Available online at www.sciencedirect.com
ScienceDirect
Coordination Chemistry Reviews 251 (2007) 111–141
COORDINATION CHEMISTRY REVIEWS
www.elsevier.com/locate/ccr

Review

Correlations between molecular structures and third-order non-linear optical functions of heterothiometallic clusters: A comparative study

Chi Zhang [a,*], Yinglin Song [b], Xin Wang [a,**]

[a] *Materials Chemistry Laboratory, School of Chemical Engineering, Nanjing University of Science and Technology, Nanjing 210094, PR China*
[b] *National Special Laboratory of Non-linear Optics and Information Processing, Department of Applied Physics, Harbin Institute of Technology, Harbin 150001, PR China*

Received 16 December 2005; accepted 13 June 2006
Available online 18 June 2006

Contents

1. Introduction 112
2. Origin and principle of non-linear optics 113
   2.1. Physical processes 113
   2.2. Experimental techniques 113
   2.3. Non-linear mechanisms 114
3. General study: structural characteristics and non-linear optical functions 116
   3.1. Linear-shaped clusters 120
   3.2. Butterfly-shaped clusters 121
   3.3. Cubane-like clusters 122
   3.4. Nest-shaped clusters 123
   3.5. Half-open cubic-cage clusters 124
   3.6. Flywheel-shaped cluster 125
   3.7. Pentanuclear planar 'open' clusters 126
   3.8. Hexagonal-prism-shaped clusters 127
   3.9. Windmill-shaped cluster 128
   3.10. Twin-nest-shaped clusters 129
   3.11. Dodecanuclear square-like cluster 130
   3.12. Supra-cage-shaped cluster 131
   3.13. Polymeric clusters 132
      3.13.1. One-dimensional cluster polymers 132
      3.13.2. Two-dimensional cluster polymers 133
      3.13.3. Three-dimensional cluster polymers 134
4. Discussions and remarks 135
   4.1. Electronic transitions 135
   4.2. Influence of skeletal atoms 135
   4.3. Influence of structural types 136
   4.4. Influence of peripheral ligands 137
   4.5. Molecular orbital analysis 138
5. Conclusions and perspectives 138
   Acknowledgements 139
   References 139

* Corresponding author. Tel.: +86 25 84318257; fax: +86 25 84315438.
** Corresponding author. Tel.: +86 25 84315500; fax: +86 25 84432747.
E-mail addresses: chizhang@mail.njust.edu.cn (C. Zhang), wangx@mail.njust.edu.cn (X. Wang).

0010-8545/$ – see front matter
doi:10.1016/j.ccr.2006.06.007

Abstract

This contribution presents an overview of the structural features and third-order optical non-linearities of the principal classes of transition heterothiometallic clusters, and demonstrates how synthetic coordination chemistry can offer a very large variety of NLO performances in relation to the different applicable heavy transition metals and the cluster configurations, the molecular symmetry and structural rigidity of the cluster compounds, the size of the energy gap between HOMO and LUMO as well as the π-donating peripheral ligands. Such clusters can very well satisfy the different heavy demands of third-order NLO materials such as absorption, refraction, switch and most importantly, optical limiting, depending on the subtle interplay of structure–function relationships. Correlations between the structural characteristics and the non-linear optical functions of these heterothiometallic clusters are discussed and examined. Recent advances and perspectives of these clusters as NLO materials are also described.

Keywords: Transition heterothiometallic clusters; Structural characteristics; Third-order non-linear optical functions

1. Introduction

Transition metal–sulfur cluster chemistry has attracted considerable attention in recent years, and presents an important and active research frontier involving advanced materials, biological processes and catalytic reactions [1–21]. This is because such clusters possess interesting electronic, biological, optical, structural and catalytic properties with a promising potential as biological active models for some nitrogenases or metalloenzymes [1–12], as active centers related to some industrial catalytic processes [1,2,13–17], and as precursor molecules of optical functional materials for optical limiting applications and optical signal detection techniques [18–24]. Currently, significant research interest in these clusters mainly stems from the search for new better materials with third-order non-linear optical (NLO) properties and superior optical limiting (OL) effects. Such materials can be not only applied to protect optical sensors and human eyes from high-intensity laser hazards, but also utilized in optical communication, optical signal processing and transmission, optical data acquisition and storage, optical computing, and optic-electronic modulation [19–21,24].

Heterothiometallic cluster compounds containing the $[MXS_3M'_n]$ (X = O, S; M = Mo, W; M′ = Cu, Ag, Au, Pt, Pd, Fe, Co, Tl, etc.) moiety [12,23,25] were first found to exhibit very large third-order NLO effects in 1994 [19,26]. The OL effects of a series of cubane-like clusters were determined to be superior to the well-known optical limiter—fullerene C_{60} [19,26]. Since then, intense research activities have been conducted on various clusters with different skeletons for exploiting new and optimized NLO materials. Among them, 13 skeletal types of clusters have been preliminarily demonstrated to display third-order NLO effects. Those clusters with skeletons of linear [27], butterfly [28], cubane-like [19,26], nest [29], half-open cubic-cage [30], pentanuclear planar 'open' [20,21,31], hexagonal-prism [32], twin-nest [33], supra-cage [34], and polymeric clusters [35–37] have been shown to possess noticeable NLO properties or large OL effects. On the other hand, inspired by the rapid development of high-power frequency-tunable lasers and optical signal techniques in both civilian and military applications particularly since the late of 1990's, research in this area had to meet the increasingly urgent demands for broadband non-linear optical materials in order to fulfill various practical NLO applications or devices [20,21,38–46]. Heterothiometallic clusters appeared to be ideal candidates to meet these requirements possibly due to their possessing the combined advantages of both organic molecules and inorganic semiconductors: large modifiable structures in addition to many heavy transition metal atoms. Heterothiometallic clusters allow, in principle, easy modifications and, eventually, optimizations on the molecular level [20,21]. All of the structural units, peripheral ligands, skeleton elements and constructing components can be altered as for the organic molecules so that alteration of the NLO properties can possibly be realized through structural manipulation. Moreover, incorporation of heavy metal atoms may introduce more sublevels into the energy hierarchy as compared to organic molecules with the same number of skeleton atoms. This permits more allowed electron transitions to take place and hence larger NLO effects, especially those beneficial to NLO applications [19–21]. Studies on these clusters show that, unlike some traditional NLO materials, the skeletons and constituent elements in these clusters have considerable influence on their NLO functions, which results in the Mo(W)–S–M′ clusters exhibiting rather diverse combinations of NLO effects [19–21].

Nevertheless, despite all research efforts in this field, not so much attention has yet been given to the influence of both coordination chemistry of these clusters and the unique possibilities offered by the various cluster molecule configurations on their NLO capabilities. The general relationships between molecular structures and NLO functions in the various existing NLO clusters are therefore yet to be well established. This turns out to be a difficult task in the effort to improve the NLO performance and OL effect through molecular structure design, and remains the bottleneck that slows down the speed of further developments and applications of these functional heterothiometallic clusters in the field of non-linear optics.

This review surveys NLO activities of the principal classes of heterothiometallic clusters, and illustrates how synthetic coordination chemistry can offer a great variety of NLO performances in relation to the cluster composition, molecular configuration, skeletal rigidity and the size of energy gap. Through a systematic examination and an intensive comparison of the structural characteristics of the clusters with particular respect to their diverse NLO properties, we expect to trigger the understanding and development of the complicated relationships between cluster

structures and NLO functions of these clusters. A brief introduction to the non-linear optical phenomena, the experimental methods and the relative non-linear mechanisms will precede the overview of various skeletal heterothiometallic clusters and their corresponding third-order NLO performances.

2. Origin and principle of non-linear optics

This section is dedicated to a brief introductory description of the nature and origin of third-order NLO effects, the related physical processes and the experimental methods, to give the readers a basic understanding for further discussion in this article regarding the structure–property relationships of heterothiometallic clusters. A more detailed description of basics, theories and methods of third-order non-linear optics can be found in the literature [38–42,44,46].

2.1. Physical processes

Non-linear optics deals with the interaction of applied electromagnetic fields with various materials to generate the polarized electric field, altered in frequency, phase, or other physical properties. In other words, optical non-linearities occur as a consequence of the modification of optical properties (absorption, refraction, or scattering, etc.) of a material system by the presence of light (especially high-energy light, like a laser beam) [38,39,41,42,44]. When a molecule is subjected to an oscillating external electric field (light), the induced change in molecular dipole moment per unit volume, or macroscopic polarization $P(t)$, can be expressed by a power series in the field strength $E(t)$ as

$$P(t) = \chi^{(1)}E(t) + \chi^{(2)}E^2(t) + \chi^{(3)}E^3(t) + \cdots \quad (1)$$

where the χ values are the macroscopic susceptibilities, $\chi^{(2)}$ and $\chi^{(3)}$ represent the molecule second-order and third-order optical non-linear susceptibilities, respectively. The reason why polarization plays a key role in the description of non-linear optical phenomena is that a time-varying polarization can act as the source of new components of the electromagnetic fields [38,39,41,42,44].

For small fields, the quadratic and cubic terms in Eq. (1) can be neglected, so that the induced polarization is proportional to the strength of the applied field (linear optical behavior). When a molecule is, however, subjected to an intense electric field such as that due to an intense laser pulse, the second and third terms in Eq. (1) become important, and the non-linear optical behavior can be observed. Note that, the "non-linear" term originates from the non-linear dependence (quadratic or cubic) of the induced polarization of the applied field.

Multifarious non-linear optical effects can occur through $\chi^{(2)}$ and $\chi^{(3)}$. In the following discussion, however, we will refer only to third-order NLO interactions. Among them, optical switching in optical communication or optical information processing, and optical limiting in the protection of optical sensors from damages induced by intense laser beams, represent the most important third-order NLO processes.

If only the third-order optical non-linearity will be taken into account, the third-order macroscopic susceptibility $\chi^{(3)}$ can be expressed as [47]:

$$\chi^{(3)} = NF^4|\gamma| \quad (2)$$

This value is related to the corresponding molecular term—the second-order hyperpolarisability γ by the Lorentz field factor, $F(F = (n_0^2 + 2)/3)$, and the number density (concentration) of cluster molecules in solution, N [38,42,47]. Actually, the $|\chi^{(3)}|$ values obtained from the Z-scan experiments consist of contributions both from a real and from an imaginary component of $\chi^{(3)}$. The imaginary component accounts for the non-linear absorption, while the real component dictates a change in the non-linear refractivity, and these two components can be distinguished by performing Z-scan measurements on the material system (cluster sample solution). The third-order NLO susceptibility can be then written as a complex quantity [48]:

$$\chi^{(3)} = \chi_R^{(3)} + i\chi_I^{(3)} \quad (3)$$

Under the applied optical field, the non-linear optical refraction and absorption of the material can then be expressed by Eq. (4) [49] and Eq. (5) [48]:

$$n(I) = n_0 + n_2 I \quad (4)$$

$$\alpha(I) = \alpha_0 + \alpha_2 I \quad (5)$$

in which, I denotes the irradiance of the laser beam, n_0 and α_0 are linear refraction index and absorption coefficient of the material, while n_2 and α_2 are non-linear refraction index and non-linear absorption coefficient of the material. In Gaussian unit system, the optical refraction index can be described as

$$n = n_0 + \frac{\tilde{n}_2}{2}|E|^2 \quad (6)$$

in which, E is the amplitude of the applied electric field, $\tilde{n}_2$ and E are in Gaussian unit system (esu), and the corresponding relation between these two unit systems can be indicated as

$$\tilde{n}_2\,(\text{esu}) = \frac{cn}{40\pi} n_2\,(\text{MKS}) \quad (7)$$

When the classical Z-scan experiments are applied, n_2 (MKS) values can be extracted directly from the performed NLO measurements. And accordingly, the real component of third-order NLO susceptibility $\chi_R^{(3)}$ is related to n_2 by $\chi_R^{(3)} = 2n_0^2\varepsilon_0 c n_2$, while the imaginary component $\chi_I^{(3)}$ is correlated to α_2 through $\chi_I^{(3)} = (n_0^2\varepsilon_0 c^2/\omega)\alpha_2$ [48].

2.2. Experimental techniques

A variety of experimental techniques have been developed to measure third-order optical non-linearity. Among them, Z-scan technique invented by E.W. Van Stryland [48], which is based on beam distortion by non-linear refraction and intensity weakening by non-linear absorption, has been shown to be applicable as a very useful tool with both simplicity and very high sensitivity [48–51]. Both the third-order non-linear optical absorption and refraction properties of cluster molecules can be investigated,

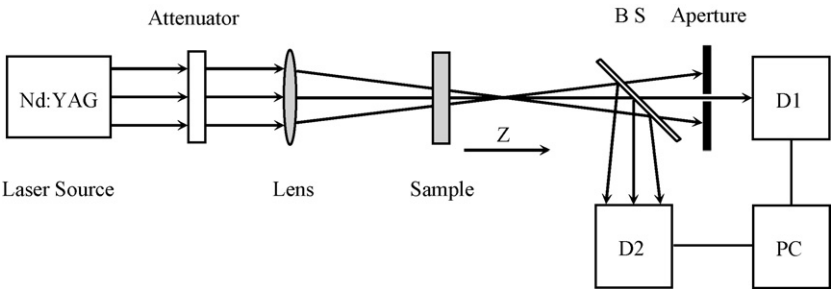

Fig. 1. Schematic illustration of the experimental set-up for the Z-scan measurements.

with the schematic illustration of the experimental set-up for the Z-scan measurements as shown in Fig. 1.

A single laser beam passing through a focused lens acts as the incident beam, while the spatial profiles of the optical pulses are of nearly Gaussian transverse mode. The cluster sample can be mounted on a translation stage that is controlled by the computer to move along the axis of the incident laser beam (*Z*-direction) with respect to the focal point instead of being fixed at its focal point. With the energy of the incident light kept constant, the cluster sample experiences different irradiances at different Z-positions. This results in a variation of the transmitted energy recorded by D1 and D2, according to the changes in position Z. A Z-scan curve (the transmittance as a function of the Z-position) will apparently show the characteristics of the non-linear optical property of the cluster sample. For determining both the sign and magnitude of the non-linear refraction of the cluster sample, an aperture is placed in front of the transmission detector D1 and the transmittance is recorded as a function of the cluster sample position on the *Z*-axis (closed-aperture Z-scan). For measuring the non-linear absorption of the cluster, the *Z*-dependent sample transmittance is taken without the aperture (open-aperture Z-scan). The non-linear refraction of the cluster sample will cause a phase distortion of the incident laser beam, as opposed to amplitude distortion due to non-linear absorption effects of the cluster.

Optical limiting measurements of cluster samples are carried out with a linearly polarized, normally 8-ns or 40-ps duration (full width at half maximum, FWHM), frequency-doubled 532 nm laser pulse produced from a Continuum Np70 ns/ps hybrid Nd:YAG laser system [51,52]. The laser pulses are operated in a nearly Gaussian transverse mode. Unsaturated cluster solutions are contained in 1 or 5-mm thick quartz cuvettes. The schematic illustration of the experimental set-up for the measurements of optical limiting effects for these clusters toward nanosecond/picosecond laser pulses is shown in Fig. 2.

The laser beam is divided into two beams by a beam splitter (BS). One is used as a reference to monitor the incident laser energy; the other is focused onto the sample cell with a 30 cm focal length mirror. Both the incident and transmitted pulse energies are measured simultaneously by two energy detectors D1 and D2 (Laser Precision, RjP-735 energy probes), which are linked to a computer by an IEEE or RS232 interface, while the incident laser energy is varied with Newport Co. Attenuator. The spot radius of the laser pulses at the focus is measured to be of either 30 ± 5 μm for the nanosecond laser beam or 55 μm for the nanosecond/picosecond laser pulse (half-width of $1/e^2$ maximum in irradiance). The interval between the laser pulses is set at 1 or 10 Hz so that every laser pulse is assured to be effectively a single shot to meet the fresh molecules in the cluster sample solution for eliminating the influence of any photo-degradation and thermal effect.

2.3. Non-linear mechanisms

Various potential mechanisms have been discussed and applied so far to define and describe the observed optical non-linearity in these heterothiometallic clusters [19–21,27–29,31–33,53–63]. As mentioned above, study on these clusters demonstrates that the constructing units, peripheral ligands, different central and skeletal metal atoms as well as structural geometry have significant influence on their optical non-linearities, and accordingly, structural, geometrical and constitutional alternations of these clusters can lead to variations in their non-linear optical properties. Thus, the relative contributions of different NLO mechanisms change consequently with the skeletal types of clusters [19–21,27–29,31–33,36,53–63].

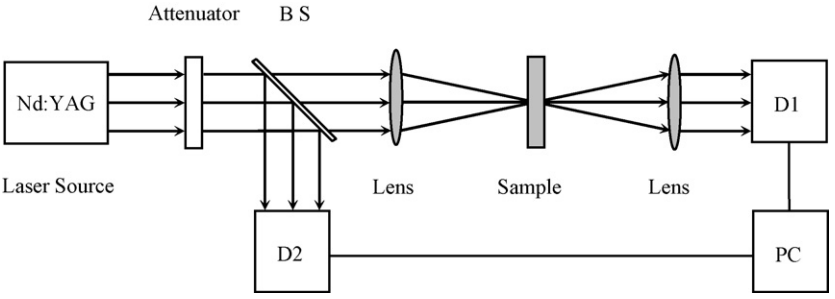

Fig. 2. Schematic illustration of the experimental set-up for the measurements of optical limiting effects.

The early investigation on butterfly-shaped clusters reveals that the good fitting between the Z-scan experimental data and the theoretical curves suggests a two-photon absorption (TPA) mechanism [28]. In contrast to butterfly clusters, non-linear scattering and excited-state absorption are possible for the observed absorptive non-linearity of the linear-shaped Au-containing clusters under the open aperture configuration of Z-scan measurements [27]. For half-open cubic-cage clusters, the explanation on the NLO mechanism has been made in terms of the individual cluster [53,54]. With 7-ns and 17-ps laser pulses, the non-linear absorption component of $[Et_4N]_3[WOS_3(CuBr)_3(\mu_2\text{-}Br)]$ was evaluated and the experimental results demonstrated that the observed optical non-linearity stemed from a fluence-dependent process [53]. Obviously, under nanosecond laser pulses, its NLO absorption is derived mainly by the excited triplet-state absorption. It is noticeable that, with nanosecond laser pulses, two consecutive one-photon absorptions appear identical to a genuine two-photon absorption. Accordingly, the magnitude of its optical non-linearity can therefore be described by an effective two-photon absorption coefficient, α_2^{eff} defined by Eq. (5) [53]. However, further investigation on its analogue cluster $[Et_4N]_3[WOS_3(CuI)_3(\mu_2\text{-}I)]$ demonstrated that both two-photon absorption and excited-state population could be responsible for the measured NLO effects [54]. The existing experimental data were insufficient to allow identification of the relative contributions of these two mechanisms, while non-linear scattering and bubble generation are not important in the NLO measurements of such half-open cubic-cage clusters. Regarding di-anionic nest-shaped cluster $[Bu_4N]_2[MoOS_3Cu_3(NCS)_3]$ [55], careful observation reveals that when the irradiance is less than 300 MW cm^{-2}, its optical limiting effect is derived predominantly from the dispersive (self-defocusing) process. When the irradiance is greater than 300 MW cm^{-2}, the dissipative mechanism becomes important. The observed NLO process is no longer pure third-order in nature, and additional excited-state absorption becomes increasingly important. As for its neutral analogue clusters $[MOS_3Cu_3L(py)_5]$, the origin of the observed reserve saturable absorption (RSA) can be attributed to excited-state absorption [29]. In contrast, the preliminary non-linearity exploration on its dimmer—twin-nest-shaped cluster indicated that, the theoretical curves qualitatively reproduced well the general pattern of the observed experimental data, and both excited-state absorption and two-photon absorption may be responsible for the measured NLO effects [33].

The non-linear mechanism of hexagonal-prism clusters has been elucidated gradually and now it tends to a conclusion. It was first discovered that the non-linear absorption of $[W_2S_8Ag_4(AsPh_3)_4]$ measured with the 7-ns width laser pulses can be viewed only as an effective third-order process. Under the influence of a nanosecond laser pulse, an excited-state absorption (two consecutive one-photon absorptions) may behave very similarly to a genuine two-photon absorption [56]. The underlying origin cannot be exactly identified of which either TPA or excited-state absorption has made the major contribution, due to insufficient experimental data [56]. Further study on its Mo-counterpart cluster $[Mo_2S_8Ag_4(PPh_3)_4]$ has shown that the non-linear absorption and refraction responsible for the limiting effect are effectively irradiance dependent, similar to two-photon absorption found in semiconductors. Although the non-linear absorption of $[Mo_2S_8Ag_4(PPh_3)_4]$ resembles TPA, it cannot be explained by TPA process. For elucidating the mechanism responsible for the observed optical limiting effect, irradiance-dependent temporal profiles of the transmitted pulses have been studied. However, no narrow temporal profiles of transmitted pulses were found, which is different from the case of C_{60}-toluene. It was then tentatively concluded that the optical limiting effect might result from absorption of a relatively short-lived excited state such as an excited singlet state or an intermediate state [32]. Subsequently, a more detailed mechanism investigation was conducted by E.W. Van Stryland and co-workers on the same hexagonal-prism cluster and the carbon-black suspension (CBS) [57]. They had performed picosecond time-resolved pump–probe measurements at 532 nm, and found that the observed pump–probe behavior is identical for $[Mo_2S_8Ag_4(PPh_3)_4]$ cluster solution and CBS. Their previous studies of CBS had documented that the primary non-linear losses were due to scattering and absorption by micro-plasmas formed after thermionic emission from heated carbon black augmented by scattering from subsequently created bubbles. The conclusion of a similar optical limiting mechanism for the two materials had also been confirmed by time-resolved shadowgraphic images taken on both samples. Although a definitive conclusion concerning the role of micro-plasmas versus bubbles in either material was still under investigation, they concluded that the non-linear mechanisms are the same for the two materials. The combination of data obtained with nanosecond pulses and with picosecond pulses showed that the dominant mechanism for optical limiting was not excited-state absorption, but non-linear scattering, the same mechanism as was dominant in CBS [57].

The later non-linearity studies on the flywheel-shaped [58], windmill-shaped [59] and dodecanuclear square-like clusters [60] preliminarily indicated that two-photon absorption, excited-state absorption, third-order bound-electronic effect and non-linear scattering were the possible mechanisms behind the observed non-linearities. As for the polymeric clusters, such as 1-D, 2-D and 3-D clusters, although these cluster polymers have been confirmed to exhibit good third-order optical non-linearities or strong OL effects which attracting considerable recent attention, it is documented that the origin of these good NLO properties are not well defined and both excited-state population and TPA could be responsible for the detected NLO performances [35,61,62]. Nevertheless, based on the previous research achievements on the third-order optical non-linearity of these heterothiometallic clusters, although the definitive conclusion concerning the underlying non-linear mechanism for each skeletal type of cluster is yet to be well established, the observed non-linearities for all type of clusters can be well described by the effective non-linear absorption coefficient α_2^{eff}, the effective non-linear refraction index n_2^{eff}, and the third-order susceptibility $\chi^{(3)}$, thus treating the system in a quasi-steady state [27,32,34,53,54,56,59–61]. These α_2^{eff}, n_2^{eff} and $\chi^{(3)}$ values of all these clusters have been documented in the literature and will be discussed later in this review.

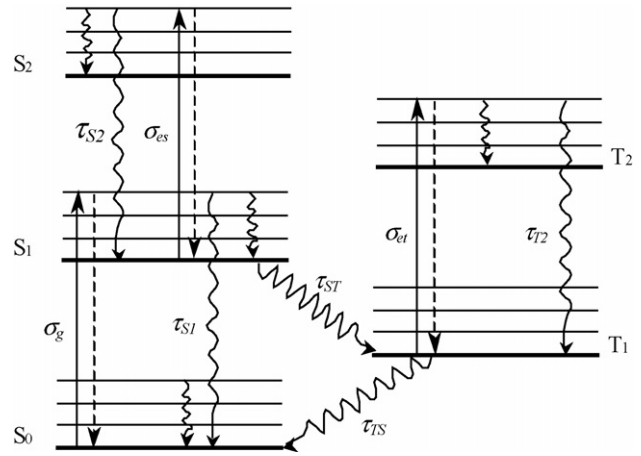

Fig. 3. Five-level energy model diagram for describing reverse saturable absorption of the heterothiometallic clusters.

However, a systematic mechanism study on these clusters is currently necessary and more NLO experimental data for each type of cluster need to be accumulated in order that the exact nature of non-linear mechanism can be well elucidated.

On the other hand, there is a general consensus that the optical limiting behaviors of those clusters with cubane-like and pentanuclear planar 'open' skeletons can be definitively attributed to the reverse saturable absorption mechanism under nanosecond pulses radiation [19–21,28,31,63], where the absorption of clusters is weak at low incident light energy but becomes extremely strong under intense light radiation, in contrast to the saturable absorption (SA) found in most materials. Physically, RSA occurs as a consequence of the absorption cross section of an excited molecular state being greater than that of the ground state. As the optical excitation intensity increases, more molecules are promoted to the excited state, thus giving rise to higher absorption at intense light excitation. Accordingly, a five-level energy model diagram (three singlet states and two triplet states, as depicted in Fig. 3) can be applied to describe the RSA process in these heterothiometallic clusters [21,63], as in other well-known RSA materials, such as fullerene C_{60} [64], the metal derivatives of phthalocyanines [50] and porphyrins [65], as well as iron–cobalt clusters [51].

Initial absorption of the laser light promotes cluster molecules from the ground state, S_0, to one of the manifold of vibration–rotational states in the first excited singlet state, S_1, which relax rapidly to the lowest level of this electronic state. Then the excited molecules in the first excited singlet state are either excited to the second excited singlet state, S_2, or transferred to the first excited triplet state, T_1, by an intersystem crossing process. Further absorption excites the cluster molecules at the T_1 state to a higher excited triplet state.

The different non-linear absorption of these clusters to nanosecond and picosecond laser pulses may be attributed to the relative contributions of excited triplet–triplet and singlet–singlet absorption for various pulse durations. For cluster molecules excited by 8 ns laser pulses, since the pulse duration is much longer than the lifetime of the excited singlet-state (~1 ns), the intersystem crossing rate is very fast. This may give rise to the contribution of the excited triplet-state absorption possessing the dominant position in the observed NLO performances [20,21,63]. Unlike for nanosecond, excitation with a 40 ps laser pulse leads to a relatively small population of the triplet state. This is because the lifetime of the singlet excited-state and the time required for intersystem crossing are both much longer than the pulse width (40 ps). Thus the optical non-linearities of these clusters are mainly caused by singlet excited-state absorption [21]. Accordingly, the variation of the beam intensity along the propagation direction (*Z*-axis) in the cluster sample solution excited by 8 ns/40 ps width laser pulses can be described as follows [21,63,66]:

$$\frac{dI}{dz} = -(\sigma_g N_g + \sigma_e N_e) I \tag{8}$$

where N_g and N_e are the molecular populations of the ground state and the first triplet excited-state (for nanosecond) or the first singlet excited-state (for picosecond), respectively; σ_g and σ_e separately represent their corresponding absorption cross sections.

3. General study: structural characteristics and non-linear optical functions

The third-order non-linear optical values of 100 heterothiometallic cluster compounds Mo(W)–S–Cu(Ag, Au, Pd and Tl), assessed by Z-scan measurements at 532 nm wavelength with nanosecond-duration laser pulses, are summarized in Table 1 [27–30,32,33–37,53–62,67–74,77,78,82–85,90–96,100–110,117,118,120,126,130,132,133]. The optical limiting threshold merits studied by 532 nm nanosecond laser pulses are collected in Table 2 [19–21,26,31,32,36,37,55,57,61,69,80–82,90,93,94,98,108,123]. At this point, one must be very cautious in comparing these NLO parameters mainly measured in two optics laboratories. For example, these values in Tables 1 and 2 have been studied by Z-scan or Optical-limiting measurements at the different widths of laser pulses, some of them are in 7 ns, and the others in 8 ns, while in several individual cases even in 40 ps. In addition, different solvent systems and cluster concentrations are also the serious concern: how the NLO merit being influenced by the interaction between cluster molecules and solvent molecules as well as the intensity and the polarity of different solvents is unclear so far and difficult to quantify. Furthermore, it is a very fact that the skeletal configuration and coordination geometry of these heterothiometallic clusters have significant influence on their third-order NLO performances. Therefore, a brief description on the cluster configuration is prior to the discussion of NLO property for each skeletal type of clusters. Following the surveys and descriptions of the structural characteristics and the corresponding non-linear optical functions of 13 types of heterothiometallic clusters in this section, the influence of skeletal atoms, structural types and peripheral ligands on the third-order optical non-linearities as well as electronic transitions and molecular orbital analysis will be preliminarily examined and discussed in detail in Section 4.

Table 1
Linear absorption data and non-linear optical parameters of the heterothiometallic cluster compounds measured at 532 nm with nanosecond-duration laser pulses

No.	Compound	Structure type	λ_{max} (nm)	α_2 (m W^{-1})	n_2 (m^2 W^{-1})	$\chi^{(3)}$ (esu)	γ (esu)	N (mol dm^{-3})	Reference
1	$[WS_4Au_2(AsPh_3)_2]$	Linear-shape	410	7.0×10^{-10}	1.0×10^{-16}	6.34×10^{-11}	6.5×10^{-29}	5.4×10^{-4}[a]	[27]
2	$[MoS_4Au_2(AsPh_3)_2]$	Linear-shape	500	5.1×10^{-10}	-5.1×10^{-17}	3.47×10^{-11}	3.0×10^{-29}	6.4×10^{-4}[a]	[27]
3	$[MoS_4Au_2(PAr_3)_2]$	Linear-shape	490		-2.25×10^{-17}			1.5×10^{-4}[b]	[67]
4	$[WS_4Au_2(PAr_3)_2]$	Linear-shape	400		-1.48×10^{-17}			9.3×10^{-4}[b]	[67]
5	$[WS_4Cu_2(dppf)_2]\cdot 4DMF$	Linear-shape	414	4.2×10^{-11}	6.1×10^{-18}	1.48×10^{-12}	6.2×10^{-31}	1.2×10^{-4}[b]	[68]
6	$[MoS_4Cu_2\{PPh_2(py)\}_4]\cdot$	Linear-shape	491	1.2×10^{-9}	-6.84×10^{-17}	3.99×10^{-11}	1.29×10^{-28}	1.55×10^{-4}[b]	[69]
7	$[MoS_4Cu_2(dppf)_2]\cdot 2DMF\cdot CH_3CN$	Linear-shape	492	1.6×10^{-9}	-1.35×10^{-17}	5.27×10^{-11}	2.04×10^{-28}	1.3×10^{-4}[b]	[69]
8	$[MoS_4Cu_2(PAr_3)_2]\cdot 0.5C_6H_{12}$	Linear-shape	490	1.41×10^{-10}	-3.52×10^{-17}	5.55×10^{-12}	1.74×10^{-29}	1.6×10^{-4}[b]	[70]
9	$[MoS_4Au_2\{PPh_2(py)\}_2]$	Linear-shape	495	5.89×10^{-12}	6.45×10^{-18}	5.90×10^{-13}	1.11×10^{-30}	2.68×10^{-4}[b]	[71]
10	$[WS_4Au_2\{PPh_2(py)\}_2]$	Linear-shape	410	4.35×10^{-11}	3.73×10^{-17}	3.53×10^{-12}	6.61×10^{-30}	2.68×10^{-4}[b]	[71]
11	$[MoS_4Ag_2(PPh_3)_3]$	Linear-shape	–	2.5×10^{-10}	-5.5×10^{-18}	8.18×10^{-12}	1.04×10^{-29}	4.0×10^{-4}[a]	[72]
12	$[Et_4N]_2[W_2S_8Pd]$	Linear-shape	398	3.5×10^{-11}	-7.5×10^{-18}	1.16×10^{-12}	4.71×10^{-31}	1.6×10^{-3}[c]	[73]
13	$[Et_4N][WS_4Pd(S_2CNC_4H_8)]$	Linear-shape	403		-6.8×10^{-18}			1.0×10^{-3}[c]	[73]
14	$[MoS_4Pd(dppp)]$	Linear-shape	486	1.0×10^{-10}	-5.5×10^{-18}	3.29×10^{-12}	3.34×10^{-30}	5.0×10^{-4}[b]	[74]
16	$[MoOS_3Cu_2(PPh_3)_3]$	Butterfly-shape	370	2.6×10^{-10}	5.0×10^{-17}	1.2×10^{-10}	9.8×10^{-28}	7.4×10^{-5}[c]	[28]
17	$[WOS_3Cu_2(PPh_3)_4]$	Butterfly-shape	345	$<10^{-12}$	8.0×10^{-18}	2.0×10^{-11}	9.0×10^{-29}	1.2×10^{-4}[c]	[28]
18	$[MoOS_3Cu_2\{PPh_2(py)\}_3]$	Butterfly-shape	378	4.4×10^{-11}	-8.23×10^{-18}	1.41×10^{-12}			[77]
19	$[MoOS_3Cu_2(PPh_3)_2(py)_2]$	Butterfly-shape	357	1.5×10^{-11}				4.0×10^{-4}[a]	[78]
20	$[MoOS_3Cu_2(PPh_3)_3(py)]$	Butterfly-shape	380	3.3×10^{-10}				2.7×10^{-4}[a]	[78]
31	$[MoS_4Cu_2Ag(\mu_3\text{-}Br)(PPh_3)_3]$	Distorted cubane-like	–	8.0×10^{-10}	3.8×10^{-16}	4.5×10^{-10}	5.5×10^{-28}	4.5×10^{-4}[c]	[72]
32	$[MoS_4Cu_3(\mu_3\text{-}Cl)\{PPh_2(py)\}_3]$	Distorted cubane-like		1.3×10^{-11}	-3.2×10^{-18}	5.09×10^{-13}	1.71×10^{-30}	1.5×10^{-4}[b]	[84]
36	$[MoOS_3Cu_3(PPh_3)_3\{S_2P(OBu)_2\}]$	Distorted cubane-like	408	5.0×10^{-10}	$<2.1 \times 10^{-18}$	2.0×10^{-11}	1.1×10^{-28}	1.0×10^{-4}[a]	[90]
37	$[MoS_4Ag_3(Ph_3P)_3\{S_2P(OCH_2CH_3)_2\}]$	Distorted cubane-like	256	8.0×10^{-10}	1.0×10^{-16}	2.4×10^{-11}	6.07×10^{-29}	2.6×10^{-4}[c]	[91]
38	$[WS_4Ag_3(Ph_3P)_3\{S_2P(OCH_2CH_3)_2\}]$	Distorted cubane-like	405	6.0×10^{-10}				5.2×10^{-4}[c]	[91]
39	$[WS_4Cu_3(PPh_3)_3\{S_2P(OCH_2Ph)_2\}]$	Distorted cubane-like	410	2.9×10^{-10}	-6.9×10^{-17}	4.74×10^{-11}	3.0×10^{-29}	8.74×10^{-4}[a]	[92]
40	$[WOS_3Ag_3(Ph_3P)_3\{S_2P(O^iPr)_2\}]$	Distorted cubane-like	360	2.5×10^{-11}	-1.5×10^{-17}	1.63×10^{-11}	7.8×10^{-30}	1.16×10^{-3}[a]	[92]
41	$[MoOS_3Cu_3(PPh_3)_3\{S_2P(OCH_2Ph)_2\}]$	Distorted cubane-like	–	7.8×10^{-11}	-7.8×10^{-18}	2.65×10^{-12}	7.67×10^{-30}	1.74×10^{-4}[b]	[93]
42	$[WOS_3Cu_3(PPh_3)_3\{S_2P(OCH_2Ph)_2\}]$	Distorted cubane-like	–	1.16×10^{-10}	4.0×10^{-18}	3.83×10^{-12}	1.67×10^{-29}	1.15×10^{-4}[b]	[93]
43	$[WOS_3Cu_3(PPh_3)_3\{S_2P(O^iPr)_2\}]$	Distorted cubane-like	434	1.23×10^{-10}	-9.3×10^{-18}	4.13×10^{-12}	1.71×10^{-29}	1.2×10^{-4}[b]	[94]
44	$[MoS_4Ag_3(PPh_3)_3\{S_2P(O^iPr)_2\}]$	Distorted cubane-like	–	1.56×10^{-10}	3.87×10^{-17}	6.08×10^{-12}	1.99×10^{-29}	1.56×10^{-4}[a]	[95]
45	$[WS_4Ag_3(PPh_3)_3\{S_2P(O^iPr)_2\}]$	Distorted cubane-like	–	1.33×10^{-10}	6.52×10^{-17}	7.08×10^{-12}	2.32×10^{-29}	1.56×10^{-4}[a]	[95]
46	$[WS_4Ag_3(Ph_3P)_3\{S_2P(OCH_2Ph)_2\}]$	Distorted cubane-like	–	1.5×10^{-10}	7.2×10^{-18}	4.94×10^{-12}	1.05×10^{-29}	2.4×10^{-4}[a]	[96]
33	$[MoOS_3Cu_3(\mu_3\text{-}Br)(2\text{-}pic)_3]$	Distorted cubane-like	495		-3.8×10^{-18}			6.2×10^{-4}[b]	[85]
34	$[WOS_3Cu_3(\mu_3\text{-}I)(2\text{-}pic)_3]$	Distorted cubane-like	427		3.5×10^{-17}			5.3×10^{-4}[b]	[85]
27	$[Et_4N]_3[MoOS_3(\mu_3\text{-}I)(AgI)_3]$	Distorted cubane-like	496	1.0×10^{-9}	8.8×10^{-17}	5.8×10^{-10}	9.07×10^{-31}	3.22×10^{-4}[b]	[82]
28	$[Et_4N]_3[WOS_3(\mu_3\text{-}I)(AgI)_3]$	Distorted cubane-like	418	1.2×10^{-9}	4.5×10^{-17}	7.3×10^{-10}	7.84×10^{-31}	4.69×10^{-4}[b]	[82]
29	$[Bu_4N]_3[MoS_4(\mu_3\text{-}Cl)Ag_3Cl_3]$	Distorted cubane-like	–	1.18×10^{-10}				2.68×10^{-4}[b]	[83]
30	$[Et_4N]_3[WOS_3(\mu_3\text{-}I)Cu_3I_3]$	Distorted cubane-like	–	1.0×10^{-10}				2.68×10^{-4}[b]	[83]
65	$[Et_4N]_3[MoOS_3(CuBr)_3(\mu_2\text{-}Br)]\cdot 2H_2O$	Half-open cubic-cage	501	1.6×10^{-10}	-2.3×10^{-16}	5.4×10^{-10}	1.6×10^{-28}	1.9×10^{-3}[c]	[30]
66	$[Et_4N]_3[WOS_3(CuBr)_3(\mu_2\text{-}Br)]\cdot 2H_2O$	Half-open cubic-cage	418	6.0×10^{-10}	1.1×10^{-16}	2.6×10^{-10}	1.6×10^{-28}	9.1×10^{-4}[c]	[53]
67	$[Et_4N]_3[WOS_3(CuI)_3(\mu_2\text{-}I)]\cdot H_2O$	Half-open cubic-cage	424	1.0×10^{-10}	-5.0×10^{-18}	1.2×10^{-11}	2.8×10^{-29}	2.3×10^{-4}[c]	[54]
68	$[MoOS_3Cu_3(PPh_3)_3(CH_3COO)]$	Half-open cubic-cage	400	3.78×10^{-14}	-1.95×10^{-17}	7.97×10^{-11}	7.0×10^{-29}	6.3×10^{-4}[a]	[109]
49	$[Bu_4N]_2[MoOS_3Cu_3(NCS)_3]$	Nest-shape	496	2.52×10^{-10}	-5.32×10^{-16}	5.3×10^{-10}	4.8×10^{-29}	6.1×10^{-3}[c]	[55]
50	$[MoI(2,2'\text{-}bpy)_2][MoOS_3Cu_3I_2(2,2'\text{-}bpy)]$	Nest-shape	420	3.0×10^{-10}	-3.0×10^{-17}	1.02×10^{-12}	1.51×10^{-30}	3.4×10^{-4}[b]	[100]
51	$[CuBr(2,2'\text{-}bpy)_2][MoOS_3Cu_3Br_2(2,2'\text{-}bpy)]$	Nest-shape				2.7×10^{-11}		7.8×10^{-4}[b]	[101]

Table 1 (*Continued*)

No.	Compound	Structure type	λ_{max} (nm)	α_2 (m W^{-1})	n_2 (m^2 W^{-1})	$\chi^{(3)}$ (esu)	γ (esu)	N (mol dm^{-3})	Reference
52	$[MoOS_3Cu_3I(py)_5]$	Nest-shape	409	6.5×10^{-10}	-3.0×10^{-17}	7.5×10^{-11}	4.73×10^{-29}	2.6×10^{-3}[c]	[29]
53	$[WOS_3Cu_3I(py)_5]$	Nest-shape	372	2.6×10^{-10}	3.2×10^{-17}	7.9×10^{-11}	2.9×10^{-29}	1.7×10^{-4}[c]	[29]
54	$[MoOS_3Cu_3(SCN)(py)_5]$	Nest-shape	400	4.8×10^{-10}	-6.7×10^{-17}	2.0×10^{-10}	5.8×10^{-27}	2.0×10^{-5}[c]	[102]
55	$[WOS_3Cu_3(SCN)(py)_5]$	Nest-shape	380	6.0×10^{-11}	-1.2×10^{-17}	8.0×10^{-11}	2.2×10^{-27}	1.9×10^{-5}[b]	[102]
56	$[MoOS_3Cu_3I(phen)_2]$	Nest-shape	400	$\sim 10^{-11}$				5.2×10^{-5}[c]	[100]
57	$[MoOS_3Cu_3I(2,2'\text{-bpy})_2]$	Nest-shape	500	6.2×10^{-10}	-3.8×10^{-17}	2.07×10^{-11}	2.81×10^{-29}	3.7×10^{-4}[b]	[103]
60	$[MoO_{0.75}S_{3.25}Cu_3Cl(2,2'\text{-bpy})_2]$	Nest-shape	–	1.2×10^{-10}	3.8×10^{-18}	3.94×10^{-12}	7.50×10^{-30}	2.68×10^{-4}[a]	[104]
58	$[WOS_3Cu_3Br(2,2'\text{-bpy})_2]$	Nest-shape	507	9.0×10^{-11}	2.72×10^{-18}	2.95×10^{-12}	1.00×10^{-29}	1.5×10^{-4}[a]	[105]
59	$[WS_4Cu_3Br(2,2'\text{-bpy})_2]$	Nest-shape	–	7.3×10^{-11}	1.24×10^{-17}	2.6×10^{-12}	2.18×10^{-30}	6.0×10^{-4}[b]	[106]
61	$[MoOS_3Cu_3(4\text{-pic})_6]\cdot Br$	Nest-shape	422	1.6×10^{-10}	1.4×10^{-17}	5.4×10^{-12}	2.51×10^{-31}	3.86×10^{-4}[b]	[107]
62	$[WOS_3Cu_3(4\text{-pic})_6]\cdot Br$	Nest-shape	372	2.8×10^{-10}	1.4×10^{-17}	5.5×10^{-12}	1.03×10^{-31}	8.89×10^{-4}[b]	[107]
63	$[WOS_3Cu_3(4\text{-pic})_6]\cdot[BF_4]$	Nest-shape	424	6.3×10^{-10}	1.85×10^{-16}	3.1×10^{-10}	4.43×10^{-31}	3.75×10^{-4}[c]	[108]
64	$[MoOS_3Cu_3(4\text{-pic})_6]\cdot 0.5[Mo_2O_7]$	Nest-shape	376	1.2×10^{-9}	3.8×10^{-16}	8.7×10^{-10}	1.32×10^{-30}	3.52×10^{-4}[c]	[108]
69	$[MoS_4Cu_3(dppm)_3]\cdot[BF_4]\cdot 2H_2O$	Flywheel-shape	560	3.96×10^{-11}	-1.98×10^{-17}	1.56×10^{-11}	2.4×10^{-29}	3.6×10^{-4}[b]	[58]
78	$[Et_4N]_2[MoS_4Cu_4(SCN)_4(2\text{-pic})_4]$	Planar 'open' shape	508	3.2×10^{-9}	-8.5×10^{-16}	8.9×10^{-10}	1.29×10^{-31}	7.44×10^{-4}[b]	[118]
79	$[Et_4N]_2[WS_4Cu_4(SCN)_4(2\text{-pic})_4]$	Planar 'open' shape	426	3.1×10^{-9}	-6.8×10^{-16}	6.5×10^{-10}	9.42×10^{-32}	6.98×10^{-4}[b]	[118]
80	$[MoS_4Cu_4(2\text{-pic})_5Br_2]\cdot 2(2\text{-pic})_{0.5}$	Planar 'open' shape	521			2.05×10^{-13}	1.06×10^{-31}	1.0×10^{-3}[b]	[120]
76	$[MoS_4Cu_4(SCN)_2(py)_6]$	Planar 'open' shape	520	4.0×10^{-10}	-4.0×10^{-17}	1.4×10^{-11}	6.98×10^{-30}	9.8×10^{-4}[b]	[117]
77	$[WS_4Cu_4(SCN)_2(py)_6]$	Planar 'open' shape	440	5.6×10^{-10}	-5.6×10^{-17}	1.9×10^{-11}	7.37×10^{-30}	1.3×10^{-3}[b]	[117]
72	$[MoS_4Cu_4Br_2(py)_6]$	Planar 'open' shape	524	1.5×10^{-9}	1.8×10^{-16}	4.6×10^{-9}	1.17×10^{-30}	3.8×10^{-4}[b]	[110]
73	$[WS_4Cu_4Br_2(py)_6]$	Planar 'open' shape	442	1.6×10^{-9}	1.1×10^{-16}	5.0×10^{-9}	1.27×10^{-30}	2.83×10^{-4}[b]	[110]
70	$[MoS_4Cu_4I_2(py)_6]$	Planar 'open' shape	526	1.0×10^{-9}	2.5×10^{-16}	5.9×10^{-9}	5.8×10^{-30}	1.39×10^{-4}[b]	[110]
71	$[WS_4Cu_4I_2(py)_6]$	Planar 'open' shape	438	2.6×10^{-9}	1.2×10^{-16}	6.2×10^{-9}	6.9×10^{-30}	5.5×10^{-4}[b]	[110]
81	$[Mo_2S_8Ag_4(PPh_3)_4]$	Hexagonal-prism-shape	256	1.8×10^{-9}	2.2×10^{-16}	5.6×10^{-10}	2.38×10^{-27}	1.3×10^{-4}[d]	[32,57]
82	$[W_2S_8Ag_4(AsPh_3)_4]$	Hexagonal-prism-shape	422	2.8×10^{-9}	5.9×10^{-17}	1.7×10^{-10}	7.2×10^{-28}	1.3×10^{-4}[c]	[56]
83	$[W_2S_8Pd_4(dppm)_2]\cdot 4DMF$	Windmill-shape	400	2.0×10^{-11}	-2.55×10^{-17}	2.29×10^{-12}	6.79×10^{-31}	1.7×10^{-3}[b]	[59]
85	$[Et_4N]_4[Mo_2O_2S_6Cu_6I_6]$	Twin-nest-shape	409	4.0×10^{-10}	-6.0×10^{-17}	1.6×10^{-10}	4.4×10^{-29}	2.0×10^{-3}[c]	[33]
86	$[Et_4N]_4[Mo_4O_4S_{12}Cu_8\{(Ph_2PS)_2N\}_4]$	Dodecanuclear square	440	1.2×10^{-11}	-2.04×10^{-18}	4.3×10^{-13}	1.81×10^{-30}	1.2×10^{-4}[b]	[60]
87	$[Bu_4N]_4[Mo_8O_8S_{24}Cu_{12}]$	Supra-cage-shape	509	2.3×10^{-9}	-3.5×10^{-16}	8.2×10^{-10}	5.7×10^{-28}	8.0×10^{-4}[a]	[34,126]
88	$[(Bu_4N)(MoS_4Tl)]_n$	1-D chain polymer	459	2.2×10^{-7}	3.1×10^{-14}	6.7×10^{-9}	8.6×10^{-27}	5.1×10^{-4}[c]	[35]
89	$[(Bu_4N)(WS_4Tl)]_n$	1-D chain polymer	398	1.8×10^{-7}	3.2×10^{-14}	5.7×10^{-9}	7.6×10^{-27}	4.9×10^{-4}[c]	[35]
90	$[\{MoOS_3Cu_3(CN)(py)_3\}\cdot 0.5C_6H_6]_n$	1-D chain polymer	395	5.0×10^{-11}	-8.0×10^{-18}	1.56×10^{-12}	1.9×10^{-29}	5.3×10^{-5}[c]	[130]
92	$[(Bu_4N)(W_2S_8Ag_3)]_n$	1-D chain polymer	–	1.11×10^{-10}	3.67×10^{-18}	3.67×10^{-12}	1.5×10^{-29}	1.2×10^{-4}[b]	[132]
93	$[\{MoS_4Cu_4(2\text{-pic})_3Br\}(\mu\text{-Br})\cdot(2\text{-pic})]_n$	1-D zigzag chain	506			2.01×10^{-13}	1.02×10^{-31}	1.0×10^{-3}[b]	[120]
94	$[(Et_4N)\{Mo_2O_2S_6Cu_6I_3(4,4'\text{-bpy})_5\}\cdot MeOH\cdot H_2O]_n$	2-D network polymer	–	3.12×10^{-9}	-5.0×10^{-16}	1.11×10^{-10}	4.66×10^{-28}	1.2×10^{-4}[b]	[36]
95	$[MoS_4Cu_6I_4(py)_4]_n$	2-D network polymer	410	1.5×10^{-9}	-2.5×10^{-17}	5.2×10^{-11}	3.56×10^{-28}	6.5×10^{-5}[e]	[61]
96	$[(Me_4N)_2\{MoOS_3Cu_3(\mu_2\text{-}I)_3\}]_n$	2-D network polymer	413	1.48×10^{-9}	-5.02×10^{-17}	4.9×10^{-11}	3.39×10^{-28}	1.08×10^{-4}[b]	[133]
97	$[(Me_4N)_2\{WOS_3Cu_3(\mu_2\text{-}I)_3\}]_n$	2-D network polymer	335	4.49×10^{-8}	1.2×10^{-16}	1.48×10^{-9}	1.02×10^{-26}	9.85×10^{-5}[b]	[133]
98	$[(Et_4N)_2\{MoS_4Cu_4(CN)_4\}]_n$	3-D framework polymer	521	1.5×10^{-9}	1.8×10^{-16}	4.58×10^{-9}	1.15×10^{-29}	3.64×10^{-5}[b]	[37]
99	$[(Et_4N)_2\{WS_4Cu_4(CN)_4\}]_n$	3-D framework polymer	443	1.6×10^{-9}	1.2×10^{-16}	5.12×10^{-9}	1.26×10^{-29}	2.93×10^{-5}[b]	[37]
100	$[\{WS_4Cu_4(4,4'\text{-bpy})_4\}\{WS_4Cu_4I_4(4,4'\text{-bpy})_2\cdot 4H_2O\}]_n$	3-D framework polymer	411	1.6×10^{-10}	1.8×10^{-17}	5.87×10^{-12}	4.44×10^{-29}	5.8×10^{-5}[e]	[62]

[a] In CH_2Cl_2.
[b] In DMF.
[c] In CH_3CN.
[d] In acetone.
[e] In DMSO.

Table 2
The limiting thresholds of some OL materials measured at 532 nm with nanosecond-duration laser pulses

No.	Compound	Structure	Solvent	Linear Transmission (%)	Limiting Threshold ($J\,cm^{-2}$)	N ($mol\,dm^{-3}$)	Ref.
	Fullerene C_{60}		Toluene	62	1.6	1.9×10^{-3}	[64]
	Phthalocyanine derivatives		Toluene	85	0.1		[52,122]
6	$[MoS_4Cu_2\{PPh_2(py)\}_4]$	Linear-shape	DMF		0.35	1.55×10^{-4}	[69]
7	$[MoS_4(Cudppf)_2]\cdot 2DMF\cdot CH_3CN$	Linear-shape	DMF		0.65	1.3×10^{-4}	[69]
21	$[Bu_4N]_3[MoS_4Ag_3BrCl_3]$	Cubane-like	MeCN	70	0.6	5.6×10^{-4}	[19]
22	$[Bu_4N]_3[MoS_4Ag_3BrI_3]$	Cubane-like	MeCN	70	0.5	1.3×10^{-4}	[19]
23	$[Bu_4N]_3[MoS_4Ag_3Br_4]$	Cubane-like	MeCN	70	0.6		[80]
24	$[Bu_4N]_3[WS_4Cu_3Br_4]$	Cubane-like	MeCN	70	1.1	5.7×10^{-3}	[26]
25	$[Bu_4N]_3[WS_4Ag_3Br_4]$	Cubane-like	MeCN	70	0.6	1.9×10^{-3}	[26]
26	$[Bu_4N]_3[MoOS_3Cu_3BrI_3]$	Cubane-like	MeCN	70	1.0		[81]
27	$[Et_4N]_3[MoOS_3Ag_3I_4]$	Cubane-like	DMF	70	0.29	3.22×10^{-4}	[82]
28	$[Et_4N]_3[WOS_3Ag_3I_4]$	Cubane-like	DMF	70	0.24	4.69×10^{-4}	[82]
36	$[MoOS_3Cu_3(PPh_3)_3\{S_2P(OBu)_2\}]$	Distorted cubane-like	CH_2Cl_2	90	5.0	1.04×10^{-4}	[90]
47	$[MoS_4Ag_3(PPh_3)_3\{S_2P(OBu^i)_2\}]$	Distorted cubane-like	CH_2Cl_2	90	0.8	8.1×10^{-4}	[90]
41	$[MoOS_3Cu_3(PPh_3)_3\{S_2P(OCH_2Ph)_2\}]$	Distorted cubane-like	DMF		0.22	1.74×10^{-4}	[93]
42	$[WOS_3Cu_3(PPh_3)_3\{S_2P(OCH_2Ph)_2\}]$	Distorted cubane-like	DMF		0.6	1.15×10^{-4}	[93]
43	$[WOS_3Cu_3(PPh_3)_3\{S_2P(OPr^i)_2\}]$	Distorted cubane-like	DMF		0.6	1.2×10^{-4}	[94]
49	$[Bu_4N]_2[MoOS_3Cu_3(NCS)_3]$	Nest-shape	MeCN	70	7.0	1.4×10^{-2}	[55]
48	$[Bu_4N]_2[MoOS_3Cu_3BrCl_2]$	Nest-shape	MeCN	73	10.0	1.49×10^{-4}	[98]
63	$[WOS_3Cu_3(4\text{-pic})_6]\cdot[BF_4]$	Nest-shape	MeCN	72	0.34	3.75×10^{-4}	[108]
64	$[MoOS_3Cu_3(4\text{-pic})_6]\cdot 0.5[Mo_2O_7]$	Nest-shape	MeCN	72	0.26	3.52×10^{-4}	[108]
84	$[Et_4N]_4[Mo_2O_2S_6Cu_6Br_2I_4]$	Twin-nest-shape	MeCN	70	2.0		[123]
94	$[(Et_4N)\{Mo_2O_2S_6Cu_6I_3(4,4'\text{-bpy})_5\}\cdot MeOH\cdot H_2O]_n$	2-D network polymer	DMF	72	0.4	1.2×10^{-4}	[36]
95	$[MoS_4Cu_6I_4(py)_4]_n$	2-D network polymer	DMSO		0.6	6.5×10^{-5}	[61]
98	$[(Et_4N)_2\{MoS_4Cu_4(CN)_4\}]_n$	3-D framework polymer	DMF	70	0.28	3.64×10^{-5}	[37]
99	$[(Et_4N)_2\{WS_4Cu_4(CN)_4\}]_n$	3-D framework polymer	DMF	70	0.15	2.93×10^{-5}	[37]
81	$[Mo_2S_8Ag_4(PPh_3)_4]$	Hexagonal-prism-shape	MeCN	92	0.1	1.3×10^{-4}	[32,57]
78	$[Et_4N]_2[MoS_4Cu_4(SCN)_4(2\text{-pic})_4]$	Planar 'open' shape	DMF	84	0.5	7.44×10^{-4}	[20,21]
79	$[Et_4N]_2[WS_4Cu_4(SCN)_4(2\text{-pic})_4]$	Planar 'open' shape	DMF	86	0.3	6.98×10^{-4}	[20,21]
77	$[WS_4Cu_4(SCN)_2(py)_6]$	Planar 'open' shape	DMF	69	0.3	1.3×10^{-3}	[31]
74	$[MoS_4Cu_4Cl_2(py)_6]$	Planar 'open' shape	DMF	78	0.15	2.6×10^{-4}	[20,21]
75	$[WS_4Cu_4Cl_2(py)_6]$	Planar 'open' shape	DMF	64	0.10	4.7×10^{-4}	[20,21]
72	$[MoS_4Cu_4Br_2(py)_6]$	Planar 'open' shape	DMF	72	0.10	3.8×10^{-4}	[20,21]
73	$[WS_4Cu_4Br_2(py)_6]$	Planar 'open' shape	DMF	72	0.08	2.83×10^{-4}	[20,21]
70	$[MoS_4Cu_4I_2(py)_6]$	Planar 'open' shape	DMF	72	0.08	1.39×10^{-4}	[20,21]
71	$[WS_4Cu_4I_2(py)_6]$	Planar 'open' shape	DMF	72	0.07	5.5×10^{-4}	[20,21]

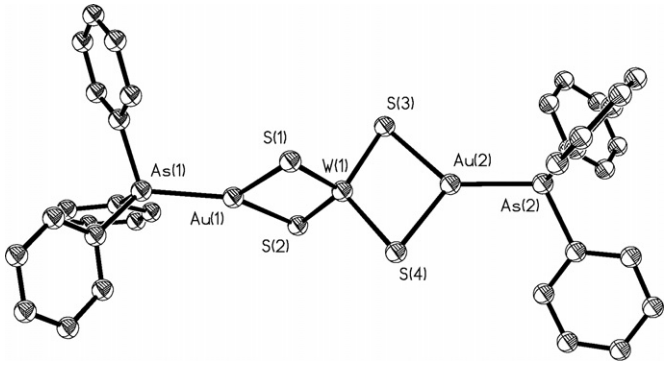

Fig. 4. Molecular configuration of the linear-shaped cluster $[WS_4Au_2(AsPh_3)_2]$ **1**. (From [27], with permission of © The Royal Society of Chemistry 1997.).

3.1. Linear-shaped clusters

Two types of clusters with the linear-shaped skeleton have been studied for their NLO performances. The first type is constructed by three metal atoms as the skeletal elements, which includes $[MS_4Au_2(AsPh_3)_2]$ (M = W, Mo) **1**–**2** [27], $[MS_4Au_2(PAr_3)_2]$ (PAr_3 = tris(4-methoxyphenyl)phosphine) **3**–**4** [67], $[WS_4(Cudppf)_2]\cdot 4DMF$ (dppf = 1,1′-bis(diphenylphosphino)-ferrocene) **5** [68], $[MoS_4Cu_2\{PPh_2(py)\}_4]$ (py = pyridine) **6** [69], $[MoS_4(Cudppf)_2]\cdot 2DMF\cdot CH_3CN$ **7** [69], $[MoS_4Cu_2(PAr_3)_2]\cdot 0.5C_6H_{12}$ **8** [70], $[MS_4Au_2\{PPh_2(py)\}_2]$ **9**–**10** [71], $[MoS_4Ag_2(PPh_3)_3]$ **11** [72], $[Et_4N]_2[W_2S_8Pd]$ **12** [73]. The second type has only two transition metal atoms in their skeletons, they are $[Et_4N][WS_4Pd(S_2CNC_4H_8)]$ **13** [73], $[MoS_4Pd(dppp)]$ (dppp = 1,3-bis(diphenylphosphino)propane) **14** [74], $[WS_4Co(dppe)]\cdot DMF$ (dppe = 1,2-bis(diphenylphosphino)ethane) **15** [75].

Exemplified by the typical linear three-metal array cluster **1** in Fig. 4, clusters with the first type of skeleton can be viewed as two planar four-membered rings MS(1)Au(1)S(2) and MS(3)Au(2)S(4) interleaving with a dihedral angle of ca. 90°, displaying essentially perpendicular to each other. The central metal atom M situated at the cluster symmetric center, has essentially tetrahedral coordination geometry. The $[MS_4]^{2-}$ acts as a tetradentate ligand coordinating to two Au atoms through its four μ_2-S atoms, and the whole molecule shows a linear structure with crystallographic C_{2v} symmetry. Each skeletal Au atom is coordinated by two μ_2-S atoms and a bulk weak electron-donating $AsPh_3$ ligand (in comparison with *S*- or *N*-containing ligands), forming a trigonal-planar geometry.

Presumably to be attributed to their symmetric molecular configuration, these linearly arranged three-metal clusters exhibit large third-order optical non-linearities. Particularly for clusters **1**–**2**, they have been demonstrated by Z-scan experiments with large non-linear absorption performance, probably owing to their heavier skeleton-metal Au atoms in addition to the symmetric cluster skeleton [27]. Likewise, the effective self-focusing in **1** and self-defocusing effects in **2**, illustrated in Fig. 5, have also been observed. In accordance with the observed α_2 and n_2 values, the modulus of second-order non-linear hyperpolarizability $|\gamma|$ were calculated as high as 6.5×10^{-29} esu **1** and 3.0×10^{-29} esu **2**, respectively. Similarly large optical

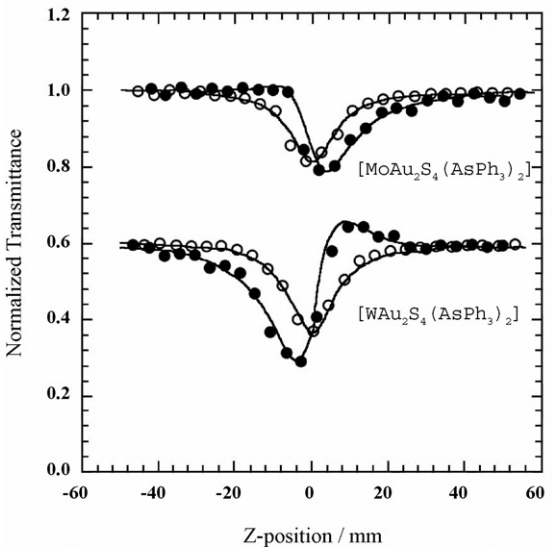

Fig. 5. Z-scan data of clusters **1** (6.4×10^{-4} mol dm^{-3}) and **2** (5.4×10^{-4} mol dm^{-3}) in CH_2Cl_2 with 532 nm 7 ns laser pulses. Optical path 1 mm. Incident energy of pulses 20 mJ. Transmittance of the aperture 0.34. The experimental data were measured with (●) and without (○) the aperture, respectively. The solid curves represent fits based on Z-scan theory. The radius of the beam waist was measured to be 30 ± 5 μm (half-width at I/e^2 maximum). The Z-scans of cluster **2** were vertically displaced by 0.4 for clarity. (From [27], with permission of © The Royal Society of Chemistry 1997.).

non-linearities have also been displayed by their Cu-analogues. Clusters **6** and **7** exhibit strong optical absorption (effective $\alpha_2 = 1.2 \times 10^{-9}$ m W^{-1} **6** and 1.6×10^{-9} m W^{-1} **7**) and optical self-defocusing effects ($n_2 = -6.84 \times 10^{-17}$ m^2 W^{-1} **6** and -1.35×10^{-17} m^2 W^{-1} **7**). Their limiting thresholds (F_{th} is defined as the incident fluence at which the actual transmittance falls to 50% of the corresponding linear transmittance) were determined to be 0.35 J cm^{-2} **6** and 0.65 J cm^{-2} **7**, which are about four and two times, respectively, better than that of C_{60} [69]. However, in contrast to the non-linear optical behaviors of clusters **1**–**2**, exceptional cases were found for their analogous clusters **3**–**4** in DMF solution investigated by the Z-scan technique at 532 nm and picosecond time-resolved pump–probe measurements at pump fluence of 5.2 J cm^{-2}. Their optical non-linearities are dominated by non-linear self-defocusing as their non-linear absorptions are negligible [67]. In general, although a precise internal comparison of NLO values cannot be made at this moment because of the lack of enough NLO results of these linear skeletal clusters, some preliminary figures have emerged. The first type clusters **1**–**2** and **9**–**10** with heavier Au atoms incorporated in their cluster skeletons exhibit good NLO properties, while a close inspection shows that in both cases, W-containing clusters (**1**, **10**) always demonstrate somewhat superior NLO performance to their Mo-counterparts (**2**, **9**) [27,71], probably due to heavier transition metal atom within the former clusters. This is consistent with the fact that the NLO performance is essentially influenced not only by the molecular configuration symmetry of the heterothiometallic cluster, but also by the modulation of heavy transition metal atoms within the cluster skeleton even for the same skeletal type [19–21,26], as found in organometallic NLO compounds [52,65,76]. In addition, the

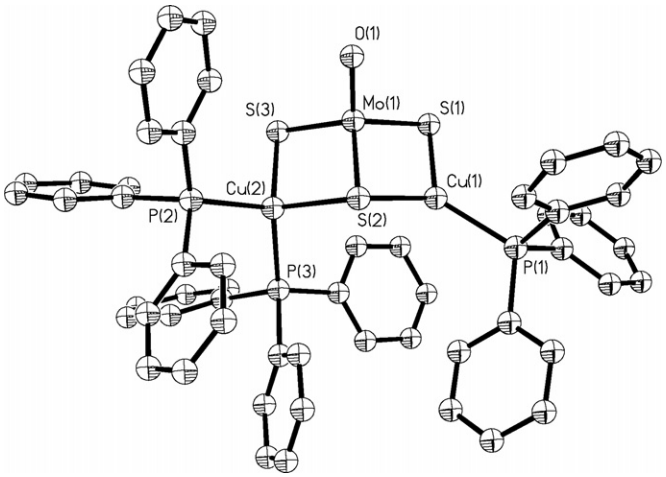

Fig. 6. Molecular configuration of the butterfly-shaped cluster $[MoOS_3Cu_2(PPh_3)_3]$ **16**. (From [28], with permission of © 1995 American Chemical Society.).

first type linear clusters **1–2** and **6–8**, having the symmetrical C_{2v} skeleton in the center, exhibit the strong NLO properties among all M–S–M′ heterothiometallic clusters.

3.2. Butterfly-shaped clusters

Neutral clusters $[MoOS_3Cu_2(PPh_3)_3]$ **16** [28], $[WOS_3Cu_2(PPh_3)_4]$ **17** [28], $[MoOS_3Cu_2\{PPh_2(py)\}_3]$ **18** [77], $[MoOS_3Cu_2(PPh_3)_2(py)_2]$ **19** [78], and $[MoOS_3Cu_2(PPh_3)_3(py)]$ **20** [78] have a butterfly-shaped configuration.

An early NLO study on such skeleton of clusters is related to cluster **16**, depicted in Fig. 6, which displays an asymmetric butterfly structure with the C_s symmetry. The central Mo atom possesses tetrahedral coordination, while the two skeletal Cu atoms have two different asymmetric coordination geometries: Cu(2) adopts a distorted tetrahedral coordination mode being ligated by two peripheral PPh_3 units—a weak π-donating ligand; Cu(1) is in a trigonal-planar environment with only one PPh_3 ligand, a μ_2-S and a μ_3-S atom. It is obvious that cluster **16** has no symmetry center and less skeletal rigidity. The similar molecular coordination geometry has been displayed by other butterfly-shaped clusters, and it is interesting that all these clusters are associated with PPh_3-containing weak π-donating ligands.

All these reported PPh_3-capped butterfly-shaped clusters exhibit only modest NLO performances in the heterothiometallic cluster family. The NLO properties of cluster **16** are shown by both non-linear absorption (absorption coefficient $\alpha_2 = 2.6 \times 10^{-10}$ m W^{-1}) and optical self-focusing performance (refraction index $n_2 = 5.0 \times 10^{-17}$ m^2 W^{-1}) as illustrated by Z-scan traces in Fig. 7 measured in 7.4×10^{-5} mol dm^{-3} CH_3CN solution [28]. In contrast, its W-counterpart with one additional PPh_3 coordinated to Cu(1) in cluster **16**, cluster **17** only exhibits a very weak optical self-focusing effect ($n_2 = 8.0 \times 10^{-18}$ m^2 W^{-1}) as measured with a 1.2×10^{-4} mol dm^{-3} CH_3CN solution, in addition to its negligibly small non-linear absorption. From the α_2 and n_2 values, the effective third-order NLO susceptibility $\chi^{(3)}$ was calculated to be 1.2×10^{-10} esu ($\gamma = 9.8 \times 10^{-28}$ esu) for **16**, which is comparable with some best performing organic polymers and semiconductors (such as 8.5×10^{-10} esu for crystal PTS (*p*-toluene sulfonate), 1.8×10^{-10} esu for poly-4-BCMU (poly{5,7-dodecadiyne-1,12-diol-*co*-bis[((*n*-butoxycarbonyl)-methyl)urethane]}), 5.0×10^{-10} esu for PA (poly-acetylene), 4.8×10^{-11} esu for GaAs, and 4×10^{-10} esu for Ge) known at that time [39,79]. The NLO performances of some similar butterfly clusters with pyridine- or 2-(diphenylphosphino)-pyridine-capped ligands have also been investigated recently [77,78], demonstrating similar NLO behaviors to those of clusters **16–17**. However, it is worth noticing that, only small change in the peripheral ligands of cluster **18** by $PPh_2(py)$ instead of PPh_3 in cluster **16** with the same other cluster skeleton components for both clusters, NLO capability in cluster **18** is significantly lower (n_2 reduces to -8.23×10^{-18} m^2 W^{-1} and α_2 to 4.4×10^{-11} m W^{-1}) [77]. This fact may suggest that the

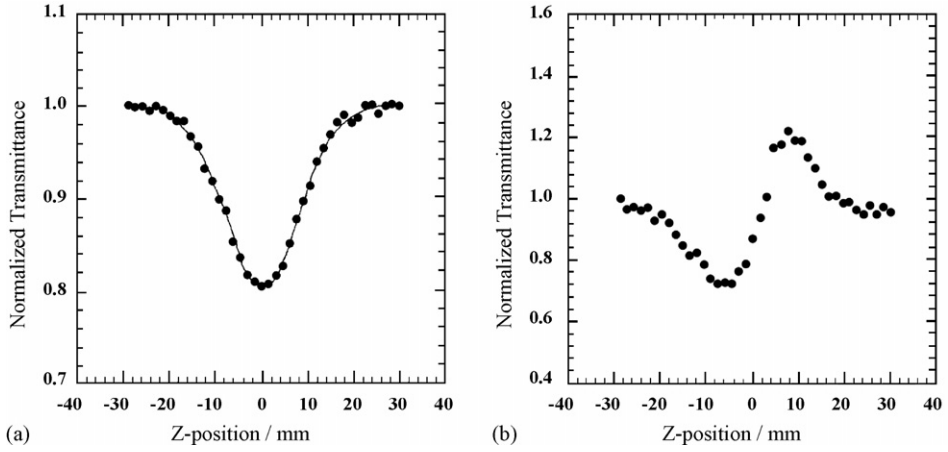

Fig. 7. Z-scan data of 7.4×10^{-5} mol dm^{-3} of cluster **16**, in a 1-mm quartz cuvette and at 532 nm 7 ns with I_0 being 2.2×10^{12} W m^{-2}: (a) collected under the open-aperture configuration showing nonlinear absorption (the solid curve is a theoretical fit based on the Z-scan theory), (b) obtained by dividing the normalized Z-scan data obtained under the closed-aperture configuration by the normalized Z-scan data in (a). The radius of the beam waist was measured to be 30 ± 5 μm (half-width at $1/e^2$ maximum). (From [28], with permission of © 1995 American Chemical Society.).

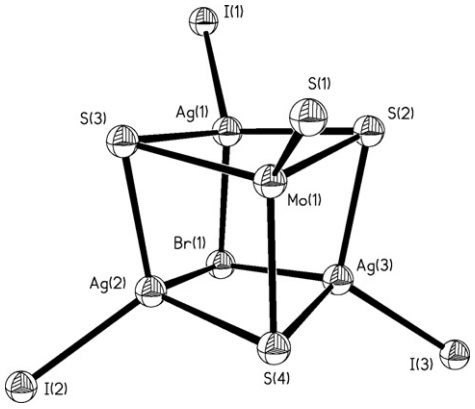

Fig. 8. Molecular configuration of the cubane-like anion cluster $[MoS_4Ag_3BrI_3]^{3-}$ **21**. (From [19], with permission of © 1994 American Chemical Society.).

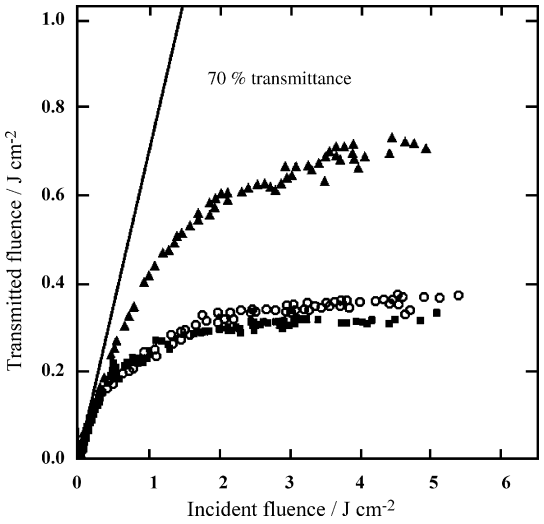

Fig. 9. Optical limiting responses to 7-ns, 532-nm laser pulses, of clusters **21** (■) and **22** (○) in acetonitrile and C_{60} (▲) in toluene, in a 1-mm-thick quartz cell. Solutions with 70% transmittance correspond to 1.4×10^{-4} mol dm^{-3} **21**, 5.6×10^{-4} mol dm^{-3} **22**, or 1.9×10^{-3} mol dm^{-3} C_{60}, respectively. (From [19], with permission of © 1994 American Chemical Society.).

peripheral ligands also play an important role in determining the NLO properties of these heterometallic clusters.

3.3. Cubane-like clusters

Cubane-like clusters with tri-anionic and neutral skeletons comprise the largest group among various skeletons of clusters and have been extensively reported for NLO study, which include anionic clusters $[R_4N]_3[MO_nS_{4-n}M'_3YL_3]$ **21–30** [19,26,63,80–83], neutral clusters $[MS_4M'_3Y(PPh_3)_3]$ **31–32** [72,84] and $[MOS_3Cu_3Y(2\text{-pic})_3]$ **33–35** [85–89] (M = Mo, W; M′ = Cu, Ag; Y, L = Cl, Br, I; R = Et, Bu; n = 0, 1). It is also documented that those clusters with a skeleton supported by $S_2P(OR)_2$ ligands, for example, $[MO_nS_{4-n}M'_3(PPh_3)_3\{S_2P(OR)_2\}]$ (M = Mo, W; M′ = Cu, Ag; R = Et, Pr^i, Bu, Bu^i, CH_2Ph; n = 0, 1) **36–47** [90–96], may also be described as a distorted cubic cage-shape.

Consisting of a ($MoAg_3$) metal tetrahedron interlocked with a (BrS_3) nonmetal tetrahedron, the skeleton of the prototypical anionic cluster $[Bu_4N]_3[MoS_4Ag_3BrI_3]$ **21** [19] in Fig. 8 (crystallized in the cubic space group F-43c) can be defined as a slightly distorted cube with very high skeletal rigidity and geometrical symmetry. The cluster core of $[MoS_4Ag_3Br]$ basically retains the C_{3v} geometry with three AgI groups coordinated to the $[MoOS_3]^{2-}$ unit across three S···S edges. The central Mo atom is tetrahedrally coordinated, while the three skeletal Ag atoms are almost equivalent and each of them is coordinated with two μ_3-S atoms, one μ_3-Br atom and one peripheral I ligand, forming three reverse distorted tetrahedrons. These three tetrahedral $MoAg_3$, BrS_3 and SI_3 moieties in the anionic cluster skeleton are co-centred.

In 1994, tri-anionic clusters of formula $[Bu_4N]_3[MoS_4Ag_3BrL_3]$ (L = I **21**, Cl **22**) were first demonstrated to possess very large optical limiting effects in such heterothiometallic clusters, which was ascribed to their highly symmetrical cage skeleton [19]. As illustrated in Fig. 9, the optical limiting threshold was measured to be 0.5 J cm^{-2} for cluster **21** and 0.6 J cm^{-2} for **22**, both with a saturation fluence transmitted to 0.3 J cm^{-2}. These threshold values are only 1/3 of that of C_{60} measured under identical conditions, and their saturation energies are about 1/2 of that of C_{60}. In other words, these values are significantly better than that of C_{60}, the benchmark molecular OL materials reported at the time [19,121]. The subsequent studies on the similar clusters $[Bu_4N]_3[WS_4M'_3Br_4]$ (M′ = Cu **24**, Ag **25**) showed that the OL performance was improved on replacement of Cu by Ag, which is attributable to the heavy atom effect [26]. Z-scan and pump–probe experiments further proved that the OL behaviors of these cubane clusters originated from a non-linear absorptive process referring to RSA [63]. It is therefore not surprising that since this observation the investigation on NLO effects of cubane-like clusters and the related heterothiometallic clusters with various types of skeletons have attracted considerable research attention.

However, further investigations on the PPh_3-capped neutral cubic clusters $[MoS_4M'_3Cl(PPh_3)_3]$ (M′ = Cu, Ag), $[WS_4Ag_3Cl(PPh_3)_3]\cdot 0.5P(S)Ph_3\cdot 3H_2O$, and $[WS_4Ag_3Br(PPh_3)_3]\cdot H_2O$ demonstrated only negligible cubic optical non-linearity and OL behavior [97]. In comparison with their tri-anionic counterparts showing large OL effects derived from the efficient RSA, the negligible NLO performances in PPh_3-capped neutral cubic clusters are evidently due to the larger HOMO–LUMO gaps and smaller ratio of σ_e/σ_g [97]. In addition, moderate to large NLO performances have been displayed by the clusters supported by $S_2P(OR)_2$ (R = Et, Pr, Bu, CH_2Ph...) ligands [90–96], shown in Table 1. Particularly in distorted cubic cage-shaped clusters $[MOS_3Cu_3(PPh_3)_3\{S_2P(OCH_2Ph)_2\}]$ (M = Mo, W) **41–42**, these two clusters exhibit large optical limiting performance with limiting threshold values of 220 mJ cm^{-2} for **41** and 600 mJ cm^{-2} for **42**, which are comparable to their tri-anionic counterparts [93]. A recent interesting discovery involved two 2-picoline-containing neutral cubic clusters $[MOS_3Cu_3X(2\text{-pic})_3]$ (M = Mo, X = Br; M = W, X = I; 2-pic = 2-picoline) **33–34**.

These two isomorphous clusters exhibit diametrically opposed non-linear refractive properties, with cluster **33** showing a self-defocusing performance (effective non-linear refractive index $n_2 = -3.8 \times 10^{-18}$ m^2 W^{-1}) and cluster **34** demonstrating a self-focusing effect ($n_2 = 3.5 \times 10^{-17}$ m^2 W^{-1}) under 10 ns laser pulses [85]. Moreover, when excited by shorter 40 ps laser pulses, the non-linear refraction performance of cluster $[MoOS_3Cu_3I(2\text{-pic})_3]$ **35** switches from self-defocusing in 10 ns pulses to self-focusing, a phenomenon attributable to the larger refraction volume of the initially populated singlet state which can not undergo significant ISC (intersystem-crossing process) to the triplet state of smaller refraction volume within the pulse duration [89].

3.4. Nest-shaped clusters

Nest-shaped clusters are another series of representative members in the family of heterothiometallic clusters, including anionic clusters $[Bu_4N]_2[MoOS_3Cu_3BrCl_2]$ **48** [98], $[Bu_4N]_2[MoOS_3Cu_3(NCS)_3]$ **49** [55,99], $[MoI(2,2'\text{-bpy})_2][MoOS_3Cu_3I_2(2,2'\text{-bpy})]$ (2,2′-bpy = 2,2′-bipyridine) **50** [100], $[CuBr(2,2'\text{-bpy})_2][MoOS_3Cu_3Br_2(2,2'\text{-bpy})]$ **51** [101], neutral clusters $[MOS_3Cu_3L(py)_5]$ (M = Mo, W; L = I, SCN) **52–55** [29,102], $[MoOS_3Cu_3I(phen)_2]$ (phen = 1,10-phenanthroline) **56** [100], $[MXS_3Cu_3L(2,2'\text{-bpy})_2]$ (M = Mo, W; X = O, S; L = Br, I) **57–60** [103–106] and cationic clusters $[MOS_3Cu_3(4\text{-pic})_6]\cdot L$ (L = Br, M = Mo **61**, W **62**; BF_4, M = W **63**; $0.5M_2O_7$, M = Mo **64**; 4-pic = 4-picoline) [107,108].

As a typical neutral cluster, $[MOS_3Cu_3I(py)_5]$ (M = Mo **52**, W **53**) exhibits a nest-shaped structure as shown in Fig. 10 [29]. With C_{3v} geometry, the core aggregate $[MOS_3Cu_3]$ of such nest-shaped clusters possesses much lower structural rigidity than that of cubane-like clusters. Three skeletal Cu atoms adopt a distorted tetrahedral geometry and two different coordination modes: one is coordinated to two μ_3-S atoms, a peripheral pyridine and an I ligand; the other two are linked by two μ_3-S atoms and two peripheral pyridine ligands. There exists a strong super-conjugation effect in clusters **52–53** and in their cationic analogues $[MOS_3Cu_3(4\text{-pic})_6]\cdot L$ **61–64** [107,108], which may result from the coordinated py or 4-pic. These strong π-donating ligands have a high tendency to coordinate strongly to the Cu atoms and accordingly, weaken the coordination between the Cu and S atoms. This has been confirmed by the shorter average Cu–S bond lengths in both neutral clusters **52–53** and cationic clusters **61–64**, in comparison with a longer Cu–S bond distance found in their anionic analogue $[Bu_4N]_2[MoOS_3Cu_3BrCl_2]$ **48** [98].

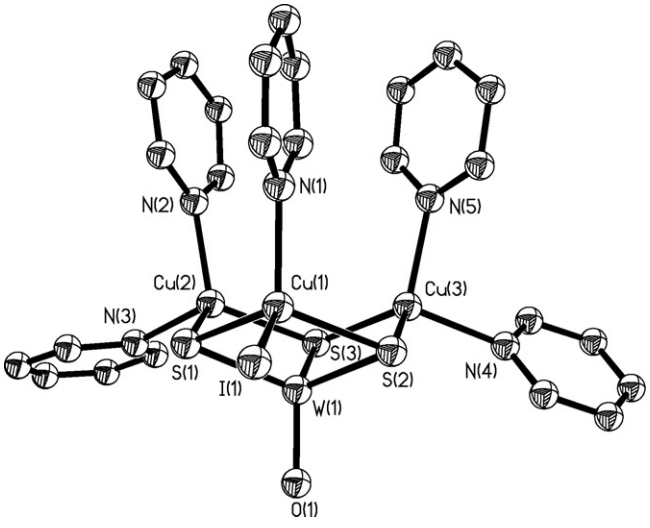

Fig. 10. Molecular configuration of the nest-shaped cluster $[WOS_3Cu_3I(py)_5]$ **53**. (From [29], with permission of © 1997 American Chemical Society.).

Open/closed-aperture Z-scan experiments demonstrate that the optical non-linearity of nest-shaped clusters is represented by both strong non-linear absorption capabilities and non-linear refraction behaviors. For neutral nest-shaped clusters $[MOS_3Cu_3I(py)_5]$ **52–53**, both clusters exhibit moderately large non-linear absorption capabilities with absorption coefficients being 2.6×10^{-10} m W^{-1} for **53** and 6.5×10^{-10} m W^{-1} for **52** [29]. Interestingly, clusters **52** and **53** are the first examples of two isomorphous clusters being found to exhibit diametrical opposite non-linear refractive properties. The data given in Fig. 11a show that **53** has a positive sign for refractive non-linearity, which gives rise to a self-focusing effect (effective non-linear refractive index $n_2 = 3.2 \times 10^{-17}$ m^2 W^{-1}), while the data in Fig. 11b indicate that **52** has a self-defocusing performance ($n_2 = -3.0 \times 10^{-17}$ m^2 W^{-1}). It is noticeable that the only difference between **52** and **53** is the nature of the central metal atom: W for **53** and Mo in **52**.

Nevertheless, neutral nest clusters $[MOS_3Cu_3(SCN)(py)_5]$ (M = Mo **54**, W **55**) with the same cluster core $[MOS_3Cu_3]$ as **52–53** reveal the exceptional large second-order hyperpolarizability γ values (5.8×10^{-27} esu for the Mo-cluster **54**, 2.2×10^{-27} esu for the W-cluster **55**). These γ values of clusters **54–55** are the biggest of all discrete heterothiometallic clusters to date [102]. On the other hand, regarding ionic nest-shaped clusters, they especially exhibit strong non-linear refraction behaviors, such as in the anionic cluster **49** ($n_2 = -5.32 \times 10^{-16}$ m^2 W^{-1}) [55] and in the cationic clusters **61–64** ($n_2 = 1.4 \times 10^{-17}$ **61**, 1.4×10^{-17} **62**, 1.85×10^{-16} **63**, 3.8×10^{-16} **64** m^2 W^{-1}) [107,108].

Furthermore, when a comparison is made on the NLO properties of the clusters with the skeletons of butterfly-shaped, nest-shaped and cubic cage, one may note that a pattern of a structure/NLO correlation exists. It seems certain that the structure alternations of butterfly ⇄ nest ⇄ cubic cage (or arachno ⇄ nido ⇄ closo) are responsible for the variation of NLO activities [28]. The addition of skeletal transition metal atoms and the enhancement of the skeletal rigidity may provide an effective route to enhancing optical non-linearity of these clusters. This is consistent with the fact that skeleton metal atom modulation induces larger changes in the NLO properties (as compared with peripheral ligand substitution), as observed in the clusters with the butterfly-shaped, nest-shaped and cubic cage skeletons [19,26,28]. However, more detailed studies on the excited-state performance of these clusters are needed to provide a theoretical frame to explain and predict their NLO behaviors.

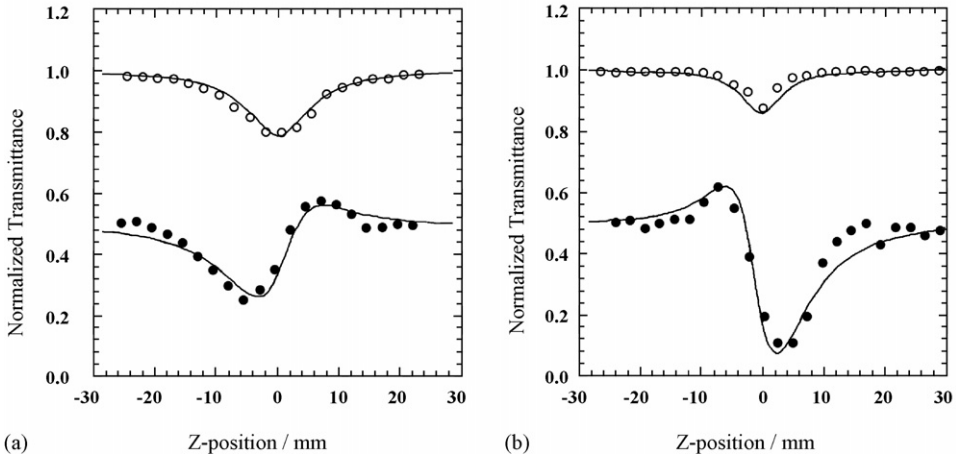

Fig. 11. Z-scan measurements at 532 nm with 7 ns laser pulses. The filled (●) and open circles (○) are the data measured with and without the aperture, respectively. The data in (a) are obtained with cluster **53** at a concentration of 1.7×10^{-4} mol dm^{-3} and a peak irradiance of 3.7×10^{8} W cm^{-2}. The data in (b) are obtained with cluster **52** at a concentration of 2.6×10^{-3} mol dm^{-3} and a peak irradiance of 6.7×10^{8} W cm^{-2}. The solid curves are the theoretical fits by using the Z-scan theory. The data (and corresponding fits) obtained with the aperture are vertically shifted by −0.5 for presentation. The spot radius of the laser pulses at the focus was measured to be of 30 ± 5 μm (half-width of $1/e^2$ maximum in irradiance). (From [29], with permission of © 1997 American Chemical Society.).

3.5. Half-open cubic-cage clusters

From the room-temperature solid-state reactions, three anionic clusters $[Et_4N]_3[MOS_3(\mu_2\text{-}Y)(CuL)_3]\cdot 2H_2O$ (M = Mo, L, Y = Br; M = W, L, Y = Br, I) **65**–**67** [30,53,54] and one neutral cluster $[MoOS_3(\mu_2\text{-}CH_3COO)Cu_3(PPh_3)_3]$ **68** [109] were constructed, which can be assigned to this structural type.

The typical cluster $[Et_4N]_3[MoOS_3(\mu_2\text{-}Br)Cu_3Br_3]$ **65** [30] in Fig. 12, crystallizing in the orthorhombic space group *Pnma*, can be envisaged as a unique half-open cage-shaped skeleton. Although the central Mo atom still retains the tetrahedral geometry and the cluster core has a C_{3v} geometry, there are two diverse coordination modes for the three skeletal Cu atoms. Two Cu atoms hold a distorted tetrahedral geometry, coordinated by two μ_3-S atoms, one μ_2-Br atom and one peripheral Br ligand. The third Cu atom is in an unusual trigonal-planar coordinated environment with two μ_3-S atoms and one peripheral Br ligand. This unique coordination mode gives rise to a symmetry plane passing through the O, Mo, Cu(1), Br(2), Br(3) and S(2) atoms, and less skeletal rigidity compared to its cubane-like cluster counterparts.

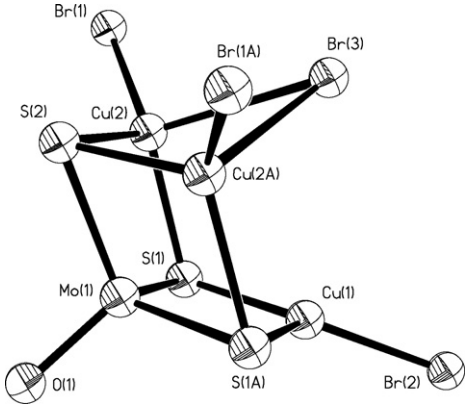

Fig. 12. Molecular configuration of the half-open cubic-cage anion cluster $[MoOS_3(\mu_2\text{-}Br)Cu_3Br_3]^{3-}$ **65**. (From [30], with permission of © 1995 American Chemical Society.).

Originating from their unusual coordination mode and the moderate skeletal rigidity, half-open cubic-cage clusters, assumed as an intermediate structure between cubane-like clusters and nest-shaped clusters, can be accordingly derived from cubane-like clusters by the cleavage of one skeletal metal Cu–Y bond. In general, such kind of clusters always exhibit a modest non-linear absorption effect ($\alpha_2 = 1.6 \times 10^{-10}$ m W^{-1} **65**, 6.0×10^{-10} m W^{-1} **66**, and 1.0×10^{-10} m W^{-1} **67**) and a large non-linear refractive performance ($n_2 = -2.3 \times 10^{-16}$ m^2 W^{-1} **65**, 1.1×10^{-16} m^2 W^{-1} **66**) under 7 ns laser pulses at 532 nm [30,53,54], in comparison with cubane-like clusters. The ensuing study demonstrates that, however, the magnitude of the optical non-linearity of cluster **66** decreases significantly if the same Z-scan experiment is carried out with 17 ps laser pulses [53]. Under the conditions of comparable irradiance (such as 2.0 GW cm^{-2}), no optical non-linearity was observed with picosecond pulses whereas the optical non-linearity is obvious with nanosecond pulses. When fluence is kept comparable, the light-dependent absorption change measured with picosecond laser pulses is still smaller than 10% of that measured with nanosecond pulses. Apparently, the observed optical non-linearity stems from a fluence-dependent process and the non-linear absorptivity of **66** is given rise mainly by excited triplet-state absorption under nanosecond pulses. The results of closed-aperture Z-scan measurements of cluster **65** are depicted in Fig. 13. The both isomorphous clusters **65** and **66**, besides their interesting non-linear refractive behaviors (**66** shows strong self-focusing, while **65** depicts strong self-defocusing) [30,53], additionally possess large second-order hyperpolarizability values ($\gamma = 1.6 \times 10^{-28}$ esu) and a large corresponding optical suscepitibility $\chi^{(3)}$ as 5.4×10^{-10} esu for **65**, 2.6×10^{-10} esu in **66**.

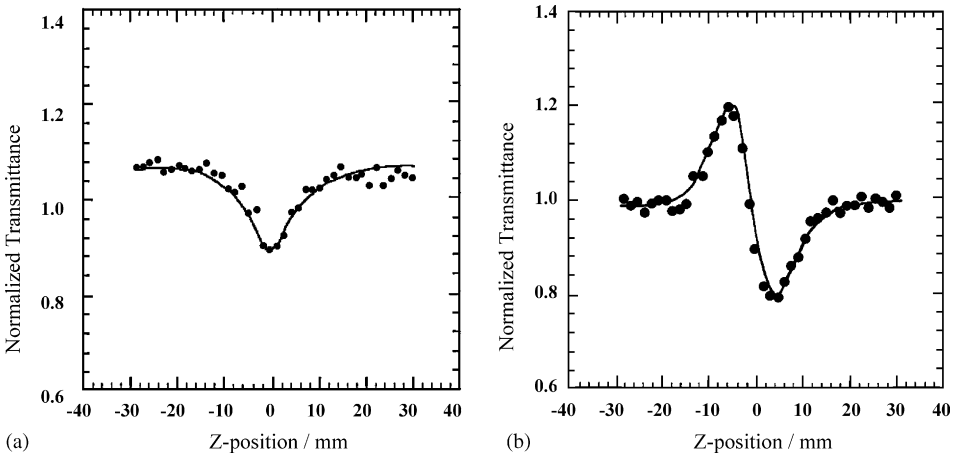

Fig. 13. Z-scan data (●) of 1.9×10^{-3} mol dm^{-3} of cluster **65**, at 532 nm with incident energy of 8 μJ/pulse: (a) collected under open-aperture configuration. The solid curve is a theoretical fit based on Z-scan theory. (b) Obtained by dividing the normalized Z-scan data obtained under closed-aperture configuration by the normalized Z-scan data in open-aperture configuration. The solid line is an eye guide. Pulse duration (full width of l/*e* maximum in irradiance) was measured to be 7 ± 1 ns. The minimum spot radius of the focused beam was 30 ± 5 μm (half-width of l/e^2 maximum in irradiance). (From [30], with permission of © 1995 American Chemical Society.).

3.6. Flywheel-shaped cluster

Only one such cluster $[MoS_4Cu_3(dppm)_3]\cdot[BF_4]\cdot 2H_2O$ (dppm = bis(diphenylphosphino)methane) **69** [58], in Fig. 14, has been synthesized and exploited for the NLO properties. The X-ray crystallography determination reveals that the whole cluster molecule crystallizes in the monoclinic system space group $P2_1$, and one $[MoS_4]^{2-}$ moiety with the three Cu atoms construct a distorted "flywheel" array, corresponding to three four-membered Mo–μ_2-S–Cu–μ_4-S rings sharing one Mo–μ_4-S edge. The related average μ_2-S–Mo–μ_2-S and Cu–μ_4-S–Cu bond angles adopt 111.6° and 113.6°, respectively, which confirms the cationic $[MoS_4Cu_3]^-$ cluster core to have approximately C_{3v} symmetrical geometry. The Mo atom has retained its initial tetrahedral coordination, and each of the three Cu atoms is in a distorted tetrahedron. There are two different coordination modes of the bridging S atoms. S(1), S(2) and S(3) are bonded to Mo and only one Cu atom, but S(4) exhibits an unprecedented μ_4-bridging mode, being asymmetrically bonded to two kinds of metal units, one Mo and three Cu atoms. With the Mo···Cu separations being rather long, one would expect only very weak intramolecular metal-metal interaction. The six-membered ring comprising Cu, S, Cu, P, C and P has a boat conformation, whereas the other related rings have a chair conformation. This is probably due to the rigidity of the $[MoS_4]^{2-}$ group and the steric crowding of the phenyl groups of dppm.

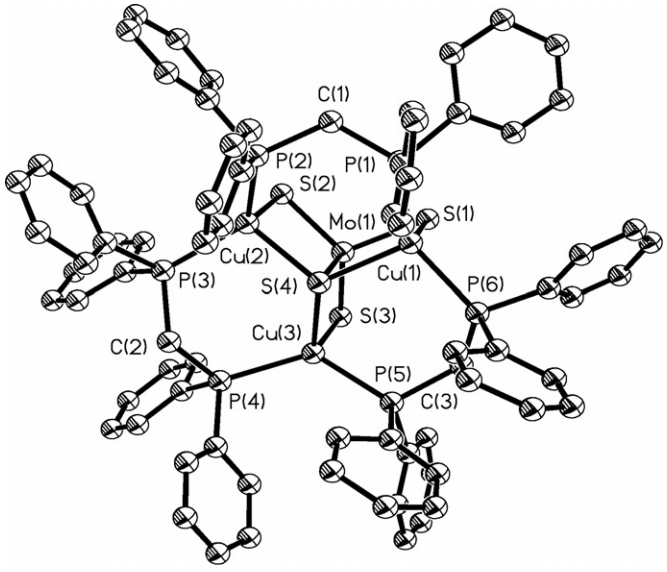

Fig. 14. Molecular configuration of the flywheel-shaped cation cluster $[MoS_4Cu_3(dppm)_3]^+$ **69**. (From [58], with permission of © 2000 Elsevier Science Ltd.).

The third-order non-linear optical performance of the flywheel-shaped cluster $[MoS_4Cu_3(dppm)_3]\cdot[BF_4]\cdot 2H_2O$ **69** has only been preliminarily investigated by applying Z-scan technique with linearly polarized 7 ns (FWHM) optical pulses at 532 nm, illustrated in Fig. 15. Its non-linear absorption is very weak (the non-linear absorption coefficient $\alpha_2 = 3.96 \times 10^{-11}$ m W^{-1} [58], in contrast to $\alpha_2 = 2.6 \times 10^{-10}$ m W^{-1} found in the butterfly cluster **16** $[MoOS_3Cu_2(PPh_3)_3]$ [28], the latter having one [SCuS] face missing as compared with cluster **69**), but it exhibits moderate third-order non-linear refractive behavior ($n_2 = -1.98 \times 10^{-17}$ m^2 W^{-1}). The corresponding optical suscepitibility $\chi^{(3)}$ and hyperpolarizability γ, based on its α_2 and n_2 values, were calculated to be 1.56×10^{-11} and 2.4×10^{-29} esu. Its optical non-linearity is obviously lower than those of most other skeleton heterothiometallic clusters such as linear, cubane-like, nest shape and half-open cube shape. This is presumably to be attributed to the absence of triply bridged μ_3-S atoms in its cluster skeleton. On the other hand, such a μ_3-S bridging binding mode may generally provide stability to the clusters (such as for cubane-like, hexagonal-prism, pentanuclear planar 'open' clusters exhibiting very strong optical non-linearities) toward light-induced fragmentation caused by the electronic transition between the skeletal bonding and anti-bonding orbitals [19,24].

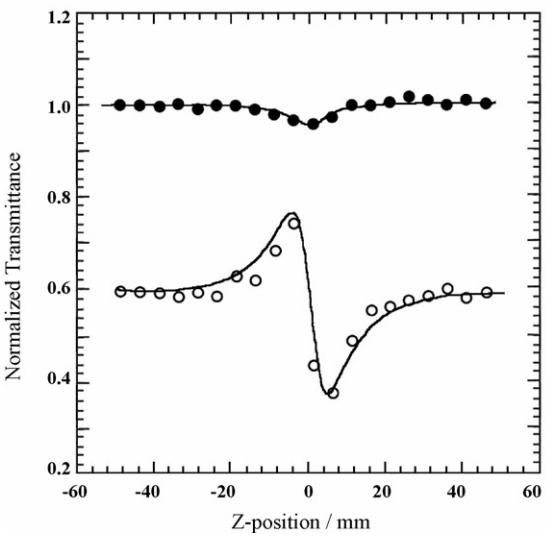

Fig. 15. The normalized Z-scan data of cluster **69** (3.6×10^{-4} mol dm^{-3}) in DMF solution with 532 nm, 7 ns laser pulses. The optical path is 1 mm. The peak incident irradiance of the pulses at focus is 420 MW cm^{-2}. The experimental data were measured without (●) an aperture. The open circles (○) were obtained by dividing the Z-scan data collected with the aperture by those collected without the aperture; they have been vertically displaced by −0.4 for clarity. The solid curves are the theoretical fits based on the Z-scan theory. The minimum beam radius of the focused laser beam was determined to be 30 ± 5 μm. (From [58], with permission of © 2000 Elsevier Science Ltd.).

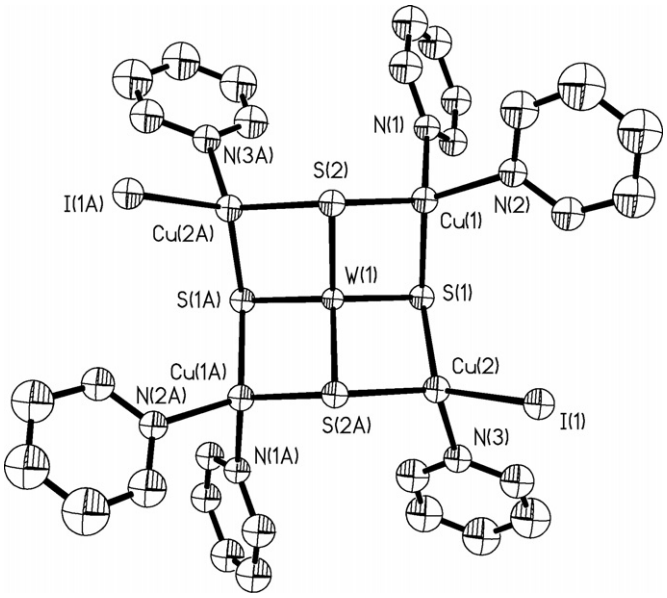

Fig. 16. Molecular configuration of the pentanuclear planar 'open' cluster $[WS_4Cu_4I_2(py)_6]$ **71**. (From [110], with permission of © The Royal Society of Chemistry 2002.).

3.7. Pentanuclear planar 'open' clusters

Pentanuclear planar 'open' clusters have been intensively investigated, both under nanosecond and picosecond laser pulses, for their third-order NLO properties. A series of pentanuclear planar 'open' clusters formulated as $[MS_4Cu_4X_2(py)_6]$ (M = Mo, W; L = I, Br, Cl, SCN) **70–77** [20,21,31,110–117] in Fig. 16, $[Et_4N]_2[MS_4Cu_4(SCN)_4(2\text{-pic})_4]$ (M = Mo, W) **78–79** [118,119], and $[MoS_4Cu_4(2\text{-pic})_5Br_2]\cdot 2(2\text{-pic})_{0.5}$ **80** [120], can be constructed by the newly developed ligand-redistribution synthesis in two steps. This route is the first rational synthesis for such a series of planar 'open' clusters.

The neutral skeleton (in the orthorhombic crystal system, space group *Fdd*2) in clusters **70–77** as the more efficient representatives of this type of compounds, is composed of one M (M = Mo, W), four Cu and four μ_3-S atoms to form a $[MS_4Cu_4]$ aggregate, in which the M atom is located in the symmetrical center of the cluster molecule while both the M and Cu atoms are essentially tetrahedrally coordinated. There are two kinds of environments for these skeletal Cu atoms: one (two mutual *trans* Cu(2) atoms) is linked with two μ_3-S atoms, one L atom and one pyridine ligand to form a distorted tetrahedral $S_2CuL(py)$ unit; the other (two Cu(1) atoms) is coordinated by two μ_3-S atoms and two pyridine ligands building up a distorted tetrahedral $S_2Cu(py)_2$ moiety. A couple of $S_2CuL(py)$ units and $S_2Cu(py)_2$ units ligate through four of the six edges of the tetrahedral $[MS_4]^{2-}$ moiety. The neutral structures of these clusters are of pseudo-D_{2d} symmetry and the five metal atoms are nearly co-planar with deviations of not more than 0.1 Å from the least-squares plane. Thus, the d^0 orbital of the central metal atom M (M = Mo, W) can well overlap with the suitable orbitals of the ligands to form a delocalized electron system, and may further decrease the orbital energy of the molecular system in such kind of planar 'open' clusters.

Due to their M-centered symmetric co-planar structure and the presence of an extensively delocalized π-conjugated electron system, this series of neutral pentanuclear planar 'open' clusters exhibit superior and ultrafast optical limiting responses toward the incident laser pulses in 8 ns width, with limiting thresholds of 0.07–0.10 J cm^{-2} for clusters **70–73** shown in Fig. 17 [20,21,110]. The strong third-order optical non-linear absorption indexes and large optical self-focusing refractive parameters of clusters **70–73** in DMF solution have also been obtained through the Z-scan measurements of an 8-ns pulsed laser at 532 nm, collected in Table 1. The corresponding effective third-order non-linear optical susceptibilities of this series of clusters were found to be the largest among all known heterothiometallic clusters. Particularly for cluster $[WS_4Cu_4I_2(py)_6]$ **71**, it has a γ value (6.9×10^{-30} esu) and the largest $\chi^{(3)}$ value (6.2×10^{-9} esu) toward 8 ns laser pulses in DMF, and possesses the strongest OL effect (with lowest F_{th} value as 0.07 J cm^{-2}) among all these heterothiometallic clusters [20,21,110]. Very interestingly, these planar 'open' clusters additionally exhibit similar very large OL performances to 40 ps laser pulses, and their F_{th} values are obviously lower than that of C_{60} (0.30 J cm^{-2}) even in an ultrafast timescale [21]. Such properties place these clusters among the most promising optical power limiting materials known to date [52,64,121,122].

The di-anionic pentanuclear planar 'open' clusters $[Et_4N]_2[MS_4Cu_4(SCN)_4(2\text{-pic})_4]$ (M = Mo, W) **78–79**, due to their lower symmetry in the cluster skeleton, show higher F_{th} values both to 8 ns and 40 ps pulsed laser, as compared with their neutral counterparts. However, their OL properties are slightly improved under 40 ps (0.26 J cm^{-2} **78**, 0.23 for **79**), as opposed to 8 ns

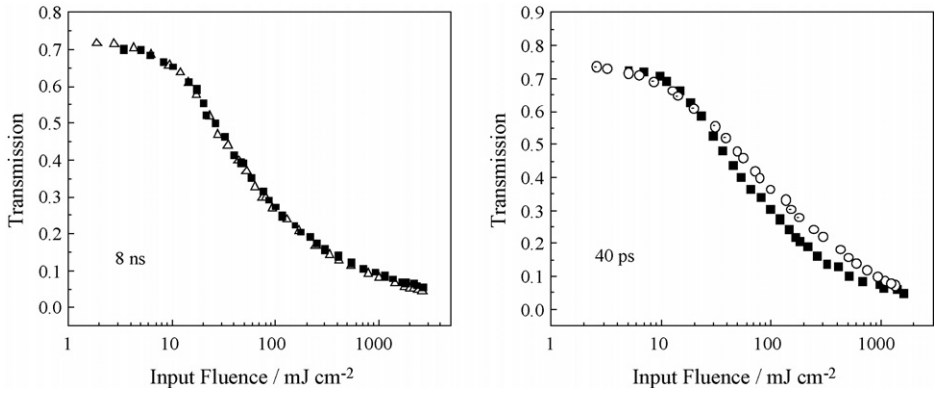

Fig. 17. Energy-dependent transmittance of clusters **70**–**71** to 8 ns/40 ps laser pulses. Optical path: 5 mm; laser wavelength: 532 nm. Left figure: pulse duration: 8 ns. Clusters **70** (■) in 1.39×10^{-4} mol dm^{-3} and **71** (Δ) in 5.5×10^{-4} mol dm^{-3} DMF solution, both with 72% transmittance. Right figure: pulse duration: 40 ps. Clusters **70** (◯) and **71** (■) both in $\sim 10^{-4}$ mol dm^{-3} DMF solution, with 75 and 73% transmittance, respectively. The spot radius of the laser pulse at the focus was measured to be 55 μm for the nanosecond/picosecond laser beam (diameter of $1/e^2$ maximum irradiance). (From [20], with permission of © The Royal Society of Chemistry 2001, and From [21], with permission of © WILEY-VCH Verlag GmbH, D-69469 Weinheim, 2002.).

($0.50\,J\,cm^{-2}$ for **78**, 0.30 for **79**) laser excitation [20,21,118]. Their non-linear optical components were evaluated by applying Z-scan measurements; both anionic planar clusters demonstrate strong non-linear absorption performances (3.2×10^{-9} m W^{-1} for **78**, 3.1×10^{-9} for **79**) and very large self-defocusing behaviors (-8.5×10^{-16} m^2 W^{-1} for **78**, -6.8×10^{-16} for **79**) [118], in sharply contrast to the strong self-focusing effects displayed by their neutral halogen-homologues **70**–**73**. In addition, cluster $[Et_4N]_2[MoS_4Cu_4(SCN)_4(2\text{-pic})_4]$ **78** was found to manifest a pulse-width-dependent self-focusing → self-defocusing transformation: under 40 ps pulses, cluster **78** possesses a self-focusing performance, which can be attributed to population transitions between singlet excited states; while for 10 ns pulses, it exhibits a self-defocusing behavior which is ascribed to the population relaxing to excited triplet states [119].

3.8. Hexagonal-prism-shaped clusters

The core of neutral clusters $[Mo_2S_8Ag_4(PPh_3)_4]$ **81** [32,57] and $[W_2S_8Ag_4(AsPh_3)_4]$ **82** [56] in the triclinic crystal system and space group *P*-1 can be viewed either as a cage that consists of two fused six-membered $[SAg_2S_2M]$ rings, or as a hexagonal prism cage that is composed of two identical butterfly shaped $[MS_4Ag_2(LPh_3)_2]$ segments (M = Mo, L = P; M = W, L = As), as shown in Fig. 18. The two central Mo atoms, as in cluster $[Mo_2S_8Ag_4(PPh_3)_4]$ **81**, are in tetrahedrally coordinated environment, while the four skeletal Ag atoms adopt a quite distorted tetrahedral geometry. The terminal positions around the Ag atoms are occupied by the PPh_3 ligands. Moreover, in both cluster cases, a crystallographic center of symmetry is located in the center of the clusters. The two identical $[MoS_4Ag_2(PPh_3)_2]$ (or $[WS_4Ag_2(AsPPh_3)_2]$) fragments are related to each other through the inversion center.

It is worthwhile noting that the above described hexagonal prism shaped cluster $[Mo_2S_8Ag_4(PPh_3)_4]$ displays very large optical limiting responses to 8-ns laser pulses in both acetone and acetonitrile solutions [32], as illustrated in Fig. 19. The limiting performance of cluster **81** in solution (limiting threshold ca. $0.1\,J\,cm^{-2}$) is one order of magnitude better than that of a C_{60}-toluene solution at a wavelength of 532 nm [64,121]. Particularly, the similar limiting performances of cluster **81** in either acetone or acetonitrile have also been observed with 8-ns laser pulses at 595, 650, and 700 nm, where the linear absorption coefficients of **81** in acetone solution are 5.3×10^3, 3.8×10^3, and 3.3×10^3 L cm^{-1} mol^{-1}, respectively. Within experimental error, there is no significant difference in the optical limiting data at these wavelengths if the same linear transmittances are used. These results along with the broad tail in the visible spectrum of the linear absorption suggest that cluster **81** should be an ideal candidate for broad-band optical limiting,

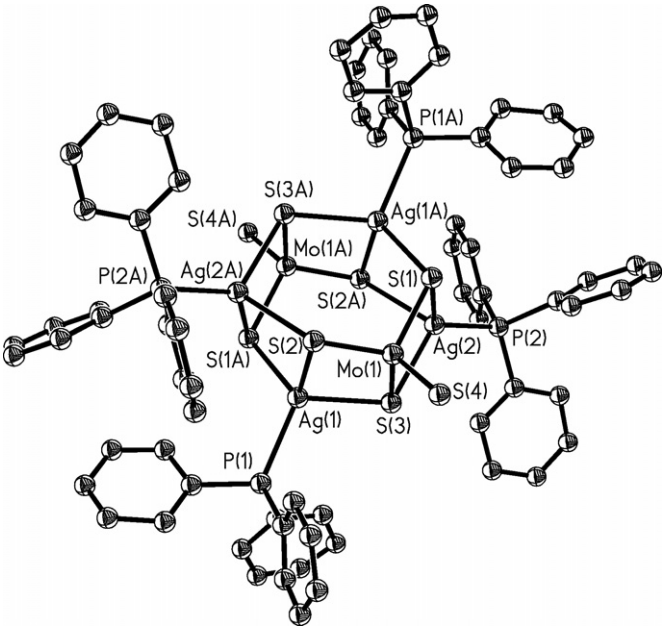

Fig. 18. Molecular configuration of the hexagonal-prism-shaped cluster $[Mo_2S_8Ag_4(PPh_3)_4]$ **81**. (From [32], with permission of © 1995 American Chemical Society.).

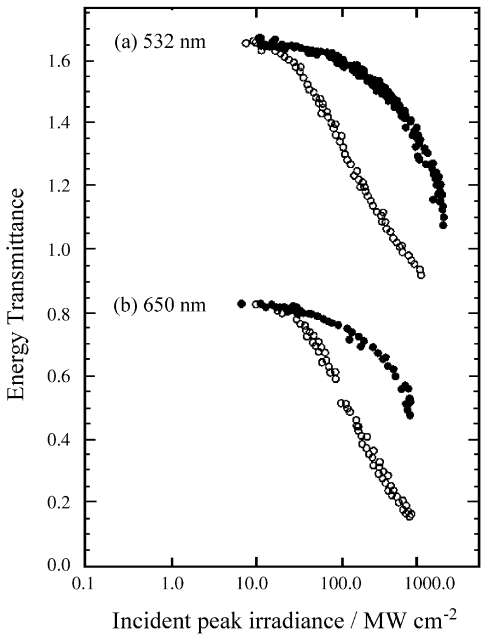

Fig. 19. Energy transmittance versus on-axis peak irradiance at (a) 532 and (b) 650 nm (with 92% internal linear transmittance). The open circles (○) and the filled circles (●) are the data measured with two cluster **81**-acetone solutions and two C_{60}-toluene solutions, in a 1-mm-thick cuvette. The concentrations of cluster **81** are 0.13 and 0.22 mmol dm^{-3} for 532- and 650-nm measurements, respectively. The concentrations of C_{60} are 2.0 and 3.8 mmol dm^{-3} for 532- and 650-nm measurements, respectively. The pulse duration is 8 ns. The upper curves have been displaced vertically by 0.8 for presentation. The spot radius (half width at e^{-2} maximum) of the laser pulses on the sample was determined to be 30 ± 5 μm. (From [32], with permission of © 1995 American Chemical Society.).

and that **81** is more attractive than phthalocyanine derivatives since all of the latter exhibit a strong linear absorption (Q-band) located between 600 and 800 nm [52]. This very fact represents the second important observation in exploring OL effects of heterothiometallic clusters. The non-linear absorption and refraction responsible for the limiting effect are effectively irradiance dependent, different from that observed in C_{60} and phthalocyanine metal-derivatives [32]. With the Z-scan technique, the effective very large third-order absorptive and refractive non-linearities have been determined (α_2 and n_2) to be 1.8×10^{-9} m W^{-1} and 2.2×10^{-16} m^2 W^{-1}, respectively, in addition to its very impressive γ value (2.38×10^{-27} esu). All these non-linear properties should define cluster **81** as a very unique optical limiter in practical application. The isostructural cluster $[W_2S_8Ag_4(AsPh_3)_4]$ **82** was also proved to possess large non-linear absorption ($\alpha_2 = 2.8 \times 10^{-9}$ m W^{-1}) and an effective self-focusing effect ($n_2 = 5.9 \times 10^{-17}$ m^2 W^{-1}) [56]. It may therefore conclude that their symmetrical cluster skeletons should be responsible for the strong broad-band OL effects and large NLO behaviors observed in hexagonal-prism clusters **81** and **82**, while the intrinsic factor of why NLO properties of cluster **81** being somewhat better than those of **82** cannot be well explained at this moment. We tend to suggest that this case may be attributed to the more efficient π-electron donating system in cluster **81** than in **82**.

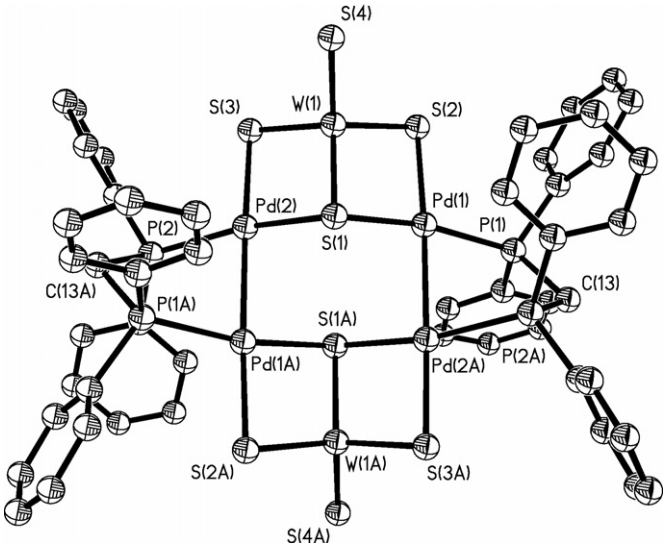

Fig. 20. Molecular configuration of the windmill-shaped cluster $[(WS_4)_2Pd_4(dppm)_2]$ **83**. (From [59], with permission of © The Royal Society of Chemistry 2000.).

3.9. Windmill-shaped cluster

A crystallographic analysis demonstrates that the compound $[(WS_4)_2Pd_4(dppm)_2]$ **83** [59], crystallized in the monoclinic system space group $P2_1/n$ with nearly D_{2h} symmetrical geometry, is a hexnuclear neutral cluster with the $[(WS_4)_2Pd_4]$ core situated on a crystallographic inversion center. Such a centrosymmertric cluster, in Fig. 20, comprises two $[Pd_2(dppm)]^{2+}$ fragments bridged by two $[WS_4]^{2-}$ moieties. Each $[WS_4]^{2-}$ tetrahedron binds two Pd centers across its two S···S edges, and the coordination geometry of the W centers remains essentially tetrahedral. A plane of four Pd atoms is symmetrically disposed around the inversion center and the coordination environment of four Pd atoms is identical. Each Pd atom is asymmetrically surrounded by one μ3-S, one μ-S, one P, and another Pd atom, resulting in a highly distorted square-planar arrangement. Such an arrangement of the palladium atoms seems to be very much dependent on the nature of the auxiliary ligands. The short Pd^I–Pd^I distance of 2.5930 (8) Å in the cluster may indicate strong Pd–Pd interactions, since the Pd–Pd distance in metallic palladium is 2.82 (2) Å. Another structural feature of cluster **83** is an almost co-planar arrangement of eight atoms, S(2), S(3), Pd(1) and Pd(2), and their symmetry equivalents S(2A), S(3A), Pd(1A) and Pd(2A), with a maximum deviation of not more than 0.053 Å from the least squares plane.

Studies on the NLO properties of Mo(W)–S–Pd clusters are much less advanced to date [59,73,74], though their group 11 counterparts have been developed for NLO material precursors for over a decade. In this regard, the optical non-linearity of the windmill-shaped cluster $[(WS_4)_2Pd_4(dppm)_2]$ has also been only preliminarily explored. Measured with 7 ns laser pulses at 532 nm, cluster **83** shows only very weak non-linear absorption ($\alpha_2 = 2.0 \times 10^{-11}$ m W^{-1}), and moderately large effective self-defocusing ability with $n_2 = -2.55 \times 10^{-17}$ m^2 W^{-1} in DMF (displayed in Fig. 21) [59].

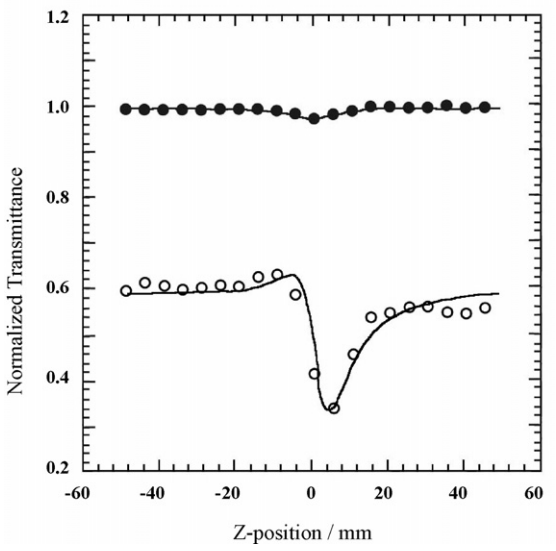

Fig. 21. The normalized Z-scan data of cluster **83** (1.7×10^{-3} mol dm^{-3}) in DMF solution with 532 nm, 7 ns laser pulses. The optical path is 1 mm. The peak incident irradiance of the pulses at the focus is 228 MW cm^{-2}. The minimum beam radius of the focused laser beam was measured to be 30 ± 5 μm. The experimental data were measured without (●) an aperture. The open circles (○) were obtained with the aperture and they have been vertically displaced by −0.4 for clarity. The solid curves are the theoretical fits based on Z-scan theory. (From [59], with permission of © The Royal Society of Chemistry 2000.).

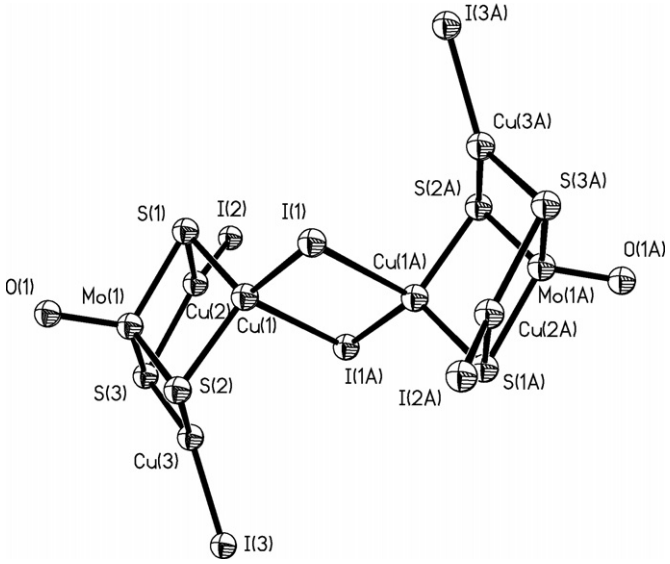

Fig. 22. Molecular configuration of the twin-nest-shaped anion cluster $[Mo_2O_2S_6Cu_6I_6]^{4-}$ **85**. (From [33], with permission of © 1996 American Chemical Society.).

The non-linear refraction behavior is comparable to that of its group 11 counterparts with linear, butterfly and nest skeletons, but larger than other group 10 counterparts, such as linear clusters $[Et_4N][WS_4Pd(S_2CNC_4H_8)]$ **13** ($n_2 = -6.8 \times 10^{-18}$ m^2 W^{-1}), $[Et_4N]_2[W_2S_8Pd]$ **12** ($n_2 = -7.5 \times 10^{-18}$ m^2 W^{-1}) [73] and $[MoS_4Pd(dppp)]$ **14** ($n_2 = -5.5 \times 10^{-18}$ m^2 W^{-1}) [74]. Apparently, the centrosymmetric structure and the co-planar arrangement of the core skeleton together with the strong Pd–Pd interactions in cluster **83** should be responsible for its better NLO properties in comparison with its M/S/Pd counterparts. Nevertheless, such Mo(W)/S/Pd clusters in general show only inferior NLO performance in a way, while the internal mechanism responsible for the weak NLO properties of M–Pd clusters is unclear so far.

3.10. Twin-nest-shaped clusters

The octanuclear anionic clusters $[Et_4N]_4[Mo_2O_2S_6Cu_6Br_2I_4]$ **84** [123], $[Et_4N]_4[Mo_2O_2S_6Cu_6I_6]$ **85** [33] (in Fig. 22) can be described as having a twin-nest-shaped structure. A crystallographic symmetry center is located at the center of the anion cluster; each anionic cluster nucleus can thus be considered to consist of two nest-shaped $[MoOS_3Cu_3L_3]^{2-}$ (L = Br, I) fragments interconnected through a four-membered CuI_2Cu ring. The central metal Mo atoms have basically retained the pseudo-tetrahedral geometry of the free $[MoOS_3]^{2-}$ anion. Notably, a distinct structural character of such type clusters is that the skeletal Cu atoms exhibit two different coordination geometries. The Cu(2) and Cu(3) atoms adopt trigonal-planar geometry (coordinated by two μ_3-S and one L atoms), while Cu(1) atom is in a distorted tetrahedral coordination (linked by two μ_3-S and two μ_2-I atoms). This structural feature is essentially different from their parents' nest-shaped clusters **48** [98] and **49** [55], where trigonal-planar coordination arrangement is adopted by all of the three skeletal Cu atoms. Additionally, relatively weak Mo···Cu (Cu of tetrahedral configuration) interactions are observed in clusters **84**–**85**.

Geometrically, these two anionic clusters can be derived from their parent nest-shaped clusters; the twin-nest-shaped skeleton may be regarded as a dimer of two nido units. The comparability in their cluster skeletons leads to the similar optical non-linearities observed in clusters **84**–**85**, as discovered in nest-shaped clusters by applying classical Z-scan measurements. Both strong non-linear absorption and non-linear refraction were observed in these clusters, with $\alpha_2 = 4.0 \times 10^{-10}$ m W^{-1} and $n_2 = -6.0 \times 10^{-17}$ m^2 W^{-1} for cluster **85** in CH_3CN [33], depicted in Fig. 23. It is obvious that these NLO data are comparable to those parameters found in linear, cubane-like, half-open cubic-cage and nest clusters [27,29,30,71]. Nevertheless, a detailed comparison between the clusters with twin-nest-shaped $[Et_4N]_4[Mo_2O_2S_6Cu_6Br_2I_4]$ **84** [123] and with nest-shaped $[Bu_4N]_2[MoOS_3Cu_3BrCl_2]$ **48** [98] skeletons reveals that, constructed by the similar anionic cluster nucleus as $[MoOS_3Cu_3BrL_2]^{2-}$ (L = Cl in **48**, I in **84**), cluster **84** (with a centrosymmetric structure) exhibits a OL effect ($F_{th} = 2.0$ J cm^{-2}, with a saturation fluence transmitted of 8.5 J cm^{-2}) superior to that of cluster **48** (with an acentric skeleton) ($F_{th} = 10.0$ J cm^{-2}), though such a OL behavior is inferior by comparison, to some extent, with those of cubane-like, hexagonal prism, and planar 'open' clusters [19,20,32]. This fact may further indicate that increasing structural symmetry may result in the enhancement of OL performance of these bimetallic clusters, even if these clusters are constructed by the same building block.

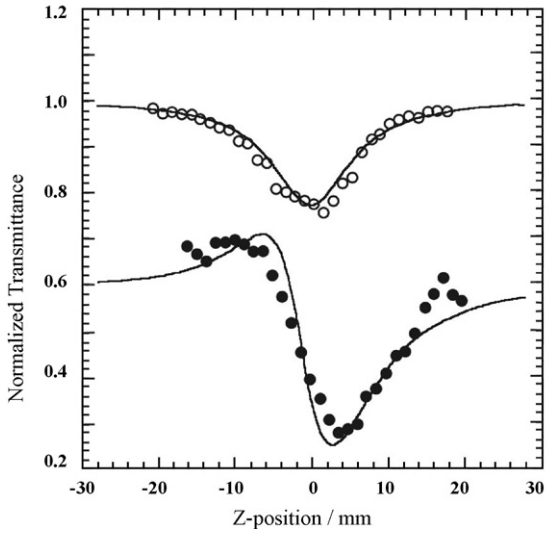

Fig. 23. Z-scan data of cluster **85**. Key: open circles (○), observed under an open-aperture configuration; filled circles (●), Z-scan data observed under a closed-aperture configuration divided by those obtained under the open-aperture configuration to filter out the influence of nonlinear absorption; upper and lower solid curves, generated by applying the Z-scan theory. Conditions: incident energy, 32 μJ; cluster concentration, 2×10^{-3} mol dm^{-3}. The radius of the beam waist was measured to be 30 ± 5 μm (half width at $1/e^2$ maximum). (From [33], with permission of © 1996 American Chemical Society.).

3.11. Dodecanuclear square-like cluster

Exemplified by $[Et_4N]_4[Mo_4O_4S_{12}Cu_8\{(Ph_2PS)_2N\}_4]$ **86** [60] (in Fig. 24), the cluster nucleus is constructed by four corner Mo atoms and four edge Cu atoms in an approximately square array (one $[Mo_4O_4S_{12}Cu_4]^{4-}$ unit), together with four capping $[CuN(Ph_2PS)_2]$ groups each attached to one $[MoOS_3]^{2-}$ moiety. The cluster anion in the crystal is located at the −4 site with four Mo atoms at the corners of a distorted square of edge length 5.48 Å (Mo···Mo). The cluster core has approximate C_{2v} symmetry, with two mirror planes intersecting at the −4 axis and individually involving the two diagonal directions of the square framework. Four diagonally related groups $[CuN(Ph_2PS)_2]$ are alternately located above and below the square framework plane as the moieties change their orientations in the $[MoOS_3]$ framework. Such an unusual coordination geometry of cluster **86** gives rise to the highly distorted tetrahedral coordination of both four edge Cu and four capping Cu atoms, while four corner moieties $[MoOS_3]^{2-}$ retain their orginal tetrahedral configuration. The short Mo···Cu distances indicate significant cluster interactions between these heteronuclear metal atoms. Another way to view the cluster core is in terms of the nest-shaped building block $[MoOS_3Cu_3]^{+}$. Four fused "nests" in alternate orientations are co-polymerized by sharing four limbic Cu atoms to form the greater oligomeric motif.

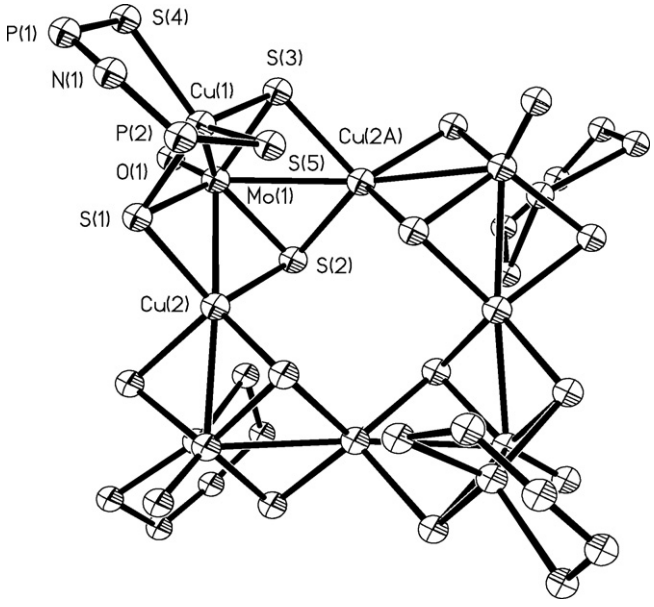

Fig. 24. Molecular configuration of the dodecanuclear square-like anion cluster $[Mo_4O_4S_{12}Cu_8\{(Ph_2PS)_2N\}_4]^{4-}$ **86**. (From [60], with permission of © The Royal Society of Chemistry and the Centre National de la Recherche Scientifique 2001.).

With an 8 ns pulsed laser at 532 nm, this dodecanuclear square-like cluster, comprising four fused nests, responses to the incident light only by a weak optical absorption ability (with open-aperature) and a self-defocusing effect (in closed-aperature) (with an absorption coefficient $\alpha_2 = 1.2 \times 10^{-11}$ m W^{-1} and a refraction index $n_2 = -2.04 \times 10^{-18}$ m^2 W^{-1} in DMF) [60] as illustrated in Fig. 25. Although

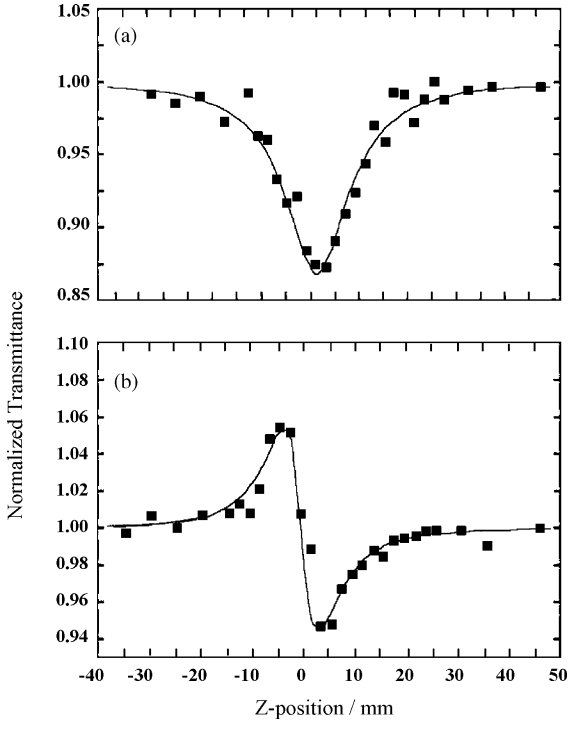

Fig. 25. Z-scan measurement of cluster **86** as a 1.2×10^{-4} mol dm^{-3} DMF solution in a 5 mm quartz cuvette, with an 8 ns laser pulse at 532 nm. The spot radius of the laser beam was measured to be 55 μm. (a) The data were collected with an open-aperture configuration. (b) The data were obtained by dividing the normalized Z-scan measured with a closed-aperture configuration by the normalized Z-scan data in (a). The solid lines present the theoretical fits by employing Z-scan theory. (From [60], with permission of © The Royal Society of Chemistry and the Centre National de la Recherche Scientifique 2001.).

these NLO data found in cluster **86** are obviously inferior to those of most of the reported heterothiometallic clusters, they are comparable with many of the best known third-order NLO materials in neat solid form, such as SiO_2 (2.0×10^{-20} m^2 W^{-1}), CdS (2.5×10^{-18} m^2 W^{-1}), $SrLaGa_3O_7$ (11.1×10^{-20} m^2 W^{-1}) and $Ca_2Ga_2SiO_7$ (6.5×10^{-20} m^2 W^{-1}) [124,125]. However, more detailed NLO experimental investigations and theoretical analysis on this four-fuse-nest cluster are currently expected for uncovering the reason why such cluster **86** with multinuclear core (4 Mo and 8 Cu atoms) shows only inferior optical non-linearity.

3.12. Supra-cage-shaped cluster

$[Bu_4N]_4[Mo_8O_8S_{24}Cu_{12}]$ **87** [34,126], in Fig. 26, is the largest discrete Mo(W)–S–Cu(Ag) heterothiometallic cluster reported so far. The cluster anion has a very high degree of symmetry with six mirror planes, four three-fold and three two-fold rotation axes, combining to molecular T_d symmetry. Its structure can formally be described as a supra-cage containing a pseudo-cubane type $[Mo_8Cu_{12}]$ core, in which the metal atoms are connected through bridging S atoms. The short Mo···Cu distances show significant interactions between heteronuclear metallic atoms. Within the core of the supra-cage, each edge of the $[Mo_8Cu_{12}]$ cubane consisting of a Cu atom and two nearest neighboring Mo atoms is nearly linear and the angles about the Cu–Mo–Cu moieties vary around 90°. The local coordination sphere around each Mo atom approaches a tetrahedron, while all Cu atoms adopt a distorted tetrahedral geometry.

The very high symmetry of its skeleton results in strong optical non-linearity of supra-cage cluster **87**, which has been manifested by Z-scan experiments [34,126]. Under the configuration without and with aperture, the supra-cage cluster demonstrates very large effective non-linear absorption ability (illustrated in Fig. 27) with α_2 equal to 2.3×10^{-9} m W^{-1}, and effective self-defocusing behavior with $n_2 = -3.5 \times 10^{-16}$ m^2 W^{-1}. Furthermore, to the best of the authors' knowledge [34], $|\gamma| = (5.7 \pm 0.8) \times 10^{-28}$ esu for cluster **87**, generated from degenerate four-wave mixing (DFWM) measurements, is the largest $|\gamma|$ value reported at the time for discrete NLO chromospheres. This value is significantly larger than those reported for C_{60} (between 4.0×10^{-31} and 1.6×10^{-29} esu) and chloroaluminum phthalocyanine (ClAlPc) (4.5×10^{-31} esu) [50,127–129]. Accordingly, the third-order susceptibility $\chi^{(3)}$ value of cluster **87** was calculated to be as high as 8.2×10^{-10} esu, which is amongst the largest cubic NLO parameters investigated for these heterothiometallic clusters up to now. In addition, its OL effect occurs at incident fluences as low as 0.7 J cm^{-2} when exposed to the 7 ns 532 nm laser pulses [34,126].

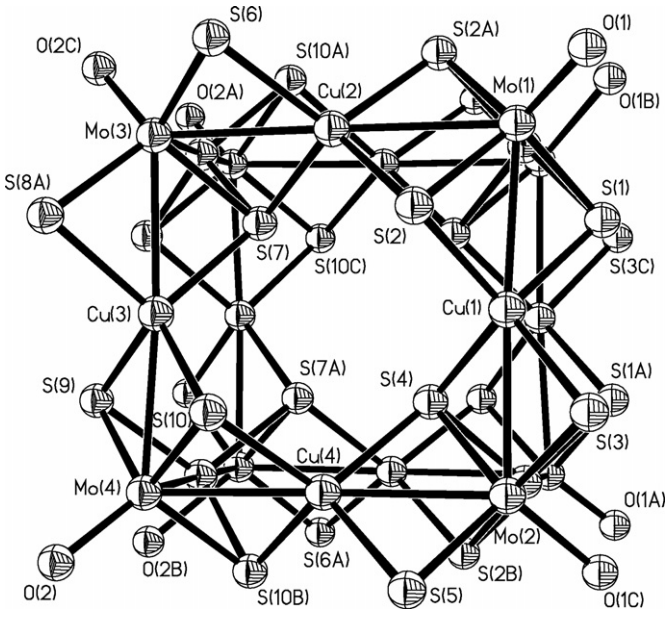

Fig. 26. Molecular configuration of the supra-cage anion cluster $[Mo_8O_8S_{24}Cu_{12}]^{4-}$ **87**. (From [34], with permission of © 1995 American Chemical Society.).

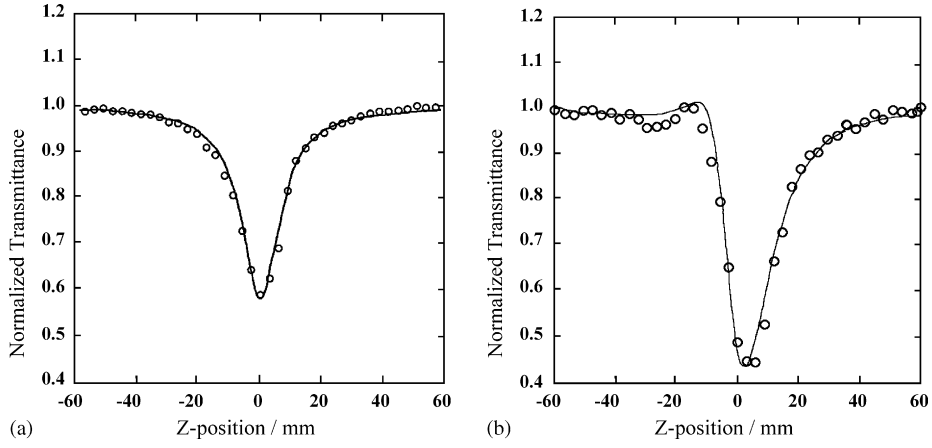

Fig. 27. Z-scan experiments of cluster **87**. The open circles are the experimental results, and the solid curves are theoretical fits by using the Z-scan theory. Experiments performed: (a) under an open-aperture configuration and (b) under a closed-aperture configuration (with an aperture of 1.8 mm diameter). The cluster concentration for this experiment is 7.99×10^{-4} mol dm^{-3} CH_3CN solution. The pulse width is 7 ns and pulse duration is 532 nm. The incident laser beam was focused with a minimum spot radius of 40 ± 5 μm. The optical length is 1 mm. (From [34], with permission of © 1995 American Chemical Society.).

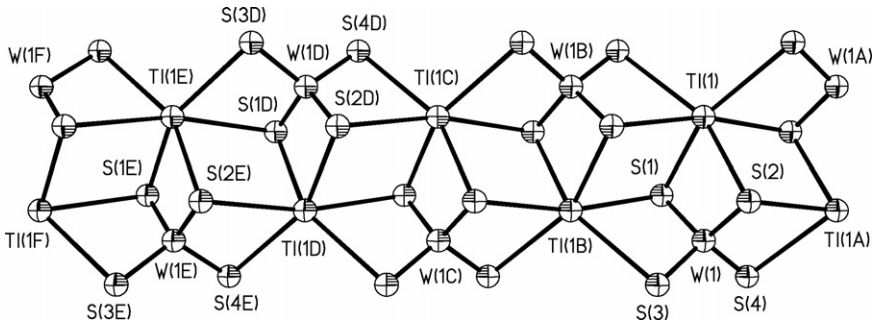

Fig. 28. Molecular configuration of the one-dimensional chain anion cluster polymer $[WS_4Tl]^-$ **89**. (From [35], with permission of © 1996 American Chemical Society.).

3.13. Polymeric clusters

3.13.1. One-dimensional cluster polymers

Considerable research interest in this area is currently attracted by the polymeric clusters. $[Bu_4N][MS_4Tl]$ (M = Mo, W) **88–89** [35], $[\{MoOS_3Cu_3(CN)(py)_3\}\cdot 0.5C_6H_6]_n$ **90** [130], $[W_2O_2S_6Cu_4(CH_3CN)_4]_n$ **91** [131], $[(Bu_4N)(W_2S_8Ag_3)]_n$ **92** [132], $[\{MoS_4Cu_4(2\text{-pic})_3Br\}(\mu\text{-Br})\cdot(2\text{-pic})]_n$ **93** [120] are such examples that belong to the class of 1-D cluster polymers.

The first reported one-dimensional polymeric chain clusters for NLO performance, to be formulated as $[MS_4Tl]_n^{n-}$ (M = Mo **88**, W **89**) [35] in the monoclinic space group *Cc*, are composed of $[MS_4]^{2-}$ tetrahedrons connected by Tl atoms as illustrated in Fig. 28. The repeating unit within the cluster chain is $[MS_4Tl]$, where M, S(1), S(2) and Tl are nearly coplanar, as are M, S(3), S(4) and Tl. This unit is stacked along the crystallographic *c*-axis with the M → Tl vectors pointing alternatively right and left. Looking down the *c*-axis, one may view the chain as a three-layered tape in which the Tl–M layer is sandwiched by two sulfur layers consisting of S(2)–S(3) and S(1)–S(4). There are four crystallographically independent sulfur atoms, which can be grouped into two classes: triply-bridging sulfurs, S(1) and S(2), and doubly-bridging sulfurs, S(3) and S(4).

The cluster polymer $[\{MoOS_3Cu_3(CN)(py)_3\}\cdot 0.5C_6H_6]_n$ **90** consists of neutral nest-shaped structural units $[MoOS_3Cu_3(\mu_2\text{-}CN)(py)_3]$, and every such structural unit forms two Cu(1)–C–N–Cu(3) bridges with two identical units leading to an infinite one-dimensional skeletal chain [130]. In every unit cell of **90**, the four structural units from four independent linear polymeric molecules are parallel to each other. Another 1-D polymeric cluster showing novel zigzag chains is $[W_2O_2S_6Cu_4(CH_3CN)_4]_n$ **91**. The molecular configuration of this polymer can be viewed as a helical chain which is propagated along the crystallographic *c*-axis. With the chain turning at each W atom, the main core of the cluster contains a nest-shaped $[W_2S_6Cu_4]$ fragment [131]. The polymeric anions of $[(Bu_4N)(W_2S_8Ag_3)]_n$ **92** feature a hanging ladder-like polymeric chain [132], which can also be described as double helical chains bridged by silver atoms. Such hanging ladder chains or double helical chains constructed by the edge-sharing distorted square units are propagating along the [010] direction. Interconnecting via μ_2-Br bridges, the repeat unit $[MoS_4Cu_4(2\text{-pic})_3Br_2]$ extends into an infinite zigzag chain along *b*-axis to construct 1-D cluster $[\{MoS_4Cu_4(2\text{-pic})_3Br\}\cdot(\mu_2\text{-Br})\cdot(2\text{-pic})]_n$ **93**. Within the asymmetric structural unit, four Cu atoms have two different coordination geometries: two Cu displaying a trigonal planar mode, while two other Cu atoms on the infinite chain adopting a distorted tetrahedral configuration [120].

The Z-scan data of the 1-D cluster polymer **89** are given in Fig. 29, which clearly shows the presence of both large non-linear optical absorption and strong non-linear optical refraction [35], probably due to its tightly constructed 1-D rigid chain skeleton. The non-linear absorptive coefficients α_2 were theoretically calculated to be 1.8×10^{-7} m W^{-1} for **89**, 2.2×10^{-7} m W^{-1} for **88** in open-aperture Z-scan. The non-linear refractive index assessed by closed-aperture configuration both gave the positive sign ($n_2 = 3.2 \times 10^{-14}$ m^2 W^{-1} **89**, 3.1×10^{-14} m^2 W^{-1} **88**), which leads to a self-focusing behavior of the light propagation in the cluster solution. The NLO

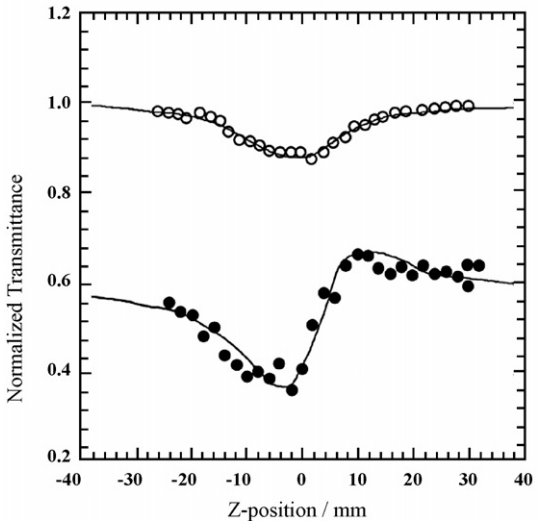

Fig. 29. The Z-scan data of cluster **89** as a 4.9×10^{-4} mol dm^{-3} CH_3CN solution in a 1-mm thick quartz cell at 532 nm 7 ns laser pulses with $I_0 = 3.48 \times 10^{-9}$ W m^{-2}. The incident beam was focused into a spot radius (ω_0) of 35 μm (half-width at $1/e^2$ maximum) by a 25 cm focal-length mirror. The data shown by open circles (○) are those collected under an open-aperture configuration, and the upper solid curve is a theoretical fit based on Z-scan theory. The data shown by filled circles (●) were obtained by dividing the normalized Z-scan data measured under closed-aperture configuration by the normalized Z-scan data under the open-aperture configuration. (From [35], with permission of © 1996 American Chemical Society.).

measurement for 1-D cyanide-bridged polymeric cluster **90** only shows weak non-linear absorption ($\alpha_2 = 5.0 \times 10^{-11}$ m W^{-1}) and modest self-defocusing refraction behavior with n_2 value as -8.0×10^{-18} m^2 W^{-1} [130]. No strong NLO property can be detected in its analogous polymeric cluster $[WOS_3Cu_3(CN)(py)_4]_n$, which holds the similar neutral nest-shaped structure unit to **90**. These facts might be attributed to the inferior skeletal rigidity of their nest-shaped 1-D chain configuations. As for the 1-D zigzag cluster polymer **91**, 40 ps pulse-width Z-scan measurements indicate that, with the non-linear absorption of about 90% at the focus, this cluster polymer possesses strong excited state absorption and a large optical limiting response, in addition to displaying an optical self-focusing performance ascribed to population transitions between singlet states [131]. In contrast, the hanging ladder-like polymeric cluster **92** exhibits only a moderate non-linear optical absorption response and a weak optical self-focusing effect (effective $\alpha_2 = 1.11 \times 10^{-10}$ m W^{-1}, $n_2 = 3.67 \times 10^{-18}$ m^2 W^{-1}) when measured with a 1.2×10^{-4} mol dm^{-3} DMF suspension [132]. Moreover, the optical limiting experimental data, measured with a linear transmittance of 94%, demonstrate that cluster polymer **92** possesses a promising OL performance. Determined by DFWM under 35 ps width laser pulses at 532 nm, cluster polymer **93** only behaves a very weak NLO performance, with $\chi^{(3)}$ and γ derived from theoretical calculations as 2.01×10^{-13} and 1.01×10^{-31} esu [120].

3.13.2. Two-dimensional cluster polymers

Clusters $[(Et_4N)\{Mo_2O_2S_6Cu_6I_3(4,4'\text{-bpy})_5\}\cdot MeOH\cdot H_2O]_n$ (4,4′-bpy = 4,4′-bipyridine) **95** [36], $[MoS_4Cu_6I_4(py)_4]_n$ **94** [61], and $[(Me_4N)_2\{MOS_3Cu_3(\mu_2\text{-}I)_3\}]_n$ (M = Mo **96**, W **97**) [133] belong to the skeletal type of 2-D cluster polymers.

A X-ray diffraction study on $[\{Mo_2O_2S_6Cu_6I_3(4,4'\text{-bpy})_5\}^-]_n$ **95** (crystallizing in the triclinic system with space group $P\bar{1}$) reveals that the structure of the cluster polymer consists of an infinite 2-D anionic coordination open-network with distorted hexagonal chair cavities [36]. As shown in Fig. 30, the configuration of the polymeric anions can be viewed as two zigzag chains propagated by cell translations along the *a*- and *b*-axes. The edges of one chain formed by $[Cu_2(\mu_2\text{-}S)(\mu_2\text{-}4,4'\text{-bpy})]_2$ double bridges and a $[Cu_2(\mu_2\text{-}4,4'\text{-bpy})]$ single bridge are alternately perpendicular to each other by the turning points of 4,4′-bpy shared Cu atoms, while another chain is extended via [Cu(μ2-S)Cu] moieties. These two zigzag chains share the same $[Cu_2(\mu_2\text{-}S)(\mu_2\text{-}4,4'\text{-bpy})]_2$ double bridges, the intersections of which are nest-shaped $[MoOS_3Cu_3]$ cluster cores.

The polymer $[MoS_4Cu_6I_4(py)_4]_n$ **94** may be regarded as an extended octahedron network, and in each basic structural unit, $[MoS_4]$ is enveloped by six copper atoms [61]. There are two types of copper atoms in the Cu_6 distorted octahedron: four equatorial Cu(1) atoms adopting a distorted tetrahedral coordination; two axial Cu(2) atoms exhibiting a triangular planar geometry. Each $[MoS_4Cu_6I_4(py)_4]$ unit forms four Cu–μ2-I–Cu bridges with four $[MoS_4Cu_6I_4(py)_4]$ units leading to the two-dimensional network structure. Two isomorphous polymers $[(Me_4N)_2\{MOS_3Cu_3(\mu_2\text{-}I)_3\}]_n$ (M = Mo **96**, W **97**) are formed from nest-shaped units $[MOS_3Cu_3]$ along the crystallographic

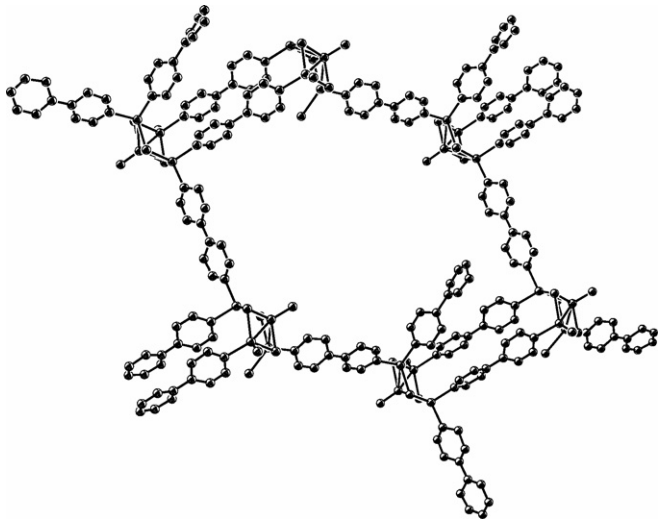

Fig. 30. Molecular configuration of the two-dimensional open network anion cluster polymer $[\{Mo_2O_2S_6Cu_6I_3(4,4'\text{-bpy})_5\}^-]_n$ **95**. (From [36], with permission of © The Royal Society of Chemistry 2001.).

b and *c* directions [133]. All these nest units aggregate into a two-dimensional network structure by μ2-I bridges. Along the crystallographic *c* direction, the two neighboring nests exist in a *trans*-position, which is extremely similar to that of the twin-nest-shaped cluster $[Et_4N]_4[Mo_2O_2S_6I_6Cu_6]$ **85** [33].

The presence of a 2-D open anionic network and the low symmetry of the skeletal configuration in cluster polymer **95** may have an important influence on its optical non-linearity. The α_2 and n_2 values extracted from 7 ns Z-scan experimental data are 3.12×10^{-9} m W^{-1} and -5.04×10^{-16} m^2 W^{-1}, respectively [36]. Both non-linear absorptive and refractive performances of **95** are obviously superior to those of its parent clusters with a nest-shaped $[MoOS_3Cu_3BrCl_2]^{2-}$ **48** [98] or a twin-nest-shaped $[Mo_2O_2S_6Cu_6I_6]^{4-}$ **85** [33] skeleton. Under the irradiation of 0.5 and 10 Hz repetition-rate laser pulses, the optical limiting results of polymeric cluster **95**, as in Fig. 31, were measured to be as low as 0.4 and 0.7 J cm^{-2}, respectively. These limiting threshold values are much lower than those received for **48** and **85** (10.0 and 2.0 J cm^{-2}), indicating that the OL performance of 2-D nest cluster polymer **95** is efficiently improved as compared with that of the nest cluster monomer **48** and dimer **85** [36]. Nevertheless, the inherent mechanism of the strong optical non-linearity for the 2-D open network cluster **95** with asymmetrical configuration remains obscure at this moment, and is waiting for further exploration.

The 2-D network polymer $[MoS_4Cu_6I_4(py)_4]_n$ **94** is the first example of a polymeric cluster showing a very large optical limiting effect [61]. Its optical limiting threshold was determined to be 0.6 J cm^{-2}, which is about three times better than that of C_{60} and this fact can be attributed to its rigid tight-capped octahedral cluster skeleton. Z-scan experiments in 6.5×10^{-5} mol dm^{-3} DMSO solution demonstrate that the extended octahedron network possesses strong non-linear absorption with index $\alpha_2 = 1.5 \times 10^{-9}$ m W^{-1} and very large non-linear self-defocusing behavior (the refractive value $n_2 = -2.5 \times 10^{-17}$ m^2 W^{-1}). It is also doc-

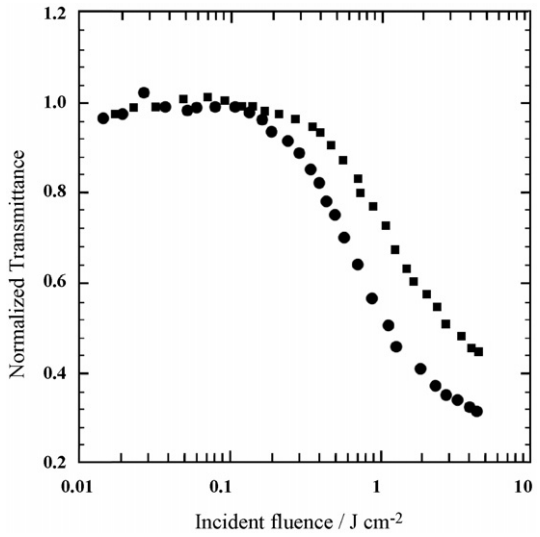

Fig. 31. Optical limiting response of cluster **95** in a 1.2×10^{-4} mol dm^{-3} DMF solution obtained for 7 ns, 532 nm laser pulses with various pulse intervals: 0.5 Hz (●) and 10 Hz (■). The solution was loaded in a 1 mm cell with a linear transmittance of 72%. (From [36], with permission of © The Royal Society of Chemistry 2001.).

umented that the isomorphous polymeric 2-D clusters $[(Me_4N)_2\{MOS_3Cu_3(\mu_2\text{-}I)_3\}]_n$ **96–97**, despite of the similarity in their polymeric structures, exhibit different non-linear refractive behaviors: **96** gives a strong self-defocusing response (-5.02×10^{-17} m^2 W^{-1}), while **97** shows a very large self-focusing effect (1.20×10^{-16} m^2 W^{-1}) [133]. Accordingly, the calculated corresponding hyperpolarizabilities γ are as large as 3.39×10^{-28} esu **96** and 1.02×10^{-26} esu **97**, ascribed to their very strong refraction non-linearities. In comparison, the above optical non-linearities observed in these isomorphous 2-D network polymers **96–97** are obviously much stronger than those of their parents clusters, in either nest-shaped skeleton **48** [98] or twin-nest-shaped skeleton **85** [33].

3.13.3. Three-dimensional cluster polymers

The 3-D open-framework polymeric anions $[(Et_4N)_2\{MS_4Cu_4(CN)_4\}]_n$ (M = Mo **98**, W **99**) [37] (Fig. 32, orthorhombic, space group *Fddd*), are built from MS_4Cu_4 units bridged by cyanide ligands. Within the MCu_4 core, each M atom is located in the center of an essentially tetrahedral $[MS_4]$ unit, while five metal atoms are perfectly coplanar with a Cu–M–Cu angle concerning the two *trans* positioned Cu atoms of 180°. This leads to an ideal crystallographic D_{2d} symmetry for the $[MS_4Cu_4]$ aggregate. Two *cis* Cu atoms, Cu(1) and Cu(2), have a distorted tetrahedral geometry with their tetrahedral apices occupied by two triply bridging S atoms and two cyanide bridging C or N atoms. These tetrahedra are mutually linked by bridged cyanide ligands, thus constructing a three-dimensional open framework of basic formula $[MS_4Cu_4(CN)_4]^{2-}$, displaying no layering but particular directionality. An alternative way to view this framework is in terms of the diamond structure, where C has alternately been replaced by $[MS_4Cu_4]$ aggregates and the C–C bonds by two parallel cyanide-bridging ligands. However, unlike the diamond lattice, microporosity is created

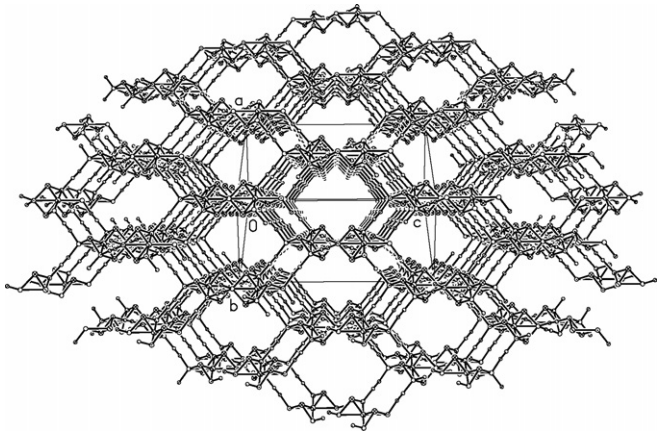

Fig. 32. Molecular configuration of the three-dimensional open framework anion cluster polymers $[\{MS_4Cu_4(CN)_4\}^{2-}]_n$ **98–99**. (From [37], with permission of © The Royal Society of Chemistry 2000.).

as a consequence of the larger size of the inorganic clusters compared to carbon atoms, which gives rise to the high rigidity in the structure of 3-D polymeric clusters **98–99** [37].

Another unprecedented 3-D polymeric cluster reported recently is $[\{WS_4Cu_4(4,4'\text{-bpy})_4\}\{WS_4Cu_4I_4(4,4'\text{-bpy})_2\cdot 4H_2O\}]_n$**100** [62] (in the tetragonal system, space group *I*4(1)/*acd*), containing intricate fourfold interpenetrating cationic and anionic 3-D diamondoid cluster coordination polymers. There is a twofold interpenetrating 3-D network in the cationic coordination polymer comprising square pentanuclear $[WS_4Cu_4]^{2+}$ building blocks, each linked by four pairs of parallel 4,4′-bpy bridges. The 3-D anionic cluster coordination polymer is almost exactly analogous to its cationic cluster counterpart, except that the building block is the $[WS_4Cu_4I_4]^{2-}$ ion, which is nearly tetrahedrally coordinated by four N atoms of four 4,4′-bpy ligands.

Attributed to a 3-D open framework with the high rigidity in their diamond-like structures, these polymeric clusters **98–100** must exhibit large optical non-linearities and very strong OL effects. Z-scan experiments confirmed the expectations of **98–100** having large non-linear absorptive performances and optical self-focusing responses. Both their absorption coefficients α_2 (1.5×10^{-9} m W^{-1} **98**, 1.6×10^{-9} m W^{-1} **99**, and 1.6×10^{-10} m W^{-1} **100**) and refraction indexes n_2 (1.84×10^{-16} m^2 W^{-1} **98**, 1.22×10^{-16} m^2 W^{-1} **99**, and 1.8×10^{-17} m^2 W^{-1} **100**) [37,62] are comparable to those of $[Mo_2S_8Ag_4(PPh_3)_4]$ **81** [32] and $[W_2S_8Ag_4(AsPh_3)_4]$ **82** [56], which have very large NLO values. In addition, these NLO merits of polymers **98–99** are superior to those of other discrete inorganic clusters but less than those of 1-D chain cluster polymers **88–89** [35].

From the perspective of their OL properties, as depicted in Fig. 33, polymers **98–99** respond linearly to the incident irradiation at very low fluence, obeying Beer's law. The light transmittance starts to deviate from Beer's law when the input light fluence rises to certain values with respect to each cluster, and the solution becomes increasingly less transparent. Their OL threshold values determined as 0.28 J cm^{-2} **98** and 0.15 J cm^{-2} **99**, with a linear transmission of 70% [37], are obviously better

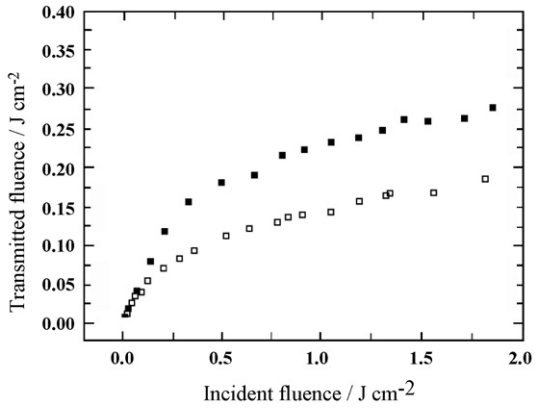

Fig. 33. Optical limiting effects of clusters **98** (3.64×10^{-5} mol dm^{-3} in DMF) (■) and **99** (2.93×10^{-5} mol dm^{-3} in DMF) (□). The cluster sample solutions were placed in a 5 mm quartz cuvette for OL measurements which were performed with linearly polarized 8 ns pulses at 532 nm. The spot radius of the laser beam was measured to be 55 μm (half-width at $1/e^2$ maximum). (From [37], with permission of © The Royal Society of Chemistry 2000.).

than those of the discrete cubane-like clusters [19,26], and 1-D [35] and 2-D [36,61] polymeric clusters.

4. Discussions and remarks

4.1. Electronic transitions

There is a general consensus that three absorptions (ν_1, ν_2, ν_3) are attributable to ligand-to-metal charge transfer transitions within the $[MoXS_3]^{2-}$ units. The intrinsic electronic spectra of heteothiometallic clusters are characterized by two absorption regions: (1) $\lambda_1 = 400$–500 nm; (2) $\lambda_2 = 200$–400 nm [12,97].

The S → Mo charge transfer transition in the region of 400–500 nm for the absorption band ν_1 is corresponding to the "$1t_1 \rightarrow 2e$" transition of the $[MoXS_3]^{2-}$ moiety in the clusters [12,18,97], i.e. from the highest occupied molecular orbital (HOMO) to the lowest unoccupied molecular orbital (LUMO). In comparison to the S → Mo charge transfer occurring at a shorter wavelength in the parent $[MoXS_3]^{2-}$ moiety, the red shift of the S → Mo transition in the clusters with respect to the $[MoXS_3]^{2-}$ can be attributed to the coordination of the M′L groups to the $[MoXS_3]^{2-}$ unit, which reduces significantly the antibonding character of the LUMOs (corresponding to the "2e" orbitals of the parent $[MoXS_3]^{2-}$). The LUMOs of the clusters are mainly Mo d orbitals that possess Mo–S antibonding and S–M′L bonding character. The HOMOs of the clusters are mainly p orbitals of S in the $[MoXS_3]^{2-}$ unit, which mix with the d and p orbitals from the M′L units in the clusters [12,18,97,134,135].

The intense absorption peaks in the region of 200–400 nm are attributable to sulfur-based transitions [12,97]. Similar features were observed with simple salts of $[MoXS_3]^{2-}$ and $[WXS_3]^{2-}$ [12,136], where S → S* ("$t_1 \rightarrow 4t_2$" and "$3t_2 \rightarrow 2e$", in relation to ν_2 and ν_3 bands, respectively) transitions were reported to occur at 316 and 241 nm in $[R_4N]_2[MoS_4]$, 277 and 216 nm in $[R_4N]_2[WS_4]$, 395 and 308 nm in $[R_4N]_2[MoOS_3]$, and 336 and 240 nm in $[R_4N]_2[WOS_3]$ [12,18,97,136]. In the Mo(W)–S–Cu(Ag) clusters, the electronic absorption of the $[MXS_3]$ (M = Mo, W) units still has the characteristics of their parent complexes ($[MoXS_3]^{2-}$ and $[WXS_3]^{2-}$). The "$3t_2 \rightarrow 2e$" transition carries certain ligand-to-metal charge transfer character. The "t_1" molecular orbitals are derived exclusively from the p orbitals of the sulfur atoms. The "$3t_2$" orbitals are the M–S bonding orbitals that are mainly sulfur p orbitals in character [97]. The "$4t_2$" and "2e" orbitals are mainly derived from metal d orbitals with M–S antibonding character.

The S → M charge transfer transition peaks are obviously blue shifted when Mo is replaced by W in the M–S–M′ clusters [12,136]. Coordination of $[WXS_3]^{2-}$ moieties to the M′L units will lead to a shift of ν_1 bands in the direction of longer wavelengths in W–S–Cu clusters. As compared with those in the Cu-homologues, the position of ν_1 bands can be observed in the region of shorter wavelengths in Mo(W)–S–Ag clusters. The higher the nuclearity, the longer is the wavelength of the ν_1 band.

4.2. Influence of skeletal atoms

An evident compositional (skeletal metal) effect on both linear and non-linear optical properties was observed when M–S–Ag (M = Mo, W) and M–S–Cu clusters were compared, such as in cubane-like clusters from $[WS_4Cu_3Br_4]^{3-}$ **24** to $[WS_4Ag_3Br_4]^{3-}$ **25** (in Scheme 1) [26]. A blue shift of the optical absorption band ν_1 was detected when the Ag-containing cubic cluster was measured instead of its Cu homologue, along with the OL threshold values reducing from 1.1 to 0.6 J cm^{-2}. This is understandable because the d orbitals of the M′ atoms (M′ = Cu, Ag) have significant contributions to the HOMOs [12,97,134,135].

On the other hand, both linear and non-linear optical performances of the clusters are also considerably influenced by the central metal atoms. By comparing the pentanuclear planar 'open' clusters $[MoS_4Cu_4I_2(py)_6]$ **70** and $[WS_4Cu_4I_2(py)_6]$ **71** (in Scheme 2) [110], an obvious effect of the central heavy metal atoms on their linear and non-linear optical performances was found similar to that found in the comparison of M–S–Cu with M–S–Ag clusters. As discussed above, the LUMOs of the clusters are primarily M (M = Mo, W) d orbitals that possess M–S antibonding and S–M′L bonding characters [12,97,134,135]. A blue shift of the optical absorption band ν_1 (corresponding to a S → M transition) was observed by replacing the central skeleton Mo atom with the heavier W atom, which increases substantially the antibonding character of the LUMOs.

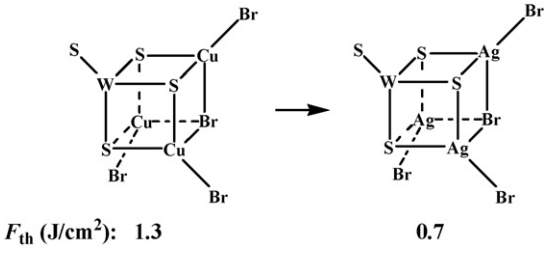

Scheme 1. Influence of skeletal metal atoms.

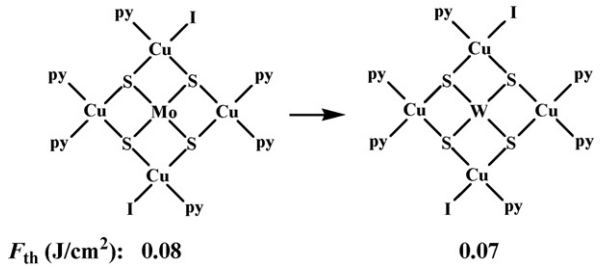

Scheme 2. Influence of central metal atoms.

Thus, a significant improvement of optical non-linearity and optical limiting effect, as observed in the cubane-like clusters from **24** to **25**, or in the planar 'open' clusters from **70** to **71**, may be derived from the heavy atom effect. First, substitution of Cu or Mo atoms by heavier Ag or W atoms may allow more efficient spin–orbital coupling, and facilitate the intersystem crossing at the excited states [19,20,41]. Large spin–orbital couplings might be very beneficial if the strong reverse saturable absorptions are associated with the electronic transitions in the desired excited states ($T_1 \rightarrow T_n$), as in the cases of fullerene C_{60} and phthalocyanine systems [41,52,64,66,121,122,137–139]. Second, the use of heavy atoms may introduce more sublevels into the energy hierarchy, and give more allowed electronic transitions for the initial excited state. The increased numbers of the allowed electronic transitions probably enhance the non-linear absorption of the initial excited state to the higher excited states.

Furthermore, an alteration of the central metal atom from Mo to W may, in some cases, lead to an essential switch in the optical non-linearity, such as from a self-focusing to a self-defocusing effect as found in neutral cubane-like clusters [$MOS_3Cu_3(\mu_3$-Y)(2-pic)$_3$] (M = Mo **33**, W **34**) [85], similar to a case mentioned above in Section 3.4 for clusters **52**–**53** [29]. A preliminary NLO investigation on clusters **33**–**34** demonstrates that the excited-state non-linear refraction can be tentatively interpreted by a multi-energy-level model. Consequently, the nonlinear refraction index n can be represented as [85,115]:

$$n = n_0 + \eta_g N_g + \eta_e N_e \tag{9}$$

where N_g and N_e are the cluster molecule populations of the ground-state and the excited-state, respectively; η_g and η_e separately denote the corresponding refractive volumes of the ground-state and the excited-state. When all the cluster molecules are in the ground-state, $n_{0s} = n_0 + \eta_g N$ is the linear refractive index of the cluster solution. For the sake of simplicity and only considering the case of steady-state, the nonlinear refraction index can then be expressed as [85,115]:

$$n = n_0 + \frac{1 + k_r(I/I_s)}{1 + (I/I_s)}\eta_g N \tag{10}$$

where $I_s = \hbar\nu/\sigma_g\tau_{s1}$ is the saturable intensity. The ratio $K_r = \eta_e/\eta_g$, the refraction volume of the excited-state to that of the ground-state, can correlate the refractive volume with the sign of the non-linear refraction. When K_r is larger than 1, it appears self-focusing; if K_r is less than 1, a negative sign will be observed. Such a model was applied to study the refractive non-linearity of **33**–**34**, and successfully fit the experimental results, which are shown in Scheme 3 (solid lines). The ratio K_r is calculated to be 0.5 from the fitting curve for cluster **33** and 2.0 for cluster **34**, respectively [85]. Although cubane-like clusters **33** and **34**, or in the case of nest-shaped clusters **52** and **53**, have similar structures, replacing the central metal atom W for Mo results in a red shift for the first absorption band ν_1. Accordingly, the non-linear refraction is switched from self-focusing to self-defocusing, due to the influence of different heavy central metal atoms.

4.3. Influence of structural types

Studies on the NLO effect of these heterothiometallic clusters have also demonstrated that their NLO performances including absorption, refraction and optical limiting are often influenced by the excited-state charge distribution and excited-state lifetime [19,21,82,110]. Constructing components, molecular symmetry and structural rigidity of these clusters are important factors in determining the locations and shapes of the potential wells of the excited states, which in turn control the lifetime of the excited states and hence the NLO performance of the clusters.

A salient feature is that strong OL effects have been observed with the tri-anionic cubane-like, hexagonal prismatic and pentanuclear planar 'open' clusters, as well as with polymeric clusters. Other clusters, such as the nest, butterfly, linear, half-open cage, flywheel, and twin-nest types only exhibit moderate, weak or almost negligible OL ability, in comparison with the former four types of clusters. It can be assumed that such different OL behavior may be attributed to the high symmetry of the cluster molecule configuration in the above first

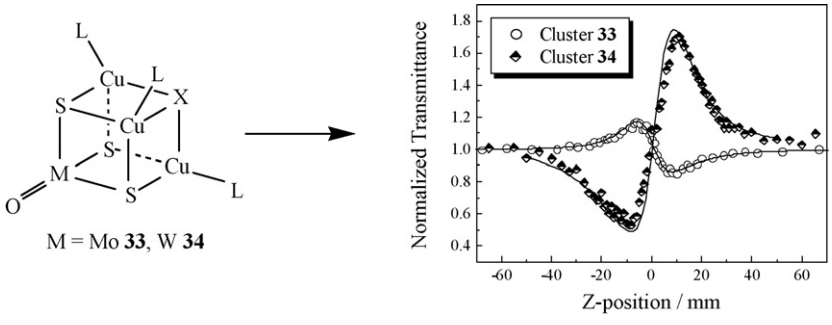

Scheme 3. Influence of the central metal atoms on the optical refractive nonlinearity.

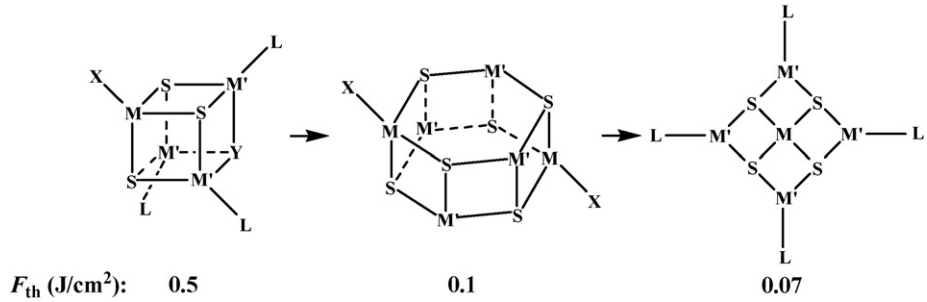

Scheme 4. Influence of the cluster skeletons on the OL performances.

group of clusters. Particularly the pentanuclear planar 'open' clusters [20,21,31,110] have higher symmetry (D_{2d}) than the cubane-like (C_{3v}) [19,26,63] and hexagonal-prismatic clusters (C_{3v}) [32,56,57]. The higher skeleton symmetry, as found in the phthalocyanine systems [52,122,137,139], may decrease the probability of the ground-state electronic transitions and give a smaller absorption cross-section σ_g and a larger σ_e/σ_g (K_α) ratio, which can be obtained from the Z-scan measurements, and eventually results in large optical non-linearities and strong OL effects (illustrated in Scheme 4).

It is also interesting to compare the NLO properties of the cubane-like clusters [82] with those of the nest-shaped [29,55,108] and half-open cubic-cage clusters [30,53,54]. These three types of clusters have the same cluster cores in C_{3v} symmetry. The difference among them arises only from the much higher structural rigidity of the cubane-like clusters in comparison with the nest-shaped and half-open cubic-cage clusters. Accordingly, only small structural changes are possible in the structure of such cubane-like clusters when electrons are pumped from ground states to excited states by laser light excitation. Much larger structural deformation is allowed with the nest-shaped clusters. If a large change in charge distribution is to occur due to electronic excitation, a nest-shaped cluster may accommodate this change better than a cubane-like cluster and hence allow the excited state to have a longer lifetime [19–21,26,29,30,53–55,82,85,108]. Cleavage of one skeletal Cu–Y (Y = I, Br) bond in a cubane-like cluster results in a half-open cubic-cage cluster, of which structural rigidity should be between that of a cubane-like cluster and a nest-shaped cluster (formed from a cubane-like structure by removal of a skeleton atom and cleavage of three skeletal bonds). The above described inference has been suggested by the measured $\chi^{(3)}$ values of these three types of clusters (5.4×10^{-12} to 7.9×10^{-11} esu for nest-shaped clusters **52–53** and **61–62** [29,107], 1.2×10^{-11} to 5.4×10^{-10} esu for half-open cubic-cage clusters **65–67** [30,53,54], and 5.8×10^{-10} to 7.3×10^{-10} esu for cubane-like clusters **27–28** [82]), as shown in Scheme 5.

4.4. Influence of peripheral ligands

The OL capability (exemplified by the limiting threshold merits or the ratios of σ_e/σ_g) and optical non-linearity (by the γ values) of a series of pentanuclear planar 'open' clusters increase systematically going from $[MS_4Cu_4(NCS)_2(py)_6]$ **76–77** [31,117] and $[Et_4N]_2[MS_4Cu_4(NCS)_4(2\text{-pic})_4]$ **78–79** [118] through $[MS_4Cu_4Cl_2(py)_6]$ **74–75** to $[MS_4Cu_4Br_2(py)_6]$ **72–73** and finally to $[MS_4Cu_4I_2(py)_6]$ **70–71** [20,21,110]. These clusters all have the identical center skeleton aggregate $[MS_4Cu_4]$ with the difference only laying in their peripheral ligands. It is the very fact that substitutions of light elements (halide ligand Cl or pseudo-halide ligand NCS) by heavy elements (Br or I) reduce the optical limiting thresholds and increase optical non-linearities. This may be attributable to the heavy atom substituting effect illustrated in Scheme 6.

In the case of cubane-like clusters [19,26], replacement of all three peripheral halides of the tri-anionic cluster $[MS_4M'_3YL_3]^{3-}$ by PPh_3 affords the neutral cluster $[MS_4M'_3Y(PPh_3)_3]$. Interestingly, after the anionic peripheral ligands (halides) of the clusters $[MS_4M'_3YL_3]^{3-}$ were replaced by neutral ligands (PPh_3), the generated neutral clusters $[MS_4M'_3Y(PPh_3)_3]$ are nearly incapable of performing OL actions under the identical experimental conditions [97]. A decrease of the OL effect in these PPh_3-containing neutral clusters may be expected, noting that PPh_3 is less π-donating than halides and the linear absorption peaks of the clusters $[MS_4M'_3Y(PPh_3)_3]$ (at λ_1 and λ_2) are blue shifted (corresponding

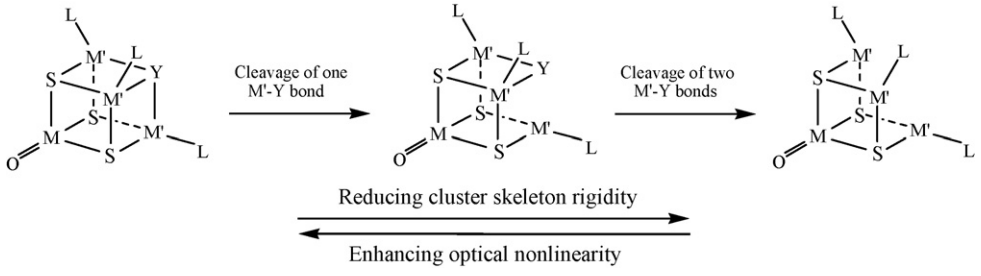

Scheme 5. Influence of the skeletal rigidity on the NLO effects.

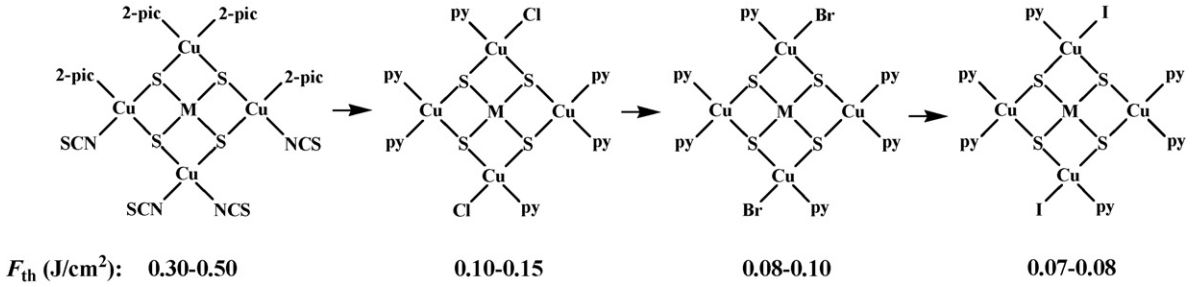

Scheme 6. Influence of the peripheral ligands on the OL capabilities.

to increase HOMO–LUMO energy gaps) with respect to their anionic counterparts.

Such an influence of peripheral ligands on the NLO performance in clusters with pentanuclear planar 'open' or cubane-like cores can also be preliminarily interpreted by the RSA mechanism. A significant extent of the photo-induced excited state population is required for a NLO chromophore of which the OL capability originates from excited state absorption. The larger the ratio of the excited state absorption cross-section over the ground state absorption cross-section (σ_e/σ_g) is, the better is the OL performance. Since most of the neutral cubane-like clusters have much smaller linear absorption at the operation wavelength (532 nm) than their anionic analogues, their relevant excited state population is inevitably smaller. Sequentially, larger irradiation is needed for the neutral clusters to operate the desired optical limiting performance (e.g., characterized by a given F_{th} value) even if the excited state absorption cross-sections of the clusters $[MS_4M'_3Y(PPh_3)_3]$ and $[MS_4M'_3YL_3]^{3-}$ are comparable. In such series of pentanuclear planar 'open' clusters, I- or Br-containing clusters have been proved to possess larger σ_e/σ_g values than their Cl- or NCS-counterparts by excited-state absorption experiments [20,21,110,118].

4.5. Molecular orbital analysis

Molecular orbital (MO) analysis has been applied to further verify the above described deductions and conclusions. The geometries of all clusters were optimized by using molecular mechanics in MM+ force fields. MOs were calculated using the extended Hückel molecular orbital (EHMO) method [97,140–143]. Results of the EHMO calculations were graphically plotted employing the plotting program of Hyperchem 6.0. Cluster bond lengths and bond angles used for the EHMO calculations were symmetrized (average bond lengths and bond angles were used to replace individual bond lengths and bond angles reported in literature [19–21,26,30,53,54,82,107,110]) to assist the assignment of symmetry representations of molecular orbitals.

The energy gap between HOMO and LUMO may play an important role in determining the NLO performance and OL effect of heterothiometallic clusters, in the viewpoint of quantum chemistry. The large energy gap ΔE may contribute to the small NLO capability and poor OL ability. This is understandable because their corresponding photoinduced excited state population is inevitably smaller. Consequently, larger incident fluence (represented by F_{in}) is required for such clusters to reach the desired level of optical limiting even if the excited state absorption cross-sections of theses clusters are comparable to those of the clusters with small ΔE values. The calculations of the energy gap ΔE clearly support the inference that the skeletal metal atoms, peripheral ligands and structural configuration of these heterothiometallic clusters have a significant influence on their NLO properties: first, replacement of all three skeletal Ag atoms with Cu in a cubane-like cluster (**24**–**25**) will increase the ΔE value from 0.36 to 0.58 eV, which is consistent with the drop in their OL capability as revealed in Scheme 1 [26,63]. Second, alteration of the cluster skeleton as described in Scheme 5 may lead to a growth of the ΔE values (0.57 eV for cubane-like clusters **27**–**28** [82], 0.76 for half-open cubic-cage clusters **65**–**67** [30,53,54] and 1.34 for nest-shaped clusters **61**–**62** [107]). As a result, their optical non-linearities significantly reduce going from cubane-like through half-open cubic-cage to nest-shaped skeletons, represented by the measured $\chi^{(3)}$ values [82]. Third, pentanuclear planar 'open' clusters (**70**–**75**) in Scheme 6 have an identical core structure and overall charge but different peripheral ligands. The change of the peripheral ligands from Cl^- through Br^- and to I^- causes a red shift in their first absorption peaks (ν_1 band). In consequence, the calculated ΔE values systematically decrease from 0.84 eV through 0.79 to 0.68, with a slow but evident enhancement of their OL effects as found in the NLO measurements [20,21,110].

5. Conclusions and perspectives

In conclusion, diverse and varied features have emerged from the examination of third-order NLO functions of heterothiometallic clusters. Especially, cubane-like, hexagonal-prism and pentanuclear planar 'open' clusters show strong non-linear absorption. Bulky non-linear refraction effects are found in nest-shaped, twin-nest-shaped, half-open cubic-cage and butterfly-shaped clusters. Twenty-nuclear supra-cage cluster possesses a very large non-linear susceptibility. Pentanuclear planar 'open' clusters, hexagonal-prismatic clusters and polymeric clusters with a 2-D network or a 3-D open framework seem to reveal large optical limiting properties. The non-linear refraction performance from self-focusing to self-defocusing can be realized through altering the central metal atom (W to Mo) in some neutral cubane-like and nest-shaped clusters. Polymeric clus-

ters hold the combined strength of both clusters and polymers, and exhibit very good NLO capabilities. These characteristics certainly not only enrich the theory but expand the application of non-linear optics. Such kinds of transition heterothiometallic clusters offer a very large variety of molecules and various structures, and can satisfy very different demands of third-order NLO materials. The concepts of optical non-linearity, NLO switching and, particularly, optical limiting are for some aspects uniquely related to such kinds of clusters.

Various classes of transition metal complexes have been investigated and the structure–property trend for most of them can be understood to some extent. The unique characteristics of heterothiometallic clusters as third-order NLO materials remain, however, still largely unexplored. Moreover, multifunctional materials involving metal clusters or complexes, such as combining optical non-linearity with magnetic, optical, or electric properties, can be envisaged. These and other topics certainly deserve further investigation in the perspective of new molecular materials. Thus, it is critically important to further explore and establish the comprehensive relationships between cluster structures and NLO functions for guiding the future rational design and development of new NLO cluster compounds. With rational molecular design and chemical synthesis, investigators could consequently tailor the optical properties to specific applications in broadband and ultrafast NLO or OL response. Such molecular engineering will pave the way to the final application of these functional molecule-based materials in practical non-linear optical devices in the near future.

Acknowledgements

The authors thank the National Natural Science Foundation of China (No. 50472048), Program for New Century Excellent Talents in University (NCET-05-0499, NCET-04-0333), and Foundations of NUST (Young Scholar Research Grant) and HIT for financial support. We are grateful to referees for their constructive comments and to editor—Professor A.B.P. Lever for his patient advice. We also thank Professor Bernt Krebs at University of Münster for his beneficial discussion.

References

[1] E.I. Stiefel, K. Matsumoto, Transition Metal Sulfur Chemistry: Biological and Industrial Significance, American Chemical Society, Washington, DC, 1996.
[2] I. Dance, K. Fisher, Prog. Inorg. Chem. 41 (1994) 637.
[3] R.H. Holm, Adv. Inorg. Chem. 38 (1992) 1.
[4] S.C. Lee, R.H. Holm, Chem. Rev. 104 (2004) 1135.
[5] R. Panda, C.P. Berlinguette, Y.G. Zhang, R.H. Holm, J. Am. Chem. Soc. 127 (2005) 11092.
[6] D. Coucouvanis, Acc. Chem. Res. 24 (1991) 1.
[7] S.M. Malinak, D. Coucouvanis, Prog. Inorg. Chem. 49 (2001) 599.
[8] M. Koutmos, D. Coucouvanis, Angew. Chem. Int. Ed. 43 (2004) 5023.
[9] Y. Ohki, Y. Sunada, M. Honda, M. Katada, K. Tatsumi, J. Am. Chem. Soc. 125 (2003) 4052.
[10] Z.L. Li, Y. Ohki, K. Tatsumi, J. Am. Chem. Soc. 127 (2005) 8950.
[11] J.B. Howard, D.C. Rees, Chem. Rev. 96 (1996) 2965.
[12] A. Müller, E. Diemann, R. Jostes, H. Bögge, Angew. Chem. Int. Ed. Engl. 20 (1981) 934.
[13] D. Sellmann, J. Sutter, Acc. Chem. Res. 30 (1997) 460, and references therein.
[14] J.C. Bayón, C. Claver, A.M. Masdeu-Bultó, Coord. Chem. Rev. 193 (1999) 73, and references therein.
[15] D.J. Evans, C.J. Pickett, Chem. Soc. Rev. 32 (2003) 268, and references therein.
[16] M. Hidai, Special publication: Perspectives in Organometallic Chemistry, R. Soc. Chem. 287 (2003) 62, and references therein.
[17] T. Weber, R. Prins, R.A. van Santen, Transition Metal Sulphides: Chemistry and Catalysis, Kluwer Academic Publishers, 1997.
[18] H.W. Hou, X.Q. Xin, S. Shi, Coord. Chem. Rev. 153 (1996) 25.
[19] S. Shi, W. Ji, S.H. Tang, J.P. Lang, X.Q. Xin, J. Am. Chem. Soc. 116 (1994) 3615.
[20] C. Zhang, Y.L. Song, B.M. Fung, Z.L. Xue, X.Q. Xin, Chem. Commun. (2001) 843.
[21] C. Zhang, Y.L. Song, F.E. Kühn, Y.X. Wang, X.Q. Xin, W.A. Herrmann, Adv. Mater. 14 (2002) 818.
[22] H. Yu, Q.F. Xu, Z.R. Sun, S.J. Ji, J.X. Chen, Q. Liu, J.P. Lang, K. Tatsumi, Chem. Commun. (2001) 2614.
[23] Y.Y. Niu, H.G. Zheng, H.W. Hou, X.Q. Xin, Coord. Chem. Rev. 248 (2004) 169.
[24] M. Feliz, J.M. Garriga, R. Llusar, S. Uriel, M.G. Humphrey, N.T. Lucas, M. Samoc, B. Luther-Davies, Inorg. Chem. 40 (2001) 6132.
[25] C. Zhang, G.C. Jin, J.X. Chen, X.Q. Xin, K.P. Qian, Coord. Chem. Rev. 213 (2001) 51, and references therein.
[26] S. Shi, W. Ji, J.P. Lang, X.Q. Xin, J. Phys. Chem. 98 (1994) 3570.
[27] H.G. Zheng, W. Ji, M.K.M. Low, G. Sakane, T. Shibahara, X.Q. Xin, J. Chem. Soc. Dalton Trans. (1997) 2357.
[28] S. Shi, H.W. Hou, X.Q. Xin, J. Phys. Chem. 99 (1995) 4050.
[29] P. Ge, S.H. Tang, W. Ji, S. Shi, H.W. Hou, D.L. Long, X.Q. Xin, S.F. Lu, Q.J. Wu, J. Phys. Chem. B 101 (1997) 27.
[30] S. Shi, Z.R. Chen, H.W. Hou, X.Q. Xin, K.B. Yu, Chem. Mater. 7 (1995) 1519.
[31] M.K.M. Low, H.W. Hou, H.G. Zheng, W.T. Wong, G.X. Jin, X.Q. Xin, W. Ji, Chem. Commun. (1998) 505.
[32] W. Ji, S. Shi, H.J. Du, P. Ge, S.H. Tang, X.Q. Xin, J. Phys. Chem. 99 (1995) 17297.
[33] H.W. Hou, D.L. Long, X.Q. Xin, X.Y. Huang, B.S. Kang, P. Ge, W. Ji, S. Shi, Inorg. Chem. 35 (1996) 5363.
[34] S. Shi, W. Ji, X.Q. Xin, J. Phys. Chem. 99 (1995) 894.
[35] J.P. Lang, K. Tatsumi, H. Kawaguchi, J.M. Lu, P. Ge, W. Ji, S. Shi, Inorg. Chem. 35 (1996) 7924.
[36] Q.F. Zhang, Y.Y. Niu, W.H. Leung, Y.L. Song, I.D. Williams, X.Q. Xin, Chem. Commun. (2001) 1126.
[37] C. Zhang, Y.L. Song, Y. Xu, H.K. Fun, G.Y. Fang, Y.X. Wang, X.Q. Xin, J. Chem. Soc. Dalton Trans. (2000) 2823.
[38] H.S. Nalwa, S. Miyata (Eds.), Non-linear Optics of Organic Molecules and Polymers, CRC Press, New York, 1997.
[39] J.L. Bredas, C. Adant, P. Tackx, A. Persoons, B.M. Pierce, Chem. Rev. 94 (1994) 243.
[40] I.R. Whittall, A.M. McDonagh, M.G. Humphrey, M. Samoc, Adv. Organomet. Chem. 43 (1999) 349.
[41] Y.P. Sun, J.E. Riggs, Int. Rev. Phys. Chem. 18 (1999) 43.
[42] S.D. Bella, Chem. Soc. Rev. 30 (2001) 355, and references therein.
[43] H. Zhang, D.E. Zelmon, L.G. Deng, H.K. Liu, B.K. Teo, J. Am. Chem. Soc. 123 (2001) 11300.
[44] C.E. Powell, M.G. Humphrey, Coord. Chem. Rev. 248 (2004) 725.
[45] H. Ma, A.K.Y. Jen, Adv. Mater. 13 (2001) 1201.
[46] Y. Chen, M. Hanack, Y. Araki, O. Ito, Chem. Soc. Rev. 34 (2005) 517.
[47] G.P. Agrawal, R.W. Boyd (Eds.), Contemporary Non-linear Optics, Academic Press, San Diego, 1992.
[48] M. Sheik-Bahae, A.A. Said, T.H. Wei, D.J. Hagan, E.W. Van Stryland, IEEE J. Quantum Electron. 26 (1990) 760.
[49] M. Sheik-Bahae, A.A. Said, E.W. Van Stryland, Opt. Lett. 14 (1989) 955.
[50] T.H. Wei, D.J. Hagan, M.J. Sence, E.W. Van Stryland, J.W. Perry, D.R. Coulter, Appl. Phys. B 54 (1992) 46.
[51] L.W. Tutt, S.W. McCahon, Opt. Lett. 15 (1990) 700.

[52] J.W. Perry, K. Mansour, S.R. Marder, K.J. Perry, D. Alvarez Jr., I. Choong, Opt. Lett. 19 (1994) 625.
[53] Z.R. Chen, H.W. Hou, X.Q. Xin, K.B. Yu, S. Shi, J. Phys. Chem. 99 (1995) 8717.
[54] H.W. Hou, B. Liang, X.Q. Xin, K.B. Yu, P. Ge, W. Ji, S. Shi, J. Chem. Soc. Faraday Trans. 92 (1996) 2343.
[55] S. Shi, W. Ji, W. Xie, T.C. Chong, H.C. Zeng, J.P. Lang, X.Q. Xin, Mater. Chem. Phys. 39 (1995) 298.
[56] G. Sakane, T. Shibahare, H.W. Hou, X.Q. Xin, S. Shi, Inorg. Chem. 34 (1995) 4785.
[57] T. Xia, A. Dogariu, K. Mansour, D.J. Hagan, A.A. Said, E.W. Van Stryland, S. Shi, J. Opt. Soc. Am. B 15 (1998) 1497.
[58] W.L. Tan, H.G. Zheng, Q.H. Jin, G.C. Jin, W. Ji, D.L. Long, X.Q. Xin, Polyhedron 19 (2000) 1545.
[59] H.G. Zheng, W.H. Leung, W.L. Tan, D.L. Long, W. Ji, J.T. Chen, F.B. Xin, X.Q. Xin, J. Chem. Soc. Dalton Trans. (2000) 2145.
[60] Y.Y. Niu, Y.L. Song, H.G. Zheng, D.L. Long, H.K. Fun, X.Q. Xin, New J. Chem. 25 (2001) 945.
[61] H.W. Hou, Y.T. Fan, C.X. Du, Y. Zhu, W.L. Wang, X.Q. Xin, M.K.M. Low, W. Ji, H.G. Ang, Chem. Commun. (1999) 647.
[62] K. Liang, H.G. Zheng, Y.L. Song, M.F. Lappert, Y.Z. Li, X.Q. Xin, Z.X. Huang, J.T. Chen, S.F. Lu, Angew. Chem. Int. Ed. 43 (2004) 5776.
[63] W. Ji, H.J. Du, S.H. Tang, S. Shi, J. Opt. Soc. Am. B 12 (1995) 876.
[64] D.G. McLean, R.L. Sutherland, M.C. Brant, D.M. Brandelik, P.A. Fleitz, T. Pottenger, Opt. Lett. 18 (1993) 858.
[65] W.J. Su, T.M. Cooper, M.C. Brant, Chem. Mater. 10 (1998) 1212.
[66] Y.L. Song, G.Y. Fang, Y.X. Wang, S.T. Liu, C.F. Li, L.C. Song, Y.H. Zhu, Q.M. Hu, Appl. Phys. Lett. 74 (1999) 332.
[67] M.H. Ma, H.G. Zheng, W.L. Tan, J.L. Zhou, S.S. Sundara Raj, H.K. Fun, X.Q. Xin, Inorg. Chim. Acta 342 (2003) 151.
[68] Y. Cai, Y.L. Song, H.G. Zheng, Y.Y. Niu, C.X. Du, X.Q. Xin, Chem. Lett. (2002) 508.
[69] Y.Y. Niu, T.N. Chen, S.X. Liu, Y.L. Song, Y.X. Wang, Z.L. Xue, X.Q. Xin, J. Chem. Soc. Dalton Trans. (2002) 1980.
[70] H.G. Zheng, J.L. Zhou, W.L. Tan, Y.Y. Niu, W. Ji, X.Q. Xin, Inorg. Chim. Acta 340 (2002) 29.
[71] J.L. Zhou, Y.L. Song, H.B. Mo, Y.Z. Li, H.G. Zheng, X.Q. Xin, Z. Anorg. Allg. Chem. 631 (2005) 182.
[72] D.L. Long, S. Shi, Y.H. Mei, X.Q. Xin, Chin. Sci. Bull. 42 (1997) 1184.
[73] D.L. Long, W.T. Wong, S. Shi, X.Q. Xin, J.S. Huang, J. Chem. Soc. Dalton Trans. (1997) 4361.
[74] H.G. Zheng, W.L. Tan, G.C. Jin, W. Ji, Q.H. Jin, X.Y. Huang, X.Q. Xin, Inorg. Chim. Acta 305 (2000) 14.
[75] K.C. Wu, P. Lin, X.T. Wu, L. Chen, Laser Chem. 18 (2000) 193.
[76] A. Krivokapic, H.L. Anderson, G. Bourhill, R. Ives, S. Clark, K.J. McEwan, Adv. Mater. 13 (2001) 652.
[77] Y.Y. Niu, H.G. Zheng, Y. Cai, X.Q. Xin, Y.L. Song, Acta Chim. Sinica 59 (2001) 1435.
[78] H.W. Hou, X.Q. Xin, L.Q. Song, Y.T. Fan, Acta Chim. Sinica 58 (2000) 283.
[79] M. Sheik-Bahae, D.C. Hutchings, D.J. Hagan, E.W. Van Stryland, IEEE J. Quantum Electron. 27 (1991) 1296.
[80] W. Ji, H.J. Du, S.H. Tang, S. Shi, J.P. Lang, X.Q. Xin, Singapore J. Phys. 11 (1995) 55.
[81] P.E. Hoggard, H.W. Hou, X.Q. Xin, S. Shi, Chem. Mater. 8 (1996) 2218.
[82] C. Zhang, Y.L. Song, X. Wang, F.E. Kühn, Y.X. Wang, Y. Xu, X.Q. Xin, J. Mater. Chem. 13 (2003) 571.
[83] J.L. Zhou, Y.L. Song, Y.Z. Li, H.G. Zheng, X.Q. Xin, Z. Anorg. Allg. Chem. 630 (2004) 609.
[84] Y. Cai, H.G. Zheng, Y.Z. Li, J.L. Zhou, Y.L. Song, X.Q. Xin, J. Coord. Chem. 56 (2003) 595.
[85] C. Zhang, Y.L. Song, F.E. Kühn, Y.X. Wang, H.K. Fun, X.Q. Xin, W.A. Herrmann, New J. Chem. 26 (2002) 58.
[86] Y.L. Song, C. Zhang, Y.X. Wang, G.Y. Fang, C.Y. Duan, S.T. Liu, X.Q. Xin, H.G. Ye, Opt. Commun. 168 (1999) 131.
[87] C. Zhang, Y.L. Song, G.C. Jin, Y.X. Wang, T. Pan, X.Q. Xin, J. Coord. Chem. 55 (2002) 33.
[88] Y.L. Song, C. Zhang, Y.X. Wang, G.Y. Fang, G.C. Jin, X.R. Zhang, S.T. Liu, L.X. Chen, X.Q. Xin, Opt. Commun. 186 (2000) 105.
[89] Y.L. Song, Y.X. Wang, C. Zhang, G.Y. Fang, S.L. Qu, X.Q. Xin, Opt. Commun. 192 (2001) 273.
[90] D.L. Long, S. Shi, X.Q. Xin, B.S. Luo, L.R. Chen, X.Y. Huang, B.S. Kang, J. Chem. Soc. Dalton Trans. (1996) 2617.
[91] X.T. Wu, Q.M. Wang, S. Shi, Polyhedron 16 (1997) 945.
[92] H.G. Zheng, W.L. Tan, M.K.L. Low, W. Ji, D.L. Long, W.T. Wong, K.B. Yu, X.Q. Xin, Polyhedron 18 (1999) 3115.
[93] H.G. Zheng, Y.X. Wang, M.H. Ma, Y. Cai, A. Usman, H.K. Fun, Y.L. Song, X.Q. Xin, Inorg. Chim. Acta 351 (2003) 63.
[94] Y. Cai, M.H. Ma, H.G. Zheng, X.Q. Xin, A. Usman, H.K. Fun, Y.L. Song, Trans. Met. Chem. 28 (2003) 137.
[95] Y. Wang, Y.L. Song, M.F. Lappert, X.Q. Xin, A. Usman, H.K. Fun, H.G. Zheng, Inorg. Chim. Acta 358 (2005) 2217.
[96] Q. Chang, Y. Wang, X.H. Li, Y.L. Song, H.G. Zheng, X.Q. Xin, S.S.S. Raj, H.K. Fun, Chin. Inorg. Chem. 19 (2003) 574.
[97] S. Shi, Z. Lin, Y. Mo, X.Q. Xin, J. Phys. Chem. 100 (1996) 10696.
[98] H.W. Hou, X.R. Ye, X.Q. Xin, J. Liu, M.Q. Chen, S. Shi, Chem. Mater. 7 (1995) 472.
[99] W. Ji, P. Ge, W. Xie, S.H. Tang, S. Shi, J. Luminescence 66/67 (1996) 115.
[100] H.W. Hou, H.G. Ang, S.G. Ang, Y.T. Fan, M.K.M. Low, W. Ji, Y.W. Lee, Inorg. Chim. Acta 299 (2000) 147.
[101] Y.L. Song, H.W. Hou, Y.T. Fan, C.X. Du, Y. Zhu, Chin. J. Chem. 19 (2001) 268.
[102] H.W. Hou, H.G. Ang, S.G. Ang, Y.T. Fan, M.K.M. Low, W. Ji, Y.W. Lee, Phys. Chem. Chem. Phys. 1 (1999) 3145.
[103] Y. Li, J. Lu, J.Q. Xu, X.B. Cui, Y.H. Sun, Q.X. Yang, L.Y. Pan, J. Mol. Struct. 690 (2004) 131.
[104] J.L. Zhou, Y.Z. Li, H.G. Zheng, X.Q. Xin, T. Yin, Y.X. Wang, Y.L. Song, Trans. Met. Chem. 29 (2004) 185.
[105] Y.H. Hu, Y.X. Wang, J.L. Zhou, Y.L. Song, Y.Z. Li, H.G. Zheng, X.Q. Xin, Chin. J. Inorg. Chem. 19 (2003) 215.
[106] Y.H. Hu, H.G. Zheng, K. Liang, Y.L. Song, Y.Z. Li, X.Q. Xin, Chin. J. Inorg. Chem. 19 (2003) 539.
[107] C. Zhang, Y.L. Song, Y. Xu, G.C. Jin, G.Y. Fang, Y.X. Wang, H.K. Fun, X.Q. Xin, Inorg. Chim. Acta 311 (2000) 25.
[108] C. Zhang, Y.L. Song, F.E. Kühn, Y. Xu, X.Q. Xin, H.K. Fun, W.A. Herrmann, Eur. J. Inorg. Chem. (2002) 55.
[109] D.X. Zeng, W. Ji, W.T. Wong, W.Y. Wong, X.Q. Xin, Inorg. Chim. Acta 279 (1998) 172.
[110] C. Zhang, Y.L. Song, F.E. Kühn, Y.X. Wang, H.K. Fun, X.Q. Xin, J. Mater. Chem. 12 (2002) 239.
[111] Y.L. Song, C. Zhang, Y.X. Wang, G.Y. Fang, G.C. Jin, C. Chang, S.T. Liu, X.Q. Xin, H.G. Ye, Chem. Phys. Lett. 326 (2000) 341.
[112] Y.L. Song, C. Zhang, X.L. Zhao, Y.X. Wang, G.Y. Fang, G.C. Jin, S.L. Qu, S.P. Wu, X.Q. Xin, H.G. Ye, Chem. Lett. (2000) 1076.
[113] Y.L. Song, C. Zhang, Y.X. Wang, G.Y. Fang, G.C. Jin, S.T. Liu, L. Chen, X.Q. Xin, Opt. Mater. 15 (2000) 187.
[114] Y.L. Song, C. Zhang, Y.X. Wang, G.Y. Fang, G.C. Jin, X.R. Zhang, S.T. Liu, L. Chen, X.Q. Xin, Mater. Lett. 46 (2000) 49.
[115] G.Y. Fang, Y.L. Song, Y.X. Wang, X.R. Zhang, C.F. Li, C. Zhang, X.Q. Xin, Opt. Commun. 181 (2000) 97.
[116] Y.X. Wang, C. Zhang, Y.L. Song, K. Yang, G.Y. Fang, X.Q. Xin, Appl. Phys. B 74 (2002) 43.
[117] H.G. Zheng, W.L. Tan, W. Ji, W.H. Leung, I.D. Williams, D.L. Long, J.S. Huang, X.Q. Xin, Inorg. Chim. Acta 294 (1999) 73.
[118] C. Zhang, Y.L. Song, G.C. Jin, G.Y. Fang, Y.X. Wang, S.S.S. Raj, H.K. Fun, X.Q. Xin, J. Chem. Soc. Dalton Trans. (2000) 1317.
[119] Y.L. Song, C. Zhang, G.P. Chen, G.Y. Fang, Y.X. Wang, X.Q. Xin, J. Opt. A 4 (2002) 199.
[120] W.H. Zhang, J.X. Chen, H.X. Li, B. Wu, X.Y. Tang, Z.G. Ren, Y. Zhang, J.P. Lang, Z.R. Sun, J. Organomet. Chem. 690 (2005) 394.
[121] L.W. Tutt, A. Kost, Nature 356 (1992) 224.
[122] J.W. Perry, K. Mansour, I.Y.S. Lee, X.L. Wu, P.V. Bedworth, C.T. Chen, D. Ng, S.R. Mardar, P. Miles, T. Wada, M. Tian, H. Sasabe, Science 273 (1996) 1533.

[123] H.W. Hou, X.Q. Xin, J. Liu, M.Q. Chen, S. Shi, J. Chem. Soc. Dalton Trans. (1994) 3211.
[124] Z. Burshtein, Y. Kostoulas, H.M. Van Driel, J. Opt. Soc. Am. B 14 (1997) 2477.
[125] M. Sheik-Bahae, D.J. Hagan, E.W. Van Stryland, Phys. Rev. Lett. 65 (1990) 96.
[126] W. Ji, W. Xie, S.H. Tang, S. Shi, Mater. Chem. Phys. 43 (1996) 45.
[127] F.J. Aranda, D.V.G.L.N. Rao, J.F. Roach, P. Tayebati, J. Appl. Phys. 73 (1993) 7949.
[128] J.S. Meth, H. Vanherzeele, Y. Wang, Chem. Phys. Lett. 197 (1992) 26.
[129] Z.X. Zhang, D.D. Wang, P.X. Ye, Y.L. Li, P.J. Wu, D.B. Zhu, Opt. Lett. 17 (1992) 973.
[130] H.W. Hou, H.G. Zheng, H.G. Ang, Y.T. Fan, M.K.M. Low, Y. Zhu, W.L. Wang, X.Q. Xin, W. Ji, W.T. Wong, J. Chem. Soc. Dalton Trans. (1999) 2953.
[131] H.G. Zheng, J.L. Zhou, M.F. Lappert, Y.L. Song, Y.Z. Li, X.Q. Xin, Eur. J. Inorg. Chem. (2004) 2754.
[132] J.L. Zhou, Y.X. Wang, Y. Wang, Y.L. Song, H.G. Zheng, Y.Z. Li, L.P. Yang, X.Q. Xin, CrystEngComm 5 (2003) 62.
[133] H.W. Hou, Y.L. Wei, Y.L. Song, Y. Zhu, Y.T. Fan, Inorg. Chim. Acta 357 (2004) 421.
[134] J. Bernholc, E.I. Stiefel, Inorg. Chem. 24 (1985) 1323.
[135] B.D. El-Issa, A.A.M. Ali, H. Zanati, Inorg. Chem. 28 (1989) 3297.
[136] J.W. McDonald, G.D. Frieson, L.D. Rosenhein, W.E. Newton, Inorg. Chim. Acta 72 (1983) 205.
[137] C.F. Li, L. Zhang, M. Yang, H. Wang, Y.X. Wang, Phys. Rev. A 49 (1994) 1149.
[138] G.Y. Fang, Y.L. Song, Y.X. Wang, X.R. Zhang, C.F. Li, L.C. Song, P.C. Liu, Opt. Commun. 183 (2000) 523.
[139] G.D.L. Torre, P. Vazquez, F. Agullo-Lopez, T. Torres, Chem. Rev. 104 (2004) 3723.
[140] R. Hoffman, J. Chem. Phys. 39 (1963) 1397.
[141] R.H. Summerville, R. Hoffman, J. Am. Chem. Soc. 98 (1976) 7240.
[142] M.M.L. Chen, R. Hoffman, J. Am. Chem. Soc. 98 (1976) 1647.
[143] S. Alvarez, F. Mota, M.J. Novoa, J. Am. Chem. Soc. 109 (1987) 6586.